Optimal Motion of a Vertically Sculling Hydrofoil System for Efficient Propulsion and Power Extraction

by

Franck Jack Billarant

Ingénieur E.S.T.A.C.A. (Ecole Supérieure des Techniques Aéronautiques et de Construction Automobile)
Titulaire d'une Maîtrise de Mécanique de la Faculté des Sciences et des Techniques de Nantes

Submitted to the Department of Aeronautics and Astronautics
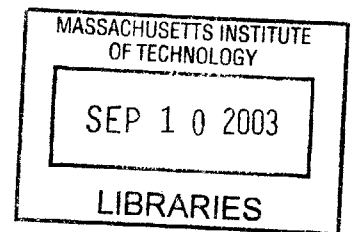in partial fulfillment of the requirements for the degree of

MASTER OF ENGINEERING IN AERONAUTICS AND ASTRONAUTICS

at the

MASSACHUSETTS INSTITUTE OF TECHNOLOGY

June 2003

Author_____
_____
Department of Aeronautics and Astronautics
May 9, 2003

Certified by_____
_____
Professor Mark Drela
Terry J. Kohler Professor of Fluid Dynamics
Thesis Supervisor

Certified by___
_____
Professor Charles Boppe
Senior Lecturer in Aeronautics and Astronautics
Thesis Supervisor

Accepted by_____
_____
Edward M Greitzer
H.N. Slater Professor of Aeronautics and Astronautics
Chair, Committee on Graduate Students

AERO

Optimal Motion of a Vertically Sculling Hydrofoil System for Efficient Propulsion and Power Extraction

by

Franck Jack Billarant

Submitted to the Department of Aeronautics and Astronautics
on May 9, 2003, in partial fulfillment of the
requirements for the degree of
Master of Engineering in Aeronautics and Astronautics

Abstract

Autonomous Marine Vehicles (AMVs) provide an efficient and cost-effective platform to accomplish a variety of maritime tasks ranging from scientific data collection to underwater mine sniffing. Because of the multirole capabilities of these vessels, military establishments around the world have expressed interest in using AMVs to close the gap in mission performance and enhance mission capabilities. In order to be a viable alternative to the current operating methods, AMV military missions involving intelligence or surveillance/reconnaissance would need to be present on site for very long periods of time to cover large areas. However, currently, mission duration is greatly limited by available on-board power supplies. Typically, endurance of autonomous marine vehicles can be improved in three ways: through 1) drag minimization, 2) highly efficient means of propulsion, and 3) the real-time extraction of energy from natural sources.

The goal of this work is to investigate a simple mechanical system to provide AMVs with all three of these attributes. The proposed system is based on a Vertically Sculling Hydrofoil (VSH) architecture, in which a horizontal wing of high aspect ratio plunges and pitches in the vertical plane. The wing provides lift to extract the hull of the vehicle to reduce wetted-surface friction drag and wave drag. The oscillation of the wing provides an efficient means of propulsion for the vessel in a way similar to birds or fish. Finally, energy can be extracted from an incoming flow by modulating the wing's incidence and damping the resulting heaving motion with an electric generator to produce power. When fitted on an autonomous marine vehicle, such a system could not only serve as a thruster but also as a means of replenishing the vehicle's power supplies to carry out long-endurance missions.

For a deeply submerged flapping wing, the unsteady loads are identical to the loads generated by a wing flapping in the air. However, when the VSH wing approaches the free surface, the problem of determining the unsteady loads is greatly complicated as a transfer of momentum between the foil and the water surface coexists. Additional drag and lift-reducing forces emanate from this free surface influence. To characterize vertically sculling hydrodynamics, a two-dimensional unsteady panel method code was devised allowing for the calculation of the unsteady loads exerted by a heaving and pitching foil with the influence of a free surface. Using this computational tool, a series of calculations were carried out to predict the optimal foil motion in order to achieve maximum efficiency for propulsion and power extraction. Based on the results, design recommendations are given for a VSH system.

Thesis Supervisor: Professor Mark Drela
Title: Terry J. Kohler Professor of Fluid Dynamics

Thesis Supervisor: Professor Charles Boppe
Title: Senior Lecturer in Aeronautics and Astronautics

Contents

List of Figures

List of Tables

Nomenclature

Roman

a_{ij}	vortex influence coefficient
A	maximum excursion of the foil's trailing edge
b_{ij}	source influence coefficient
c_j	weight vector component for numerical integration
c	mean wing chord
C	constant, lift deficiency function
C_{d0}	drag polar interpolation constant
C_{d2}	drag polar interpolation constant
C_l	lift force coefficient
C_{l0}	drag polar interpolation constant
C_m	moment coefficient, $\overline{M}_y/0.5\rho U_\infty^2 \ell_{ref}^2$
C_p	total power coefficient, $\overline{P}/0.5\rho U_\infty^3 \ell_{ref}$
$C_{t\alpha}$	pitch contribution to the total thrust coefficient
C_{th}	plunge contribution to the total thrust coefficient
C_{tc}	cross-contribution to the total thrust coefficient
C_x	vertical force coefficient, $\overline{F}_x/0.5\rho U_\infty^2 \ell_{ref}$
C_z	horizontal force coefficient, $\overline{F}_z/0.5\rho U_\infty^2 \ell_{ref}$
d	depth of foil with respect to the free surface
d_{ij}	influence coefficient
D_{wave}	normalized wave drag, $-(d/c)C_x/C_z^2$
f	frequency in Hertz
F	complex stream function, real part of lift deficiency function C
F_x	horizontal force
F_z	vertical force
$\mathcal{F}$	objective function

15

$\mathcal{F}_r$	second Froude number with ℓ_{ref} as the characteristic length, U_∞^2/g
Fr_d	first Froude number with d as the characteristic length, $U_\infty/\sqrt{gd}$
Fr_c	first Froude number with c as the characteristic length, $U_\infty/\sqrt{gc}$
g	gravitational acceleration
G	imaginary part of lift deficiency function C
$\mathcal{G}$	constraint function
h_{max}	maximum heave amplitude of travel
h_n	heaving motion Fourier coefficient
H	Hankel function
i	$\sqrt{-1}$
k	reduced frequency, $\omega c/2U$
ℓ_{ref}	reference length
$\ln$	natural logarithm
L	number of panels for free surface discretization
L_C	circulatory part of the lift
L_{NC}	non-circulatory part of the lift
L_s	free surface length
L_w	wake length
M	number of panels for wake discretization
M_y	pitching moment
n	harmonic number
n_T	number of periods in the wake
N	number of panels on foil
p	pressure
P	power, maximum number of modes
q	source distribution strength per unit length
Q	number of control points
$\mathcal{R}$	residual function
$\mathbb{R}$	the set of real numbers
Re	Reynolds number, $U_\infty \ell_{ref}/\nu$
S	leading edge suction velocity
t	time
T	period
u	x-component of perturbation velocity, $\partial\varphi/\partial x$
$\mathcal{U}$	unknown

U	x-component of total velocity, $\partial\Phi/\partial x$
U_∞	x-component of free stream velocity
W	z-component of total velocity, $\partial\Phi/\partial z$
W_∞	z-component of free stream velocity
w	z-component of perturbation velocity, $\partial\varphi/\partial z$
x	horizontal cartesian coordinate
x_{rot}	horizontal pitching axis location
$\mathcal{X}$	vector of design parameters
z	vertical cartesian coordinate

Greek

α_e	effective (aerodynamic) angle-of-attack
$\alpha_{e_{max}}$	maximum effective angle-of-attack
β	angle
χ	complex variable
Δx	panel length
∇	Laplacian operator
ν	kinematic viscosity
η_P	propulsive efficiency, C_x/C_p
η_E	power extraction efficiency, C_p/C_x
γ	vorticity strength, running circulation
Γ	total circulation
ω	circular frequency, $2\pi f$
φ	perturbation potential
ϕ	phase between plunge and pitch
Φ_∞	freestream flow potential
Φ	total velocity potential
ψ	stream function
ρ	freestream density
σ	complex source strength
θ	pitch angle
θ_{max}	maximum pitch angle
ξ	dummy integration variable

ζ vorticity

Subscripts

$(\ )_u$	upper surface
$(\ )_l$	lower surface
$(\ )_n$	mode n
$(\ )_{spec}$	specified
$(\ )_i$	control point index, panel index
$(\ )_j$	foil and wake panel node index
$(\ )_m$	free surface panel node index
$(\ )_x$	first derivative w.r.t x

Superscripts

$(\ )^a$	foil
$(\ )^s$	surface
$(\ )^w$	wake
$\hat{(\ )}$	amplitude at fixed mode
$\bar{(\ )}$	period averaged value
$\dot{(\ )}$	rate of change w.r.t time

Operators

$\Re$	real part
$\Im$	imaginary part
$\frac{D}{Dt}$	substantial derivative

Acronyms

ALTEX	Atlantic Layer Tracking Experiment
AMV	Autonomous Marine Vehicle

AUV	Autonomous Underwater Vehicle
DOF	Degree Of Freedom
LB	Lower Bound
MAV	Micro Air Vehicle
SQP	Sequential Quadratic Programming
UB	Upper Bound
VSH	Vertically Sculling Hydrofoil, Vertically Sculling Hydrodynamics

Acknowledgments

I would like to thank Professor Charles Boppe for the support and guidance he has provided me these past years at MIT. I also wish to thank him for his suggestions and the productive comments he has made throughout this thesis. My gratitude also goes to Professor Mark Drela for giving me the opportunity to do this research and for teaching me about the field of aerodynamics. His insightful suggestions throughout this work have been very helpful. This project would not have been possible without Tim Smith who has come forward with the idea of using Vertically Sculling Hydrodynamics for the proposed application.

I am also indebted to Professor John Hansman for providing me with the opportunity to work as a teaching assistant to fund my studies at MIT.

These last few years at MIT would not have been the same without the support of all my friends here and abroad. It would be impractical to list all of you here, but you know who you are ! A big thank you.

Finally, I wish to thank my family for all the moral support they've given me these last few years away from home, while I've been in Michigan and in Massachusetts. Thank you for encouraging me in all my endeavors.

Chapter 1

Introduction

1.1 Introduction-Project Motivation

Research and use of Autonomous Marine Vehicles (AMVs) have been expanding in recent years as they provide an efficient and cost-effective platform to accomplish a variety of maritime tasks. Whether operating on the ocean surface or underwater, such vessels are a desirable alternative to carrying out missions that would otherwise require a large investment in manpower and equipment. They also provide an attractive means of performing hazardous tasks and can operate in regions into which no manned underwater vessel or remotely operated vehicle can penetrate (e.g. ALTEX Arctic mission).

The vital source of energy, raw materials, nutrients, and climatic clues provided by the oceans can be surveyed and monitored with these autonomous vessels with minimal human intervention and logistic support. In fact, with approximately 150 AMVs designed around the world in nearly 40 years of development [16], the scientific and industrial community has clearly realized the benefits of using such platforms for:

- pollution detection and other environmental surveys

- seabed mapping

- pelagic fisheries surveys

- undersea search and survey

- communication and navigation aids

Because of the multirole capabilities of these vessels, the military around the world has also expressed interest in using AMVs in an effort to close the gap in mission performance and enhance

mission capabilities [34]. Kongsberg Simrad AS, for example, is currently working on a military Autonomous Underwater Vehicle (AUV) prototype called *HUGIN 1000* for the Royal Norwegian Navy to perform mine countermeasure and rapid environmental assessment operations. In the United States, MIT Sea Grant's Autonomous Underwater Vehicle's Lab is developing a low-cost AUV called *CETUS*^{TM} for underwater intervention and sea mine warfare.

Although most of the applications stated above are feasible with the available technology, for many other applications to become reality, certain technological challenges still need to be overcome. For intelligence, surveillance/reconnaissance missions (e.g. harbor security) or long-duration data sampling, AMVs would need to be present on site for very long periods of time (sometimes months) to cover large areas, in order to be a viable alternative to the current operating methods. However, mission duration is greatly limited by available on-board power supplies and means of improving duration are actively sought.

Improvement of the long-endurance capabilities of autonomous marine vehicles can typically be achieved in three ways:

1. Through drag minimization of the vehicle's hull and other appendages.

2. Through the investigation of highly efficient means of propulsion.

3. Through the real-time extraction of energy from natural sources.

The goal of this work is to investigate a simple mechanical system based on a Vertically Sculling Hydrofoil (VSH) architecture that can provide an autonomous marine vehicle with all three of these attributes.

1.2   VSH Description

A Vertically Sculling Hydrofoil is essentially a system composed of a rigid wing of high aspect ratio (hydrofoil) positioned horizontally and undergoing pitching and heaving oscillations in the vertical plane.

1. The horizontal placement of the hydrofoil provides high lift-to-drag capabilities to the marine vehicle to extract its hull from the water, thus reducing wetted-surface friction drag and wave drag generated by the hull.

2. The oscillating motion of the hydrofoil produces thrust in a way similar to birds or fish. Much theoretical work claims that propulsive efficiencies rivaling with that of propellers can be achieved with flapping propulsion.

3. Finally, energy can be extracted from an incoming flow by modulating the wing's incidence and damping the resulting heaving motion with an electric generator to produce power. One could imagine the scenario where the autonomous marine vehicle surfs the waves and extracts energy from the flowstream to recharge its power supplies.

When fitted on an AMV, such a system could not only serve as a thruster but also as a means of replenishing the vehicle's power supplies to carry out long-endurance missions.

The VSH architecture has multiple advantages over conventional systems for both propulsion and power extraction. From a mechanical standpoint, it can be designed to have few moving parts, thus reducing manufacturing/assembly costs and the likelihood of failing. In fact, if only propulsion is of interest, one could imagine a simple design involving no mechanical linkage to the foil with an offset mass on a motor inducing an oscillating motion on the hydrofoil.

Although this architecture has multiple benefits for an AMV, one of its major drawback stems from the fact that the hydrofoil operates in the vicinity of the water surface where the effects of *free-surface induced drag* are most significant. To assess the potential and the viability of such a system for the proposed application, it would be desirable to accurately characterize and quantify these effects.

1.3 Previous Work

1.3.1 Theoretical and Experimental Work

Numerous theoretical and experimental investigations pertaining to flapping-wing propulsion and flapping-wing flight have been completed throughout the years in an attempt to understand and mimic both fishlike swimming and avian flight.

Knoller and Betz were the first to provide scientific theories relating to thrust generation of a heaving airfoil in independent studies in 1909 and 1912 [22], [5]. Although a flurry of unsteady aerodynamic theories and experimental investigations followed from that point on, it was not until 1935 that Theodorsen, von Kármán and Sears, provided the ground work for many flapping-foil propulsion mathematical models. In 1936, Garrick [11] applied Theodorsen's [31] linear, inviscid unsteady aerodynamics theory to derive compact expressions for the thrust force generated by a flat plate undergoing harmonic oscillations. Garrick found that the efficiency of a heaving and plunging airfoil approaches unity as the motion frequency approaches zero. He also found that thrust was proportional to the square of the frequency.

In 1970, Lighthill investigated lunate tail propulsion and derived formulas for the thrust and efficiency of a thuniform swimmer. In his work, Lighthill proposed a *proportional feathering parameter* Θ corresponding to the ratio of slopes between the effective angle-of-attack of the tail and the angle

formed by the caudal fin trail and the swimming path of the fish. Lighthill calculated that values of Θ between 0.6 and 0.8 yielded optimal combinations of leading-edge suction and hydromechanical efficiency [24],[30].

In 1981, Delaurier and Harris [7] carried out experiments on oscillating-wing propulsion to serve as a data base for future experimental and theoretical work. Their experiments were limited to small amplitude flapping and corroborated Garrick's theoretical work. Later that year, McKinney and Delaurier [26] conducted a series of experimental tests on an oscillating-wing windmill. They determined that this *wingmill* system, as they termed it, could achieve efficiencies comparable to those of conventional windmill designs.

More recently, Triantafyllou et al. [32], [33] focused on the wake dynamics of large-amplitude oscillating foils and found conditions leading to optimal thrust production. They determined that the thrust coefficient was nearly a linear function of the Strouhal[1] number St_a, and that it should be between 0.25 and 0.35 for optimal efficiency. Their definition of the Strouhal number is $St_a = fA/U_\infty$, where A is the width of the wake taken to be equal to the maximum excursion of the foil's trailing edge, f is the frequency of motion in Hertz, and U_∞ is the average forward velocity. An optimal Strouhal number, however, does not give any indication of the optimal frequency, simply because frequency and motion amplitude can be varied to fix the Strouhal number.

With the advent of Micro Air Vehicles (MAV), Hall & Hall [13] devised a three-dimensional vortex lattice model to investigate the power requirements for flapping flight. They computed an optimal circulation distribution along the span of a flapping wing that simultaneously provides thrust and lift. They showed the existence of optimum flapping amplitudes and frequencies.

Lately, Jones and Platzer [18], [19], performed extensive numerical investigations on flapping-foil systems using a non-linear, deforming wake model to compute the unsteady flow about an airfoil undergoing pitch and plunge motions. They investigated the influence of interference effects on flapping-wing propulsion and looked at various configurations involving multiple airfoils with the intent of developing a MAV [17]. A preferred configuration where two airfoils work in opposed plunge was identified, and it was shown through numerical and experimental tests that high efficiencies could be attained.

Jones, Davis and Platzer [20] also looked at flapping-foil power generators or *wingmills*. For a prescribed maximum effective angle-of-attack, optimal plunge velocities and optimal ratios between the heaving and frequency of motion were identified. Although an experimental setup was designed, no results are currently available.

---

[1] The Strouhal number is used to characterize the structure of wakes and is essentially the ratio of unsteady to inertial forces
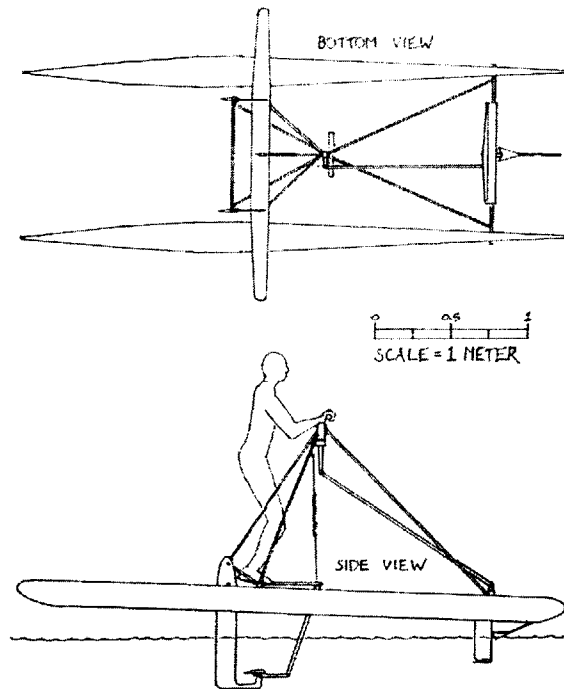
Figure 1-1: Two-view of the *Preposterous Pogo Foil*.

1.3.2 VSH Vehicle Concepts

Until now, VSH propulsion vehicles have been designed and built mostly for recreational purposes.

Parker MacCready [25] designed and built two experimental human-powered hydrofoil boats with flapping-wing propulsion in the mid 1980s. In his first boat called *the Mutiny on the Boundary Layer*, the pilot sat on a standard bike frame linked to catamaran hulls for flotation before take-off. A complex mechanism pushed a wing/strut assembly up and down as the rider pedaled to generate lift and thrust. *The Mutiny on the Boundary Layer* did not prove efficient, with propulsive efficiencies on the order of 40% and an average speed of 3m/s, but it did accomplish the goal of flying while achieving flapping-wing propulsion. MacCready claims that the low propulsive efficiencies were mainly due to mechanical friction in moving parts and suboptimal wing angles during the flapping cycle. Specifications pertaining to the craft are summarized in Table 1.1 along with estimated Reynolds number and Froude number based on the chord.

Later in 1993, MacCready experimented with a boat similar to the *the Mutiny on the Boundary Layer*, but mechanically much simpler, which he called the *Preposterous Pogo Foil* (see Figure 1-1). This boat had few moving parts (< 10), and the heaving motion of the foil was accomplished by the pilot bending at the knees. The first tests; however, showed that the craft was more limited by control problems than by excessive power requirements.

Recently, Alexander Sahlin unveiled the *Trampofoil®* in Sweden, a vehicle similar to the *Pogo*

27

	Mutiny	*Trampofoil*®
Mass, m	50kg	12kg
Wing span, b	$2.0m$	$2.87m$
Wing mean chord, c	$0.12m$	$0.15m$
Stall velocity, V_s	N/A	$2.5m/s$
Maximum velocity, V_{max}	N/A	$5.5m/s$
Cruise velocity, V_c	$3.2m/s$	$3 - 4m/s$
Estimated Froude number, Fr_c	2.9	3.3
Estimated depth of foil, d	$0.5c - 2.0c$	$0.5c - 2.0c$

Table 1.1: Specifications for the *Mutiny* and the *Trampofoil*®

Foil in the way it operates. By hopping on a footplate rigidly attached to the wing, the pilot induces an oscillating motion on the wing which propels the craft. Unlike the *Pogo Foil*, the *Trampofoil*® does not have any hulls or moving parts. Maximum speeds of 5.5m/s with stall speeds of 2.5m/s have been recorded with the *Trampofoil*® but no information regarding the efficiency of the device could be found. The specifications for the craft are summarized in Table 1.1. Figure 1-2 shows the *Trampofoil*® and its operation.

1.4 Statement of Project Objectives

Although a lot of theoretical and experimental investigations have been done in the field of flapping-wing propulsion and power extraction, no attention has been paid to the interference effects of a *free surface* on a foil flapping below the water. Also, all theories and experimental work described above draw on sinusoidally plunging and heaving foil motions without considering if a more complex motion might be more efficient from either a propulsion or power extraction standpoint. The objectives of this work are thus twofold:

1. To devise an unsteady computer-based engineering analysis tool to characterize Vertically Sculling Hydrodynamics. The tool should permit the calculation of the unsteady loads imparted on a foil undergoing arbitrarily specified motions in the presence of the ocean's free wave surface.

2. To use this computational tool to identify a preferred functional mode for regenerative power extraction and propulsion. The functional mode encompasses describing the optimal foil motions and the relevant flow parameters associated with unsteady hydrodynamics (i.e. Froude number, depth of the foil from the free surface, etc...).

The present document is organized in the following manner. In Chapter 2 a theoretical model based on inviscid, incompressible, unsteady aerodynamics for a two-dimensional VSH system is

28
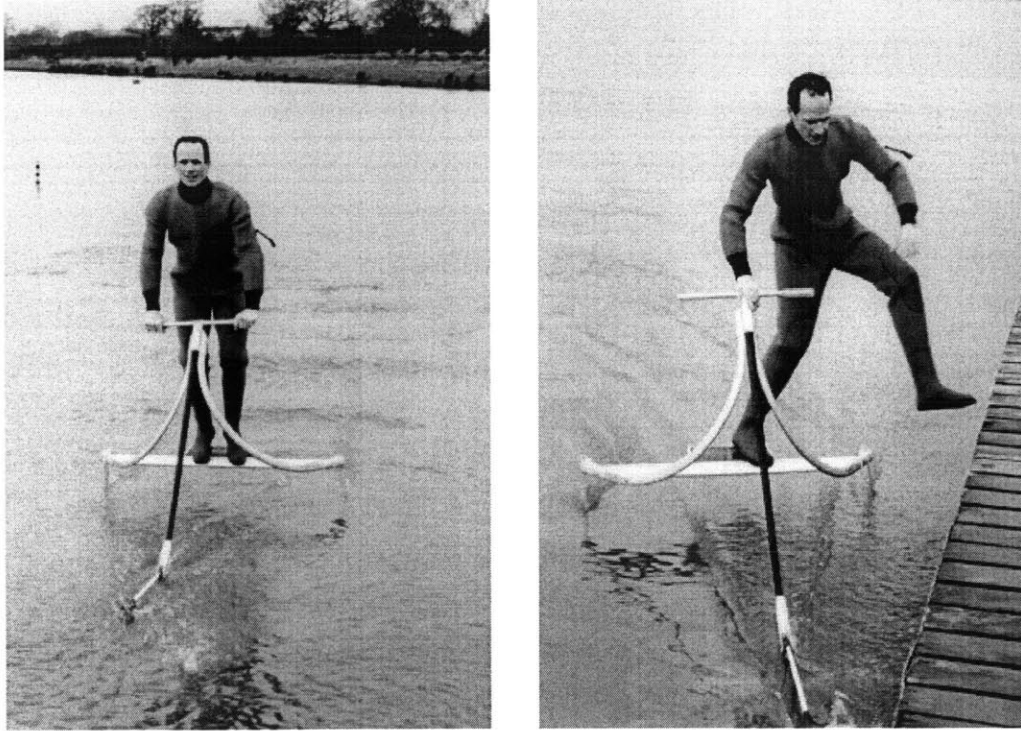
Figure 1-2: The inventor of the *Trampofoil*® riding the craft.

presented. In Chapter 3 a numerical implementation of the model is described in great detail for anyone who wishes to reproduce the computer-based tool. Testing of this tool on various cases is carried out in Chapter 4. Finally, computed VSH results are presented in Chapter 5 and design recommendations for a generic VSH system are made based on the computed results. Conclusions and recommendations for future work are given in Chapter 6.

Chapter 2

Vertical Sculling Hydrodynamic Model

The goal of this section is to formulate a mathematical model for a Vertical Sculling Hydrodynamic (VSH) system. A system composed of a two-dimensional foil moving in a flow of constant velocity U_∞ and undergoing periodic heaving $h(t)$ and pitching $\theta(t)$ motions below the surface of a body of water is considered. The governing equations of the flow are described and various assumptions about the system are made. From these assumptions, a flowfield idealization of the VSH system using vortex and source sheets is presented. Finally, a solution procedure for the flowfield unknowns is described.

2.1 Fluid Flow Governing Equations

In order to derive a model of the flowfield describing the Vertical Sculling Hydrodynamic system, the underlying fundamental physical principles of fluid dynamics must first be evoked.

2.1.1 Continuity Equation

The first physical principle is that mass is conserved throughout the flow. For a compressible, unsteady fluid moving around an airfoil fixed in space, the conservation of mass is given by:

$$\frac{\partial \rho}{\partial t} + \nabla \cdot (\rho \mathbf{V}) = 0$$
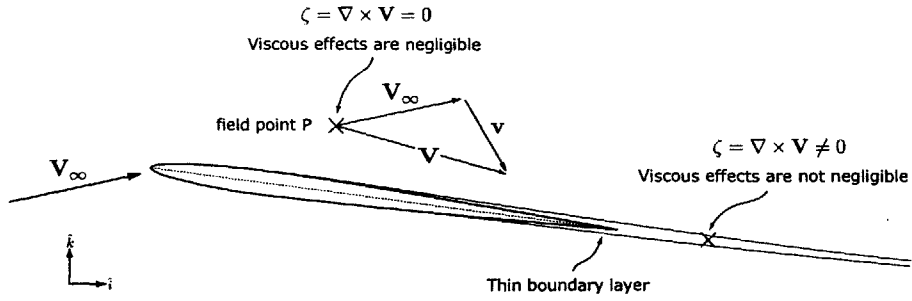
Figure 2-1: Flow regions in a high Reynolds number flow.

Where ρ and $\mathbf{V}$ are respectively the *scalar density field* and the *total vector velocity field*. These fields are a function of both space and time and are given in two-dimensional cartesian space by:

$$
\begin{aligned}
\mathbf{V} &= U(x,z,t)\,\hat{i} + W(x,z,t)\,\hat{k} \\
\rho &= \rho(x,z,t)
\end{aligned}
$$

Incompressible Flow

If the flow is assumed to be incompressible, the scalar density field is then invariant in both space and time and the continuity equation reduces to,

$$
\nabla \cdot \mathbf{V} = 0 \tag{2.1}
$$

Irrotational Flow

For a solid body immersed in a real flow, dissipative transport phenomena of viscosity leads to the creation of thin boundary layers and narrow wakes in the fluid domain (see Figure 2-1). In these regions, shear stresses induce rotational flow. Outside of these regions on the other hand, the flow is barely affected by the viscosity of the fluid and can be considered to be irrotational. Although vorticity ζ exists in boundary layers and wake regions of the flow, a good approximation of the overall flowfield can be made through the irrotational flow assumption for flows where the inertial effects dominate the viscous effects. For an irrotational flow, the curl of the total vector velocity field is zero,

$$
\zeta = \nabla \times \mathbf{V} = 0 \tag{2.2}
$$

31

and there exists a total scalar velocity potential Φ, such that the total vector velocity field is given by the gradient of this scalar function:

$$\mathbf{V} = \nabla \Phi \tag{2.3}$$

Laplace Equation

From these considerations, by substituting (2.3) into (2.1), the continuity equation reduces to the Laplace equation, which in two-dimensional cartesian space is given by:

$$\nabla^2 \Phi = \left(\frac{\partial^2 \Phi}{\partial x^2} + \frac{\partial^2 \Phi}{\partial z^2} \right) = 0 \tag{2.4}$$

Since the Laplacian is a linear operator, the superposition principle can be used to decompose the total velocity potential Φ into a velocity potential due to the free stream flow and a perturbation potential φ.

$$\Phi = \phi_\infty + \varphi \tag{2.5}$$

Taking the gradient of (2.5), the total vector velocity field may be expressed as,

$$\mathbf{V} = \mathbf{V}_\infty + \mathbf{v} = (U_\infty \hat{i} + W_\infty \hat{k}) + (u\hat{i} + w\hat{k}) \tag{2.6}$$

2.1.2 Conservation of Momentum

The second physical principle is that the fluid is governed by Newton's second law. Conservation of momentum for an inviscid incompressible fluid is given by the Euler equation:

$$\frac{\partial \mathbf{V}}{\partial t} + \mathbf{V} \cdot \nabla \mathbf{V} = -\frac{\nabla p}{\rho} + \mathbf{f} \tag{2.7}$$

where $\mathbf{f}$ is a body force. If the body force is assumed to be conservative, then $\mathbf{f}$ derives from a potential E such that,

$$\mathbf{f} = -\nabla E \tag{2.8}$$

The gravitational acceleration can be included in the momentum equation by selecting a potential $E = gz$, where g is the gravitational constant and the z axis points upwards.

Unsteady Bernoulli Equation

Rewriting (2.7) in terms of the total velocity potential leads to the *unsteady Bernoulli equation*,

$$\nabla\left(\frac{\partial \Phi}{\partial t} + (\nabla\Phi)^2 + \frac{p}{\rho} + gz\right) = 0 \rightarrow \frac{\partial \Phi}{\partial t} + (\nabla\Phi)^2 + \frac{p}{\rho} + gz = C(t) \tag{2.9}$$

If an arbitrary point and a reference point are considered in the flow where conditions are chosen such that $\Phi_\infty = const.$, the pressure p at any point in the flow can be calculated from the velocity potential by:

$$p_\infty - p = \rho\frac{\partial \Phi}{\partial t} + \frac{\rho}{2}(\nabla\Phi)^2 + \rho gz \tag{2.10}$$

The momentum equation thus connects the velocity potential to the pressure. This is useful to determine the pressure distribution on the body surface to allow for a calculation of the aerodynamic forces and moments.

2.1.3 Flow Equation Summary

From these explanations we see that in the case of an inviscid, incompressible and irrotational fluid, the conservation of mass reduces to the Laplace equation which is the governing equation for the velocity potential. It is an elliptic differential equation that results in a boundary-value problem. By prescribing appropriate boundary conditions to represent the flow, one can thus solve for the velocity potential.

Once the velocity potential is known, Bernoulli's equation, which is a consequence of the conservation of momentum, is used to calculate aerodynamic loads.

2.2 VSH Model Assumptions

Certain assumptions about the VSH system need to be made to come up with an appropriate mathematical model.

2.2.1 Perfect Fluid Assumption

The first assumption is that the ratio between the inertial and viscous forces in the fluid is expected to be high since the kinematic viscosity of water is very small ($\nu \approx 1.0 \times 10^{-6} m^2/s$) . For such flows where the Reynolds number is high ($Re >> 1$), viscous terms can be neglected from the momentum equation and irrotationality of the flow is assumed outside the immediate neighborhood of streamlined bodies present in the flow. Also, water is assumed to be an incompressible fluid. From

these considerations, the flow resulting from a wing undergoing a plunging and pitching motion below the surface of a body of water is governed by the Laplace equation (2.4).

2.2.2 Foil Shape Assumption

The shape of the foil is assumed to have little influence on the inviscid unsteady loads, and is therefore modeled by a flat plate. As shown by K.D. Jones and M.F. Platzer in [18], this is a valid assumption for the range of frequencies considered in this study. Also, since the flow is governed by the Laplace equation, the effects of the foil shape can easily be incorporated into the model by linear superposition if deemed necessary.

2.2.3 Foil Motion Assumption

Small amplitudes relative to the foil chord are assumed in the various degrees of freedom. Furthermore, the motion of the airfoil is assumed to be periodic in time with period T in the heaving and pitching degrees of freedom. By limiting the model to small amplitudes with periodic motion the VSH model can be linearized, greatly simplifying the theoretical model and allowing for the use of Fourier decomposition to represent the time dependent flow unknowns. Also, the frequencies at which the foil flaps are assumed to be within the range of low-frequencies observed in cetaceans.

2.2.4 Wake Assumption

It is assumed that the wake behind the foil does not roll up and is not convected in the flow. From our previous small amplitude considerations, shed vorticity behind the airfoil is assumed to be accurately modeled by a non-deforming, planar wake. Although, physically, the wake behind the airfoil rolls up, it has been shown by numerous investigators [13], [19] that this roll up effect has very little influence on the unsteady loads imparted on the foil and can be safely neglected for the range of frequencies and flapping amplitudes considered in this study.

2.2.5 Free Surface Assumption

The wing of the VSH system is assumed to operate below the water surface at a depth where the deformation of the free surface significantly perturbs the flowfield around the foil and its wake resulting in wave resistance effects.

Since the deformation of the free surface is not known a priori and changes in time, the resulting boundary condition is greatly complicated. To keep the complexity of the model within reasonable bounds, wave motions are assumed to be sufficiently small to linearize the free surface wave boundary condition and a planar free surface sheet is adopted to represent the wave induced effects [28],[21].
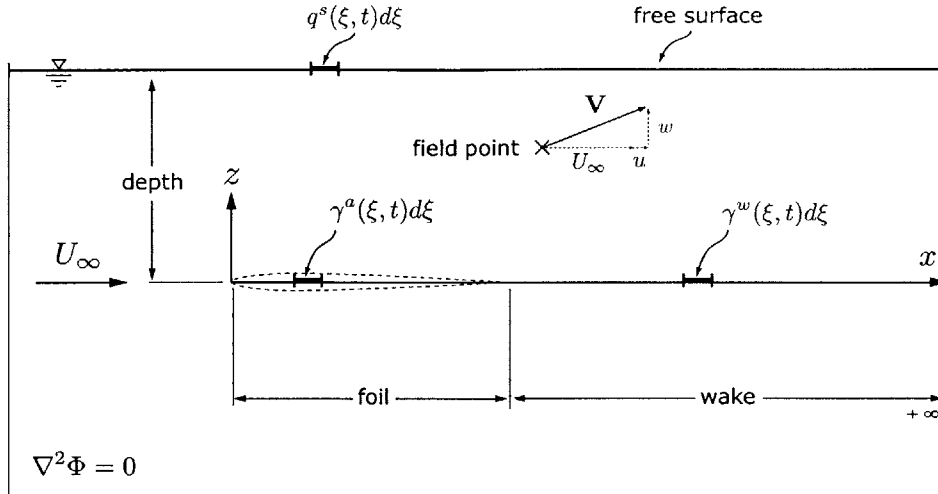
Figure 2-2: VSH flowfield idealization by means of vortex and source sheets.

Also, the floor bed is assumed deep enough not to affect the water surface, allowing deep water wave theory to be applicable.

2.3 VSH Flowfield Idealization

2.3.1 Flowfield Modeling Using Vortex and Source Sheets

As a result of applying the perfect fluid assumption, the flowfield may be represented by vortex and source sheets to account for the various elements perturbing the flow [21],[4],[1]. As depicted in Figure 2-2 and following the fore mentioned assumptions, the foil is modeled as a flat plate and is represented by a sheet of bound vorticity of unknown strength γ^a per unit length. The wake behind the foil is represented by a sheet of shed vorticity γ^w. Finally, we introduce the free surface effects of the body of water in which the VSH system is immersed by means of a source sheet of source strength distribution q^s per unit length.

2.3.2 Boundary Conditions in Time Domain

To solve for the the flowfield unknowns, $\mathcal{U} = \{\gamma^a, \gamma^w, q^s\}$, various conditions must be imposed on the boundaries of the fluid domain to ensure that a unique solution to Laplace's equation for our particular engineering problem will be found:

- a *kinematic boundary condition* of zero normal flow is imposed on the foil. This condition enforces the foil to be a streamline of the flow.
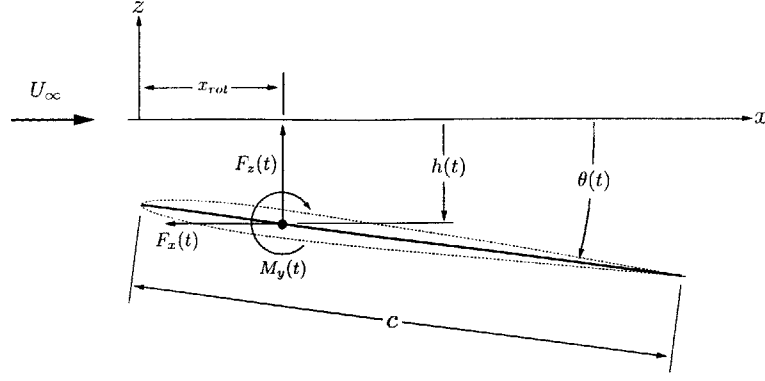
Figure 2-3: Chordline of the foil undergoing heaving and pitching displacements. All quantities positive, as shown.

- a circulation-fixing *Kutta condition* at the trailing edge of the foil is imposed for the flow to have physical meaning.

- a *dynamic boundary condition* is imposed on the wake sheet to relate the wake vortex distribution to the total foil circulation.

- a *free surface boundary condition* is enforced on the source sheet representing the surface of water.

Kinematic Boundary Condition

For a foil moving in a flow of constant velocity $\mathbf{V} = \nabla\Phi$, the kinematic boundary condition on the body's surface is such that the perpendicular component of the fluid velocity is fixed by the body's motion. Fluid particles in the vicinity of the body must thus share the body's normal motion. If the surface of a body is defined by a function $F(x, z, t) = 0$, then the boundary condition at the surface is given by:

$$\frac{DF}{Dt} = \frac{\partial F}{\partial t} + \nabla\Phi \cdot \nabla F = 0 \tag{2.11}$$

Physically, equation (2.11) states that the fluid particles on the surface of the body move with velocity $\mathbf{V}$ such that F remains zero.

Referring to Figure 2-3, the instantaneous small displacement of the chordline of a two-dimensional chordwise-rigid foil undergoing heaving (h) and pitching (θ) oscillations in a frame of reference moving with the foil is given by:

$$z^a(x, t) = -h(t) - (x - x_{rot})\theta(t) \tag{2.12}$$

Where x_{rot} is the pitching axis location.

36

Introducing the expression of the camberline $F = z - z^a = 0$ into equation (2.11) yields for the total velocity W normal to the camberline of the foil,

$$W = \frac{\partial \Phi}{\partial z} = -\dot{h}(t) - (x - x_{rot})\dot{\theta}(t) - U\theta(t) \tag{2.13}$$

Now, assuming that the horizontal perturbation velocity is small compared to the freestream velocity ($\frac{\partial \varphi}{\partial z} << U_\infty$), and recalling that the vertical freestream velocity component W_∞ is zero, the boundary condition on the foil reduces to:

$$w^a(x, t) = -\dot{h}(t) - (x - x_{rot})\dot{\theta}(t) - U_\infty \theta(t) \tag{2.14}$$

From potential flow theory [21], the time dependent vertical induced velocity w due to the vortex and source sheets at a point x on the foil is expressed as:

$$w(x, 0, t) = \frac{-1}{2\pi} \int_0^c \frac{\gamma^a(\xi, t)}{x - \xi} d\xi - \frac{1}{2\pi} \int_c^\infty \frac{\gamma^w(\xi, t)}{x - \xi} d\xi + \frac{1}{2\pi} \int_{-\infty}^\infty q^s(\xi, t) \frac{d}{(x - \xi)^2 + d^2} d\xi \tag{2.15}$$

For the foil to be a streamline of the flow, the velocity normal to the camberline of the foil of a fluid particle must equate the vertical velocity induced by the vortex and source sheet distributions. In other words, the vortex and source strengths of the singularity distributions must be adjusted appropriately for this condition to be satisfied. The kinematic boundary condition of zero normal flow thus translates into:

$$w(x, 0, t) = w^a(x, t) \tag{2.16}$$

Kutta Condition

In addition to satisfying the kinematic boundary condition, the vorticity distribution must also satisfy the Kutta condition. The Kutta condition introduces a circulation-fixing relation by making sure that the flow leaves the foil's sharp trailing edge smoothly and that the velocity there is finite.

For the steady case, this condition translates into having the vorticity at the trailing edge vanish ($\gamma(c) = 0$). In the unsteady case, the Kutta condition is that no pressure discontinuity exists at the trailing edge ($\Delta p(c) = 0$). This makes physical sense since the wake that emanates from the trailing edge of the foil is usually very thin and cannot support a pressure difference. From the unsteady Bernoulli equation (2.10) the pressure jump Δp across a vortex sheet in terms of the total velocity

37

potential is,

$$\Delta p = p_l - p_u = \rho \frac{\partial}{\partial t} \Delta \varphi + \frac{\rho}{2} \left(\Phi_{u_x}^2 - \Phi_{l_x}^2 \right)$$

$$= \rho \frac{\partial}{\partial t} \Delta \varphi + \frac{\rho}{2} \underbrace{\left(\Phi_{u_x} + \Phi_{l_x} \right)}_{\approx 2U_\infty} \underbrace{\left(\Phi_{u_x} - \Phi_{l_x} \right)}_{\frac{\partial \Delta \varphi}{\partial x}}$$

Where Φ_{u_x} and Φ_{l_x} respectively correspond to the x-derivative of the total velocity potential on the upper surface and on the lower surface of the sheet.

Assuming that the x-component of the perturbation velocity $u = \frac{\partial \varphi}{\partial x}$ is small compared to the free stream velocity U_∞, one may write a linearized form of the pressure jump across the vortex sheet representing the foil and its wake:

$$\Delta p \approx \rho \left(\frac{\partial}{\partial t} \Delta \varphi + U_\infty \frac{\partial}{\partial x} \Delta \varphi \right) \tag{2.17}$$

By definition, the vortex sheet strength γ is equal to the jump in tangential velocity on the vortex sheet:

$$\gamma = \frac{\partial \Delta \varphi}{\partial x} \tag{2.18}$$

and the pressure jump at position x along the vortex sheet written in terms of the vorticity distribution is:

$$\Delta p(x,t) = \rho \frac{\partial}{\partial t} \int_0^x \gamma(\xi,t) d\xi + \rho U_\infty \gamma(x,t) \tag{2.19}$$

Evaluating (2.19) at the foil's trailing edge ($x = c$) yields for the linearized unsteady Kutta condition,

$$\rho \frac{\partial}{\partial t} \int_0^c \gamma(\xi,t) d\xi + \rho U_\infty \gamma(c,t) = 0 \tag{2.20}$$

Dynamic Wake Boundary Condition

Since the vorticity in the wake γ^w is a direct consequence of a change in the bound vorticity γ^a, the shed vorticity distribution can be expressed in terms of the the total foil circulation Γ^a. This is done by using Kelvin's circulation theorem which states that in the potential flow region the angular momentum cannot change, and thus the total circulation Γ around a fluid curve enclosing the foil

38

and its wake is conserved,

$$\frac{D\Gamma}{Dt} = \frac{\partial\Gamma}{\partial t} + U_\infty\frac{\partial\Gamma}{\partial x} = 0 \tag{2.21}$$

The total circulation Γ around a fluid curve enclosing the foil and a wake of length $(x - c)$ is expressed in terms of the foil and wake running circulations by:

$$\Gamma = \Gamma^a + \Gamma^w = \int_0^c \gamma^a(\xi, t)d\xi + \int_c^x \gamma^w(\xi, t)d\xi \tag{2.22}$$

Taking the substantial derivative of (2.22) and setting it to zero gives an expression relating the foil and wake vorticity distribution unknowns. This condition reduces the number of unknowns from $\{\gamma^a, \gamma^w, q^s\}$ to just $\{\gamma^a, q^s\}$.

Free Surface Boundary Condition

To account for the free surface effects in the model a boundary condition describing the two-dimensional behavior of surface wave motion must be enforced on the source sheet representing the water surface. Since the relative wave height is assumed to be small, a planar source sheet is used to represent the mean ocean surface. It is relevant to point out that this surface does not move with the surface waves but that the deformation of the free surface is taken into account by changing the source strength distribution $q^s(x, t)$.

The linear progressive wave model boundary condition is given by Katz and Plotkin [21] in terms of the perturbation potential φ below:

$$\frac{U_\infty^2}{g}\frac{\partial^2\varphi(x, d, t)}{\partial x^2} + \frac{\partial\varphi(x, d, t)}{\partial z} = 0 \tag{2.23}$$

Where d is the depth of the foil relative to the water's undisturbed surface. Introducing the Froude-number $\mathcal{F}_r = U_\infty^2/g$ which is defined as the ratio of the inertial force to the gravitational force, the boundary condition in terms of perturbation velocities is,

$$\mathcal{F}_r\frac{\partial}{\partial x}\,u(x, d, t) + w(x, d, t) = 0 \tag{2.24}$$

Note that in the limiting case where the Froude number is set to zero, the free surface boundary condition describes a rigid wall ($w(x, d, t) = 0$). Ground/anti-ground effects can thus easily be incorporated into the model by setting the Froude number to zero.

39
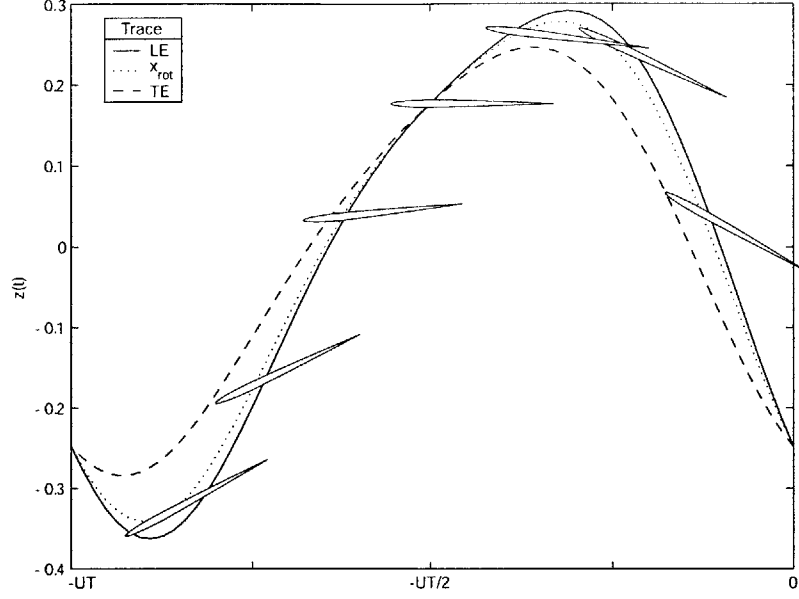
Figure 2-4: Leading edge, pivot point and trailing edge trace of the foil undergoing a complex motion described by seven Fourier coefficients. The Fourier coefficients in this example are: $h_0 = 0$, $h_1 = 0.3$, $h_2 = 0.05$, $\theta_0 = 0$, $\theta_1 = 5$, $\theta_2 = 2$ and $\phi_1 = 135$.

2.4 Flowfield Solution Methodology

2.4.1 Fourier Expansion Approach

The flowfield is fully determined by solving Laplace's equation subject to the boundary conditions defined above. Since Laplace's equation is linear and the various boundary conditions have all been linearized, a way to solve for the unsteady flowfield is to describe the foil motion and the singularity distributions as Fourier expansions and use linear superposition to reconstruct the time-dependent unknown distributions.

Foil Motion Description

The first step involves describing an arbitrary periodic foil motion with frequency ω by using a Fourier expansion,

$$h(t) = \sum_{n=0}^{P} \hat{h}_n e^{i(n\omega t + \phi_n)} \ , \ \ \theta(t) = \sum_{n=0}^{P} \hat{\theta}_n e^{in\omega t} \tag{2.25}$$

Where n is referred to as the *mode*, and ϕ_n is a heaving phase lead with the pitching motion for mode n. Using expressions (2.25), any foil motion can be described by carefully selecting P Fourier coefficients h_n, θ_n, $\phi_n \in \mathbb{R}$. As an example, Figure 2-4 shows one period of a complex foil motion obtained with seven Fourier coefficients.

40

Singularity Distribution Description

Likewise, the singularity distributions are expressed as Fourier expansions:

$$\gamma^a(x,t) = \sum_{n=0}^{P} \hat{\gamma}_n^a(x)e^{in\omega t} \ , \ \gamma^w(x,t) = \sum_{n=0}^{P} \hat{\gamma}_n^w(x)e^{in\omega t} \ , \ q^s(x,t) = \sum_{n=0}^{P} \hat{q}_n^s(x)e^{in\omega t} \tag{2.26}$$

Where $\hat{\gamma}_n^a$, $\hat{\gamma}_n^w$ and $\hat{q}_n^s$ are complex functions of the spatial coordinate x, thus allowing for phase differences between the motion and the resulting flowfield.

Using this approach, the boundary conditions are rewritten in the frequency domain, and enforced on the surfaces of the fluid region. For every mode $n = 0, 1...P$, the singularity unknowns are solved for and the time-dependent singularity distributions are reconstructed by summing over the modes using equation (2.26).

2.4.2 Boundary Conditions in Frequency Domain

The various boundary conditions on the fluid domain surfaces are rewritten in the frequency domain by means of the Fourier descriptions (2.25) and (2.26) introduced above.

Kinematic Boundary Condition

Substituting the fore mentioned Fourier expansions for the foil motion and the singularity distributions in equation (2.16) results in the kinematic boundary condition for a given mode n.

$$
\begin{aligned}
0 \ = \ & in\omega\hat{h}_n(x)e^{i\phi_n} + \left(in\omega(x - x_{rot}) + U_\infty\right)\hat{\theta}_n \\
& + \frac{-1}{2\pi}\int_o^c \frac{\hat{\gamma}_n^a(\xi)}{x - \xi} \ d\xi \\
& + \frac{-1}{2\pi}\int_c^\infty \frac{\hat{\gamma}_n^w(\xi)}{x - \xi} \ d\xi \\
& + \frac{1}{2\pi}\int_{-\infty}^\infty \hat{q}_n^s(\xi)\frac{d}{(x - \xi)^2 + d^2} \ d\xi
\end{aligned}
\tag{2.27}
$$

Unsteady Kutta Condition

Evaluating (2.19) at the trailing edge ($x = c$), results in the following expression for every mode n.

$$in\omega\underbrace{\int_0^c \hat{\gamma}_n(\xi)d\xi}_{\hat{\Gamma}_n^a} + U_\infty\hat{\gamma}_n(c) = 0 \tag{2.28}$$

41

Finally, the linearized unsteady Kutta condition is given by:

$$\hat{\gamma}_n(c) = \frac{-in\omega}{U_\infty}\hat{\Gamma}_n^a \tag{2.29}$$

For the steady case where $n = 0$, we find that the vorticity at the trailing edge vanishes.

Dynamic Boundary Condition

Substituting equation (2.22) into (2.21) and making use of the Fourier expansions for the foil motion and singularity distributions as defined per (2.25) and (2.26), one obtains for the Kelvin condition,

$$\sum_{n=0}^{P}\left(in\omega\hat{\Gamma}_n^a + in\omega\int_c^x \hat{\gamma}_n^w(\xi)d\xi + U_\infty\hat{\gamma}_n^w(x)\right)e^{in\omega t} = 0 \tag{2.30}$$

Where $\hat{\Gamma}_n^a$ is the total foil circulation for a given mode n. Eliminating time and taking the derivative with respect to x of (2.30) allows one to find a solution for $\hat{\gamma}_n^w(x)$,

$$U_\infty\frac{\partial\hat{\gamma}_n^w(x)}{\partial x} + in\omega\hat{\gamma}_n^w(x) = 0 \;\rightarrow\; \hat{\gamma}_n^w(x) = C\,e^{-in\omega x/U_\infty} \tag{2.31}$$

where C is a constant found by substituting (2.31), evaluated at the trailing edge ($x = c$), into (2.30). Finally, introducing a dimensionless *reduced frequency*, $k \equiv \omega c/2U_\infty$ gives the following expression[1] for the wake vorticity distribution in terms of the foil circulation for a mode n:

$$\hat{\gamma}_n^w(x) = \frac{-in\omega}{U_\infty}\,\hat{\Gamma}_n^a\,e^{2ink}e^{-in(\omega x/U_\infty)} \tag{2.32}$$

Free Surface Boundary Condition

Likewise, the free surface boundary condition (2.24) is rewritten in terms of the Fourier coefficients.

---

[1]Note that (2.32) evaluated at the trailing edge leads to result (2.29)

42

Chapter 3

Numerical Implementation of Model

In Chapter 2 a mathematical model of the Vertically Sculling Hydrodynamic system was described. A methodology for finding the unknown properties of the flowfield by means of a Fourier expansion approach was also introduced. The object of this chapter is to describe the numerical implementation of the Fourier approach to obtain a solution for the singularity distributions and evaluate the loads imparted on the foil.

3.1 Numerical Solution Outline

The numerical solution to the unsteady flow is obtained through a five-step process:

1. The user provides information about the geometry of the fluid domain, the motion of the foil as well as the flow conditions at which the unsteady loads need to be evaluated.

2. From the user inputs, the lengths of the foil, wake and the free surface are defined and the fluid boundaries are discretized into panels of linearly-varying strengths. A description of the discretization process is given in Section 3.3.

3. The velocities induced by the various panels representing the boundaries of the flow are determined from the geometry. Section 3.4 and Appendix 6.2 explain how this process is done.

4. For all modes n chosen to represent the motion, the boundary conditions described in Chapter 2 are enforced and a matrix system is setup for the flow. A solution to the unsteady flow for a mode n is obtained.

User Input	Variable	Units
Number of panels	N, M, L	none
Number of periods in the wake	n_T	none
Motion amplitudes for mode n	h_n, θ_n	units of ℓ_{ref}
Motion phase for mode n	ϕ_n	rads
Motion reduced frequency	k	none
Chord length	c	units of ℓ_{ref}
Depth of foil	d	units of ℓ_{ref}
Froude number based on the chord	Fr_c	none

Table 3.1: User inputs for the numerical solution to the VSH flow.

5. From the solution of the flowfield, postprocessing of the flow unknowns is carried out to calculate unsteady loads. Section 3.6 describes how the loads are calculated.

3.2 User Inputs

The motion of the foil is prescribed by the user through a set of Fourier coefficients and the frequency of motion. Information about the geometry of the system and the flow conditions at which the loads need to be estimated is also provided by the user and is summarized in Table 3.2. From the Froude number based on the foil's chord Fr_c the Froude number $\mathcal{F}_r$ is calculated,

$$\mathcal{F}_r = c \, Fr_c{}^2 \tag{3.1}$$

Note that in the code, the incoming flow velocity is assumed to be $1m/s$ and the gravitational constant is $g = 1m/s^2$.

3.3 Discretization of the Geometry

The first step to the numerical calculation involves discretizing the vortex and source sheets into panels of lengths $\Delta x_i = (x_{i+1} - x_i)$. The continuous vortex and source distributions are respectively approximated by a collection of panels of linearly varying vorticity and source strengths.

Figure 3-1 shows the nomenclature used for the discretization of the foil, wake and free surface regions. The foil of chord c is discretized using N panels connected by $N + 1$ nodes. The wake of length L_w is discretized using $M - N$ panels and the free surface source sheet, whose length is L_s, is discretized with $L - M - N$ panels. There are L panels in all to discretize the geometry. A *control point* i is placed on the foil and free surface panels where boundary conditions need to be enforced. There are Q control points in all. In what follows, index i refers to a control point and index j refers to a panel node.
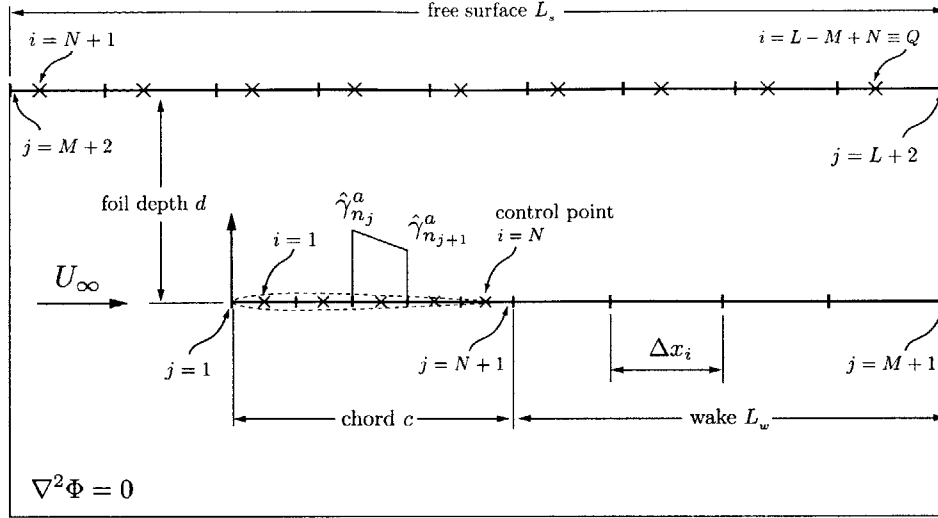
Figure 3-1: Discretization of the foil, wake and free surface regions.

3.3.1 Foil Discretization

Foil Panel Distribution

From thin airfoil theory, it is clear by looking at the analytical solution for the vorticity distribution along a flat plate that the gradient of the vorticity rapidly varies near the edges of the plate. In order to numerically capture this rapidly varying gradient in vorticity it is necessary to refine the mesh of the foil near the leading and trailing edges. A *full-cosine* spacing method which concentrates the nodes near the leading and trailing edges is thus adopted for the foil. For a foil of chord c divided into N panels, the x station of a panel node j is found by using the following cosine spacing formula:

$$x_j^a = \frac{c}{2}\left(1 - \cos\beta_j\right) \text{ with } \beta_j = \frac{(j-1)\pi}{N} \tag{3.2}$$

Foil Control Point Location

Since the kinematic boundary condition of zero normal flow needs to be satisfied on the foil, a control point is positioned on every foil panels. The control points are positioned at the center of each foil panels where the induced velocity is not singular [27].

3.3.2 Wake Discretization

Wake Panel Distribution

The foil deposits vorticity in the wake in the vicinity of the trailing edge. The wake paneling must therefore be refined in that zone in order to fully capture the physics of the flow (i.e. in order for the wake to correctly influence the foil and vice-versa). Also, since the influence of a vortex on a field

45

point at some distance r diminishes as $1/r$, the wake panels far downstream will have a negligible effect on the foil and the panel discretization in that zone can be sparse.

From these considerations a *half-cosine* discretization for the wake is chosen. Since the wake begins at the foil's trailing edge, the panel node index j runs from $N + 1$ to $M + 1$. For a wake of length L_w divided into $M - N$ panels, the x coordinate of the $j^{\,th}$ panel node is given by,

$$x_j^w = x_{N+1}^a + L_w \left(1 - \cos\beta_j\right) \text{ with } \beta_j = \frac{(j - (N+1))\pi}{2(M-N)} \tag{3.3}$$

Wake Length

In order to compare loads obtained for different frequencies of the motion, the length of the wake L_w must be adjusted to capture a fixed number of periods n_T of the motion. The length of the wake is made proportional to the period T of the motion according to the following formula:

$$L_w = n_T U_\infty T \tag{3.4}$$

3.3.3   Free Surface Discretization

Free Surface Panel Distribution

The free surface sheet panel is discretized using a constant panel distribution. The number of panels used to discretize the free surface is set by the user and must be such that the free surface panel length is always less than the depth of submergence of the foil to ensure the accuracy of the numerical method.

Free Surface Length

To compare loads obtained for varying Froude numbers F_{r_c} or F_{r_d}, the length of the free surface L_s is adjusted to capture a fixed amount of wave periods. This is done by setting the length of the free surface proportional to $\mathcal{F}_r$. In the case of a zero Froude number to account for ground effect, the length of the free surface is set to be equal to some constant C chosen by the user. The value of this constant depends on the height of the foil relative to the ground/anti-ground surface, and on the number of panels used for discretization.

Free Surface Control Point Location

Figure 3-2 shows the influence of the position of the free surface control point in obtaining accurate numerical results. Since the free surface boundary condition has terms involving both the vertical induced velocity and the first derivative of the horizontal induced velocity, the control point needs
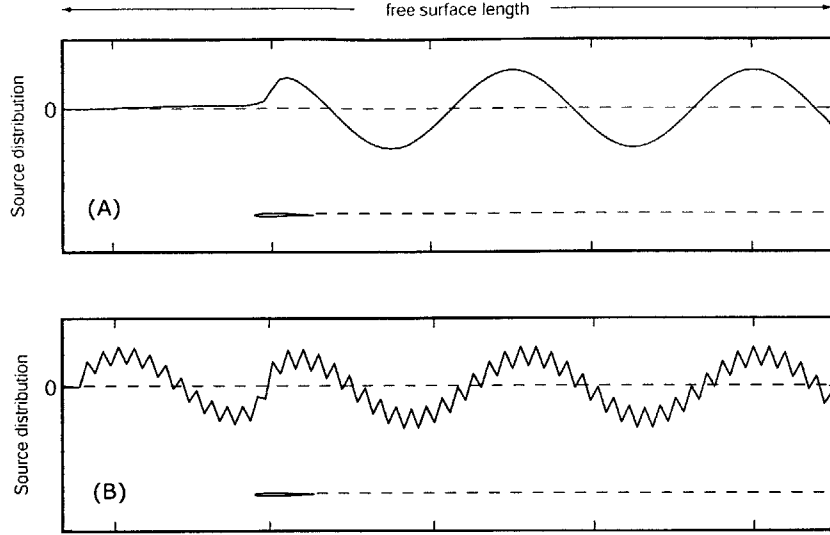
Figure 3-2: Source strength distributions obtained with the control points located at: (A) 40% of panel length, and at (B) 50% of panel length.

to be located at a position on the panel where both of these induced quantities will be seen by the control point. Numerical investigations have shown that positioning the control point at 40% of the free surface panel length gives satisfactory results when the Froude number $\mathcal{F}_r$ is different from zero. When the Froude number is set to zero by the user to model ground/anti-ground interference effects, the best results have been obtained with the control point positioned at the panel midpoint.

3.4 Panel Induced Velocities

In seeking a numerical solution to the flow, the continuous sheets are approximated by a collection of panels of linearly-varying strength. The perturbation velocities induced by these panels at some control point i in the domain are evaluated in Appendix A and are represented in a format suitable for computer manipulation by means of *influence coefficients* a_{ij}, b_{ij}. Induced velocities are evaluated by scanning the panels and summing their influences. As an example, the z-component of the velocity induced by N panels of linearly-varying vorticity is given by:

$$w(x,z) = \sum_{j=1}^{N+1} a_{ij}^z \gamma_j^a \tag{3.5}$$

For the VSH problem, the x and z-components of the velocity at a control point i for a mode n are obtained by summing the velocities induced by the foil, the wake vortex sheets and the free

47

surface source sheet:

$$\hat{u}_{n_i} = \sum_{j=1}^{N+1} a_{ij}^x \hat{\gamma}_{n_j}^a + \sum_{l=N+2}^{M+1} a_{il}^x \hat{\gamma}_{n_l}^w + \sum_{m=M+2}^{L+2} b_{im}^x \hat{q}_{n_m}^s \qquad (3.6)$$

$$\hat{w}_{n_i} = \sum_{j=1}^{N+1} a_{ij}^z \hat{\gamma}_{n_j}^a + \sum_{l=N+2}^{M+1} a_{il}^z \hat{\gamma}_{n_l}^w + \sum_{m=M+2}^{L+2} b_{im}^z \hat{q}_{n_m}^s \qquad (3.7)$$

where a_{ij}^x is the x-component of the perturbation velocity evaluated at the ith control point due to a unit strength vortex distribution on the jth panel. Likewise, b_{im}^x is the x-component of the perturbation velocity at control point i due to a unit strength source distribution on the mth panel.

As seen previously, the vorticity distribution shed into the wake is a function of the foil circulation and is given by equation (2.32),

$$\hat{\gamma}_n^w(x) = \frac{-in\omega}{U_\infty} \hat{\Gamma}_n^a \, e^{2ink} e^{-in(\omega x/U_\infty)}$$

In the discrete version of this equation, $\hat{\gamma}_n^w$ evaluated at a panel node of coordinate x_j is approximated by:

$$\hat{\gamma}_{n_j}^w = \hat{\gamma}_n^w(x_j) = \frac{-in\omega}{U_\infty} e^{in(2k - \omega x_j/U_\infty)} \sum_{j=1}^{N+1} c_j \hat{\gamma}_{n_j}^a \qquad (3.8)$$

where, $\hat{\Gamma}_n^a$, the total foil circulation, is calculated by means of (3.9),

$$\hat{\Gamma}_n^a = \int_0^c \hat{\gamma}_n^a(\xi) d\xi \approx \sum_{j=1}^N \left(\frac{\hat{\gamma}_{n_j}^a + \hat{\gamma}_{n_{j+1}}^a}{2} \right) \Delta x_j = \sum_j^{N+1} c_j \hat{\gamma}_{n_j}^a \qquad (3.9)$$

Since the computational model uses panels with piecewise linear-vorticity distributions, c_j simply corresponds to the jth component of the trapezoidal rule weight vector.

Using the discrete expression of the wake vorticity (3.8), equations for the induced velocities are rewritten in terms on the bound vorticity and the source strength unknowns:

$$\hat{u}_{n_i} = \sum_{j=1}^{N+1} d_{ij}^x \hat{\gamma}_{n_j}^a + \sum_{m=M+2}^{L+2} b_{im}^x \hat{q}_{n_m}^s \qquad (3.10)$$

$$\hat{w}_{n_i} = \sum_{j=1}^{N+1} d_{ij}^z \hat{\gamma}_{n_j}^a + \sum_{m=M+2}^{L+2} b_{im}^z \hat{q}_{n_m}^s \qquad (3.11)$$

48

where the effects of the wake panels are lumped into a new influence coefficient d_{ij}. For every control point $i = 1..N$ on the foil, d_{ij} is given by:

$$d_{ij} = a_{ij} + \sum_{l=N+2}^{M+1} a_{il} \left(\frac{-in\omega}{U_\infty} e^{in(2k - \omega x_l/U_\infty)} \right) c_j \quad \text{for all} \quad i \in [1, N] \tag{3.12}$$

3.5 Residual Formulation

The discretized boundary conditions are expressed in residual form, and a matrix system is setup to solve for the flowfield unknowns.

3.5.1 Definition of Residuals

Foil Kinematic Boundary Condition Residual

For every mode n, a residual for the boundary condition of zero normal flow on the foil is defined for the control points $i = 1..N$:

$$
\begin{aligned}
R_{n_i}^a(\hat{\gamma}_{n_j}^a, \hat{q}_{n_m}, \hat{\theta}_n, \hat{h}_n) &\equiv \sum_{j=1}^{N+1} d_{ij}^z \hat{\gamma}_{n_j}^a + \sum_{m=M+2}^{L+2} b_{im}^z \hat{q}_{n_m} \\
&+ U_\infty \hat{\theta}_n + in\omega \hat{h}_n e^{i\phi_n} + in\omega \hat{\theta}_n (x_i - x_{rot}) = 0
\end{aligned} \tag{3.13}
$$

Unsteady Kutta Condition Residual

From (2.29) and (3.9) the discretized form of the unsteady Kutta condition written in residual form becomes:

$$R_{n_{i=N+1}}^a \equiv \hat{\gamma}_{n_{N+1}} + \frac{in\omega}{(in\omega c_{N+1} + U_\infty)} \sum_{j=1}^{N} c_j \hat{\gamma}_{n_j}^a = 0 \tag{3.14}$$

Free Surface Boundary Condition Residual

The boundary condition on the free surface in residual form for a control point i running from $(N+1) \rightarrow Q = (L - M + N)$ is given for a mode n by:

$$
\begin{aligned}
R_{n_i}^s(\hat{\gamma}_{n_j}^a, \hat{q}_{n_m}^s) &\equiv \mathcal{F}_r \left(\sum_{j=1}^{N+1} d_{x_{ij}}^x \hat{\gamma}_{n_j}^a + \sum_{m=M+2}^{L+2} b_{x_{im}}^x \hat{q}_{n_m}^s \right) \\
&+ \sum_{j=1}^{N+1} d_{ij}^z \hat{\gamma}_{n_j}^a + \sum_{m=M+2}^{L+2} b_{im}^z \hat{q}_{n_m}^s = 0
\end{aligned} \tag{3.15}
$$

where $d_{x_{ij}}^x$ and $b_{x_{im}}^x$ are respectively the first derivatives of the vortex and the source influence coefficients in the x-direction as described in Appendix A.

49

The free surface boundary condition provides $(Q - N) = (L - M)$ equations. Yet, with $(L - M)$ panels on the free surface $(L - M + 1)$ source strengths are unknown, and one more equation is necessary to obtain a determined system. For the flow to be physical, two upstream end conditions are imposed. The vertical velocity of the free surface far upstream of the foil (for the first free surface control point $i = N + 1$) is set to zero and its derivative with respect to x is also set to zero.

$$R_{n_{N+1}}^{s1} \equiv w_{i=N+1} = \sum_{j=1}^{N+1} d_{N+1j}^z \hat{\gamma}_{n_j}^a + \sum_{m=M+2}^{L+2} b_{N+1m}^z \hat{q}_{n_m} = 0 \tag{3.16}$$

$$R_{n_{N+1}}^{s2} \equiv \frac{\partial w}{\partial x}\Big|_{i=N+1} = \sum_{j=1}^{N+1} d_{xN+1j}^z \hat{\gamma}_{n_j}^a + \sum_{m=M+2}^{L+2} b_{xN+1m}^z \hat{q}_{n_m} = 0 \tag{3.17}$$

Note that through this approach the first upstream residual substitutes the previous free surface boundary condition evaluated at control point $i = N + 1$, and the second residual introduces the $(L - M + 1)^{th}$ equation necessary in obtaining a determined system.

Prescribed Motion Residual

To prescribe the motion of the foil two more residuals are introduced. The values of $\hat{h}_{n_{spec}}$ and $\hat{\theta}_{n\,spec}$ are defined by the user to prescribe the motion.

$$R_n^h \equiv \hat{h}_n - \hat{h}_{n_{spec}} = 0 \tag{3.18}$$

$$R_n^\theta \equiv \hat{\theta}_n - \hat{\theta}_{n_{spec}} = 0 \tag{3.19}$$

Total Residual

Finally, a total residual vector $\mathcal{R}_n$ is defined,

$$\mathcal{R}_n = \left\{ R_{n_i}^a \,,\, R_{n_{i=N+1}}^a \,,\, R_{n_i}^s \,,\, R_{n_{N+1}}^{s1} \,,\, R_{n_{N+1}}^{s2} \,,\, R_n^h \,,\, R_n^\theta \right\}^T \tag{3.20}$$

3.5.2 System Matrix Setup

The derivatives of the residuals with respect to the flowfield unknowns and prescribed motion are evaluated to form a matrix $\left[\partial \mathcal{R}_n / \partial \mathcal{U}_n \right]$ and a direct application of Newton's method is used to solve for the unknowns $\mathcal{U}_n = [\hat{\gamma}_{n_j}^a, \hat{q}_{n_m}^s]^T$. The solution is obtained with one inversion of a matrix.

$$\delta \mathcal{U}_n = -\left[\partial \mathcal{R}_n / \partial \mathcal{U}_n \right]^{-1} \mathcal{R}_n \,,\, \mathcal{U}_n \leftarrow \mathcal{U}_n + \delta \mathcal{U}_n \tag{3.21}$$

$$[\partial \mathcal{R}_n / \partial \mathcal{U}_n] = \begin{pmatrix} \mathbf{A}_{(N+1)\times(N+1)} & \mathbf{B}_{(N+1)\times(L-M+1)} & \mathbf{C}_{(N+1)\times(2)} \\ \mathbf{D}_{(L-M+1)\times(N+1)} & \mathbf{E}_{(L-M+1)\times(L-M+1)} & \mathbf{F}_{(L-M+1)\times(2)} \\ \mathbf{G}_{(2)\times(N+1)} & \mathbf{H}_{(2)\times(L-M+1)} & \mathbf{I}_{(2)\times(2)} \end{pmatrix} \qquad (3.22)$$

A few explanations are given on the submatrices:

A Matrix

Matrix $\mathbf{A}$ contains the derivatives of the foil residual terms with respect to the vortex strength unknowns as well as the Kutta condition. The size of this matrix is $(N+1) \times (N+1)$.

$$\mathbf{A} = \begin{pmatrix} \frac{\partial R_1^a}{\partial \hat{\gamma}_1^a} & \frac{\partial R_1^a}{\partial \hat{\gamma}_2^a} & \cdots & \frac{\partial R_1^a}{\partial \hat{\gamma}_{N+1}^a} \\ \frac{\partial R_2^a}{\partial \hat{\gamma}_1^a} & \frac{\partial R_2^a}{\partial \hat{\gamma}_2^a} & \cdots & \frac{\partial R_2^a}{\partial \hat{\gamma}_{N+1}^a} \\ \vdots & \vdots & \vdots & \vdots \\ \frac{\partial R_N^a}{\partial \hat{\gamma}_1^a} & \cdots & \frac{\partial R_N^a}{\partial \hat{\gamma}_N^a} & \frac{\partial R_N^a}{\partial \hat{\gamma}_{N+1}^a} \\ \frac{\partial R_{N+1}}{\partial \hat{\gamma}_1^a} & \cdots & \frac{\partial R_{N+1}}{\partial \hat{\gamma}_N^a} & 1 \end{pmatrix}$$

B Matrix

Matrix $\mathbf{B}$ contains the derivatives of the foil residual terms with respect to the source strength unknowns as well as the Kutta condition. The size of this matrix is $(N+1) \times (L-M+1)$.

$$\mathbf{B} = \begin{pmatrix} \frac{\partial R_1^a}{\partial \hat{q}_{M+2}} & \frac{\partial R_1^a}{\partial \hat{q}_{M+3}} & \cdots & \frac{\partial R_1^a}{\partial \hat{q}_{L+2}} \\ \frac{\partial R_2^a}{\partial \hat{q}_{M+2}} & \frac{\partial R_2^a}{\partial \hat{q}_{M+3}} & \cdots & \frac{\partial R_2^a}{\partial \hat{q}_{L+2}} \\ \vdots & \vdots & \vdots & \vdots \\ \frac{\partial R_N^a}{\partial \hat{q}_{M+2}} & \cdots & \frac{\partial R_N^a}{\partial \hat{q}_{L+1}} & \frac{\partial R_N^a}{\partial \hat{q}_{L+2}} \\ \frac{\partial R_{N+1}^a}{\partial \hat{q}_{M+2}} & \cdots & \cdots & \frac{\partial R_{N+1}}{\partial \hat{q}_{L+2}} \end{pmatrix}$$

C Matrix

Matrix $\mathbf{C}$ contains the derivatives of the foil residual terms with respect to the foil motion. The size of this matrix is $(N+1) \times (2)$.

$$
\mathbf{C} = \begin{pmatrix}
\dfrac{\partial R_1^a}{\partial h_n} & \dfrac{\partial R_1^a}{\partial \theta_n} \\[2mm]
\dfrac{\partial R_2^a}{\partial h_n} & \dfrac{\partial R_2^a}{\partial \theta_n} \\[2mm]
\vdots & \vdots \\[2mm]
\dfrac{\partial R_N^a}{\partial h_n} & \dfrac{\partial R_N^a}{\partial \theta_n} \\[2mm]
0 & 0
\end{pmatrix}
$$

D Matrix

Matrix $\mathbf{D}$ contains the derivatives of the free surface residual terms with respect to the vortex strength unknowns. The first two lines of this matrix represent the free surface upstream end conditions. The size of this matrix is $(L - M + 1) \times (N + 1)$.

$$
\mathbf{D} = \begin{pmatrix}
\dfrac{\partial R_{N+1}^{end^1}}{\partial \hat{\gamma}_1^a} & \dfrac{\partial R_{N+1}^{end^1}}{\partial \hat{\gamma}_2^a} & \cdots & \dfrac{\partial R_{N+1}^{end^1}}{\partial \hat{\gamma}_{N+1}^a} \\[2mm]
\dfrac{\partial R_{N+1}^{end^2}}{\partial \hat{\gamma}_1^a} & \dfrac{\partial R_{N+1}^{end^2}}{\partial \hat{\gamma}_2^a} & \cdots & \dfrac{\partial R_{N+1}^{end^2}}{\partial \hat{\gamma}_{N+1}^a} \\[2mm]
\dfrac{\partial R_{N+2}^s}{\partial \hat{\gamma}_1} & \cdots & \dfrac{\partial R_{N+2}^s}{\partial \hat{\gamma}_N^a} & \dfrac{\partial R_{N+2}^s}{\partial \hat{\gamma}_{N+1}^a} \\[2mm]
\vdots & \vdots & \vdots & \vdots \\[2mm]
\dfrac{\partial R_Q^s}{\partial \hat{\gamma}_1} & \cdots & \vdots & \dfrac{\partial R_Q^s}{\partial \hat{\gamma}_{N+1}}
\end{pmatrix}
$$

E Matrix

Matrix $\mathbf{E}$ contains the derivatives of the free surface residual terms with respect to the source strength unknowns. Just like matrix $\mathbf{D}$, the first two lines of $\mathbf{E}$ account for the far upstream end conditions. The size of this matrix is $(L - M + 1) \times (L - M + 1)$.

$$
\mathbf{E} = \begin{pmatrix}
\dfrac{\partial R_{N+1}^{end^1}}{\partial \hat{q}_{M+2}} & \dfrac{\partial R_{N+1}^{end^1}}{\partial \hat{q}_{M+3}} & \cdots & \dfrac{\partial R_{N+1}^{end^1}}{\partial \hat{q}_{L+2}} \\[2mm]
\dfrac{\partial R_{N+1}^{end^2}}{\partial \hat{q}_{M+2}} & \dfrac{\partial R_{N+1}^{end^2}}{\partial \hat{q}_{M+3}} & \cdots & \dfrac{\partial R_{N+1}^{end^2}}{\partial \hat{q}_{L+2}} \\[2mm]
\dfrac{\partial R_{N+2}^s}{\partial \hat{q}_{M+2}} & \cdots & \dfrac{\partial R_{N+2}^s}{\partial \hat{q}_{L+1}} & \dfrac{\partial R_{N+2}^s}{\partial \hat{q}_{L+2}} \\[2mm]
\vdots & \vdots & \vdots & \vdots \\[2mm]
\dfrac{\partial R_Q^s}{\partial \hat{q}_{M+2}} & \cdots & \cdots & \dfrac{\partial R_Q^s}{\partial \hat{q}_{L+2}}
\end{pmatrix}
$$

F, G, H Matrices

Matrices $\mathbf{F}$, $\mathbf{G}$ and $\mathbf{H}$ contain zeros and are respectively of sizes $(L - M + 1) \times 2$, $2 \times (N + 1)$, and $2 \times (L - M + 1)$.

I Matrix

Matrix **I** is a (2 × 2) identity matrix containing the prescribed motion information.

$$\mathbf{I} = \begin{pmatrix} \dfrac{\partial R_n^h}{\partial h_{n_{spec}}} & \dfrac{\partial R_n^h}{\partial \theta_{n_{spec}}} \\[2mm] \dfrac{\partial R_n^h}{\partial \theta_{n_{spec}}} & \dfrac{\partial R_n^\theta}{\partial \theta_{n_{spec}}} \end{pmatrix} = \begin{pmatrix} 1 & 0 \\ 0 & 1 \end{pmatrix}$$

3.6 Post processing - Load Evaluation

Now that the flowfield unknowns $\mathcal{U}_n$ have been determined by solving the system of equations defined per (3.21), period averaged loads generated by the foil motion can be evaluated.

From $\mathcal{U}_n$, the pressure jump across the foil for every mode can be obtained by means of the linearized form of the unsteady Bernoulli equation introduced in Chapter 2 (c.f. equation 2.17). To determine the pressure jump, however, the potential jump across the sheet representing the foil must first be calculated.

By definition, the potential jump is the running sum of the vorticity distribution along the sheet representing the foil,

$$\gamma(x,t) = \frac{\partial \Delta\varphi}{\partial x} \rightarrow \Delta\varphi(x,t) = \int_0^x \gamma(\xi,t)d\xi \tag{3.23}$$

The potential jump evaluated at a panel node $j \in [1..N+1]$ on the foil is approximated by,

$$\Delta\hat{\varphi}_{n_j}^a \approx \sum_{k=1}^{j-1}\left(\frac{\hat{\gamma}_{n_{k+1}}^a + \hat{\gamma}_{n_k}^a}{2}\right)\Delta x_k = \sum_{k=1}^{j} c_k \hat{\gamma}_{n_k}^a \tag{3.24}$$

and the pressure jump evaluated at j is,

$$\Delta\hat{p}_{n_j}^a \approx \rho\left\{ in\omega\sum_{k=1}^{j} c_k\hat{\gamma}_{n_k}^a + U_\infty\hat{\gamma}_{n_j}^a \right\} \tag{3.25}$$

From 3.25, the time-dependent pressure jump is reconstructed. Recalling that γ is complex, only the real part of the function is kept,

$$\Delta p_j^a = \Re\left\{ \sum_{n=0}^{P} \Delta\hat{p}_{n_j}^a e^{in\omega t} \right\} \tag{3.26}$$

3.6.1 Vertical Force - Lift

The vertical force is simply calculated by integrating the pressure jump across the foil vortex sheet,

$$F_z(t) = \int_0^c \Delta p^a(x,t)dx \approx \sum_{i=1}^{N} \left(\frac{\Delta p_{i+1}^a + \Delta p_i^a}{2}\right)\Delta x_i = \sum_{j=1}^{N+1} c_j \Delta p_j^a \tag{3.27}$$

and the average vertical force over one period of the motion is found by calculating,

$$\overline{F}_z = \frac{\omega}{2\pi} \int_0^{2\pi/\omega} F_z(t)\ dt \tag{3.28}$$

3.6.2 Horizontal force - Thrust

To calculate the horizontal force, our approach follows the one taken by von Kármán and Burgers [35], where the period-averaged horizontal force is derived by means of the horizontal projection of the vertical force $F_z(t)$ and the leading edge suction force. Assuming small amplitudes, the time-dependent horizontal force[1] is given by Garrick [11] as:

$$F_x(t) = \pi\rho S(t)^2 - \theta(t)F_z(t) \tag{3.29}$$

where S, the *leading edge suction velocity*, is a function of the foil vorticity distribution γ^a and is found for a flat plate by using the relation:

$$S(t) = \lim_{x\to 0} \gamma^a(x,t)\sqrt{\frac{x}{4}} \quad \rightarrow \quad S(x,t) = \frac{1}{x}\int_0^x \gamma^a(\xi,t)\sqrt{\frac{\xi}{4}}\ d\xi \tag{3.30}$$

Note that the value of S is finite since γ^a is infinite in the order of $\frac{1}{\sqrt{x}}$ at the leading edge ($x = 0$). Getting rid of the time dependency and integrating by part yields for the leading edge suction velocity at some position x in the vicinity of the leading edge,

$$
\begin{aligned}
\hat{S}_n(x) &= \frac{1}{x}\int_0^x \hat{\gamma}_n^a(\xi)\sqrt{\frac{\xi}{4}}d\xi \\
&= \frac{1}{x}\left\{\left[\frac{2}{3}\hat{\gamma}_n^a(\xi)\sqrt{\frac{\xi^3}{4}}\right]_0^x - \frac{2}{3}\int_0^x \frac{\partial\hat{\gamma}_n^a(\xi)}{\partial\xi}\sqrt{\frac{\xi^3}{4}}d\xi\right\}
\end{aligned} \tag{3.31}
$$

---

[1]Note that although the x-axis is defined as being positive to the right, $F_x > 0$ corresponds to a thrust force.

Numerically, equation (3.31) evaluated at a node point $j > 1$ can be approximated by,

$$\hat{S}_n(x_j) = \hat{S}_{n_j} \approx \frac{2}{3x_j} \left\{ \hat{\gamma}_j^a \sqrt{\frac{x_j^3}{4}} - \sum_{i=1}^{j-1} \left(\hat{\gamma}_{n_{i+1}}^a - \hat{\gamma}_{n_i}^a \right) \sqrt{\frac{x_i^3}{4}} \right\} \tag{3.32}$$

but unlike the analytical expression, the numerical value of (3.32) is singular as x_j approaches 0. To remedy this situation, the value of the leading edge suction velocity is calculated at various panel nodes in the vicinity of the leading edge, and the value *at* the leading edge is obtained by interpolation. The value of the leading edge suction velocity is reconstructed in the time domain, and equation (3.29) is used to obtain the time-dependent horizontal force. The period averaged horizontal force is then calculated.

3.6.3 Pitching Moment

The pitching moment about the pitching axis location x_{rot} is simply evaluated by:

$$
\begin{aligned}
M_y(t)_{x_{rot}} &= -\int_0^c (x - x_{rot}) \Delta p(x,t) \, dx \\
&\approx -\sum_{i=1}^N \left(\frac{\Delta p_{i+1}^a + \Delta p_i^a}{2} \right)(x_i - x_{rot}) \Delta x_i
\end{aligned} \tag{3.33}
$$

and the period-averaged pitching moment is found by calculating:

$$\overline{M}_{y_{x_{rot}}} = \frac{\omega}{2\pi} \int_0^{2\pi/\omega} M_y(t)_{x_{rot}} \, dt$$

3.6.4 Motion Power

The power necessary in maintaining the motion of the foil is the contribution of the rate of work done by the pitching and heaving motions:

$$P(t) = -(F_z(t) \, \dot{h}(t) - M_{y_{x_{rot}}}(t) \, \dot{\theta}(t)) \tag{3.34}$$

and the averaged power over one cycle of the motion is:

$$\overline{P} = \frac{\omega}{2\pi} \int_0^{2\pi/\omega} P(t) \, dt \tag{3.35}$$

55

3.6.5 Coefficient Form

The hydrodynamic loads defined above are presented in non-dimensional form using standard co-efficient definitions with $\ell_{ref}{}^2$ as the reference length. For the horizontal and vertical forces the corresponding coefficients have the form:

$$C_x = \frac{\overline{F}_x}{1/2\rho U_\infty^2 \ell_{ref}} \ , \ C_z = \frac{\overline{F}_z}{1/2\rho U_\infty^2 \ell_{ref}}$$

(3.36)

and for the moment coefficient about a pitching location x_{rot},

$$C_{m_{x_{rot}}} = \frac{\overline{M}_{y_{x_{rot}}}}{1/2\rho U_\infty^2 \ell_{ref}^2}$$

(3.37)

Finally, the power coefficient is defined by,

$$C_p = \frac{\overline{P}}{1/2\rho U_\infty^3 \ell_{ref}}$$

(3.38)

3.6.6 Efficiency Calculation

From the calculated forces, and the rate at which work is done in maintaining the foil oscillation, propulsive and power extracting efficiencies can be calculated.

Propulsive Efficiency

A common measure of propulsive efficiency is the *Froude efficiency* and is defined as the ratio of the net thrust power to the net shaft power provided by an external source to move the foil:

$$\eta_P = \frac{\overline{F}_x U_\infty}{\overline{P}} = \frac{C_x}{C_p} \le 1$$

(3.39)

If no losses occur in the process of tranforming mechanical input to thrust, then the ideal thrust efficiency is 1. Note that for negative values of C_x and positive C_p, the efficiency can be negative. This coresponds to the case where work is needed to move the foil but only drag is generated.

Power Extraction Efficiency

In the case of a power extracting system such as a windmill for example, efficiency is typically defined as the inverse of the propulsive efficiency:

$$\eta_E = \frac{\overline{P}}{\overline{F}_x U_\infty} = \frac{C_p}{C_x} \le 1$$

(3.40)

$^2\ell_{ref}$ is implied by the input c, d and h_n

Chapter 4

Model Validation

Chapter 3 covered the numerical aspect of the VSH computational tool. A series of computer tool validations need to be performed in order to ensure that the results it predicts are correct. The code validation process is carried out in two steps:

The first step involves showing that the code gives valid results in the case of infinite depth flow where the ocean free surface effect is negligible. Calculations involving both stationary and unsteady foil motions are performed and compared to available analytical results.

The second step involves validating the code with the influence of the free surface effect. Although drag predictions are available for a stationary hydrofoil below the surface of water, the author was unable to find results in the literature on the loads imparted on a moving foil with the effect of a free surface. It is hoped at this stage that the former validations are sufficient to prove that the code will predict correct trends and values in the case of the foil undergoing unsteady motion with the free surface effect.

4.1 Infinite Depth Flows

4.1.1 Steady Flow Validation

The very first validation involves comparing the computed result for the lift per unit area of a flat plate at a given angle-of-attack to the analytical solution given by thin airfoil theory. From thin airfoil theory, the running circulation across a flat plate of chord c is found to be [23]:

$$\gamma^a(x) = 2\theta_0 U_\infty \sqrt{\frac{c-x}{x}} \tag{4.1}$$

From Figure 4-1, one sees that the computed vorticity distribution along the airfoil is in excellent
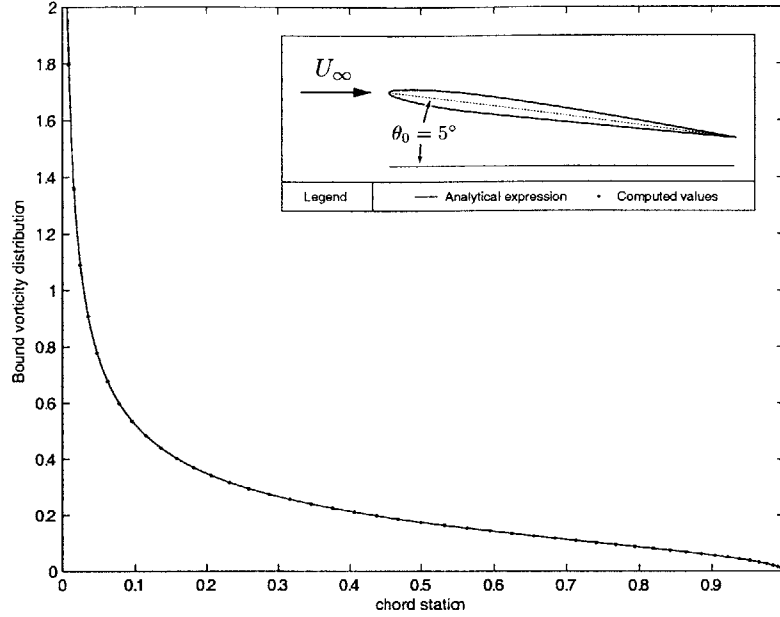
Figure 4-1: Comparison of computed and analytical results for the γ-distribution on a flat plate. ($N = 50$ panels on the airfoil).

agreement with the analytical result. This first validation ensures that the γ-distribution calculation is done properly.

4.1.2 Unsteady Flow Validation

Vertical Forces

Theodorsen [31] derived expressions for the unsteady lift and moment acting on a two-dimensional flat plate in a constant velocity flow. He showed that the unsteady lift of a flat plate undergoing small amplitude harmonic oscillations can be decomposed into two parts :

$$L = L_{NC} + L_C \tag{4.2}$$

Where L_{NC} is the *non-circulatory* or apparent mass effect of the lift and corresponds to the part of the lift resulting from flow acceleration effects. L_C is the *circulatory* part of the lift arising from the circulation Γ^a around the foil. Using the nomenclature introduced in this work, the circulatory and non-circulatory parts of the lift are respectively defined by Theodorsen as [31],[6]:

$$
\begin{aligned}
L_{NC} &= \pi\rho\frac{c^2}{4} \left[U_\infty\dot{\theta}_1 + \ddot{h}_1 + (\frac{c}{2} - x_{rot})\ddot{\theta}_1 \right] \\
L_C &= \pi\rho U_\infty c \left[U_\infty\theta_1 + \dot{h}_1 + (\frac{3c}{4} - x_{rot})\dot{\theta}_1 \right] C(k)
\end{aligned}
\tag{4.3}
$$

58
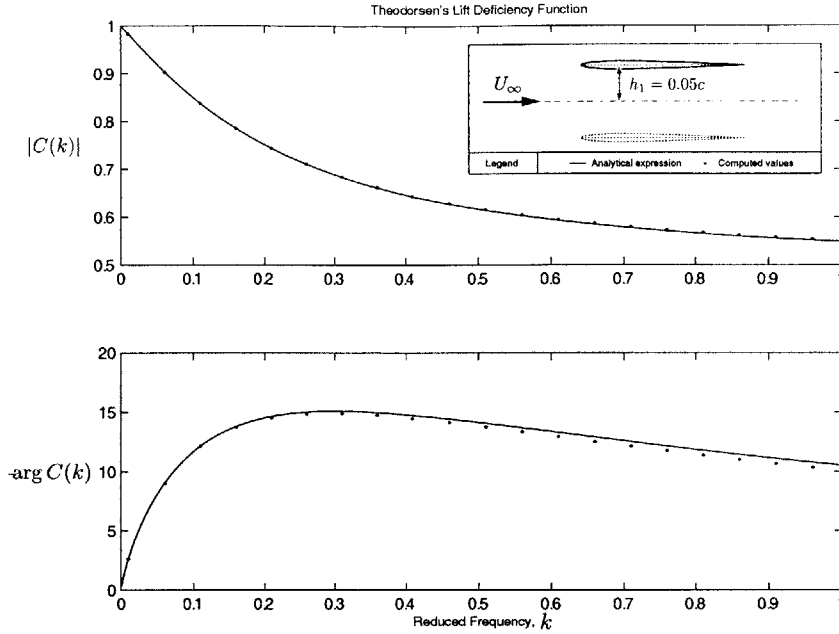
Figure 4-2: Comparision of computed and analytical results for the lift deficiency function $C(k)$.($N = 50, M = 200$ panels, $n_T = 30$)

In the circulatory lift, the complex function $C(k) = F + iG$ accounts for the effects of the shed wake on the unsteady foil and is known as Theodorsen's *lift deficiency function* or lift-reduction factor. This function is given in terms of Hankel functions H with the reduced frequency k as an argument by:

$$C(k) = F + iG = \frac{H_1^{(2)}(k)}{H_1^{(2)}(k) + iH_0^{(2)}(k)} \tag{4.4}$$

Comparison between the analytical expression of Theodorsen and the values computed by the panel method code for the absolute value ($|C(k)| = \sqrt{F^2 + G^2}$) and argument ($\tan^{-1}(G/F)$) of the lift deficiency function $C(k)$ is shown in Figure 4-2 and gives a good indication of the validity of the computed unsteady lift.

Horizontal Forces

Garrick extended Theodorsen's aeroelastic theory by including the horizontal aerodynamic loads on an airfoil undergoing harmonic plunging and pitching motions. Garrick [11], [12] has shown in his work that the period averaged horizontal force coefficient, or thrust coefficient[1] can be expressed as:

$$C_t = \pi k^2 (C_{t\alpha} + C_{th} + C_{tc}) \tag{4.5}$$

---

[1]As pointed out by Jones, Platzer, and Davids in [20], the thrust formulation given by Garrick in [11] for a pitching airfoil is incorrect. The correct formulation is found in reference [12]

59
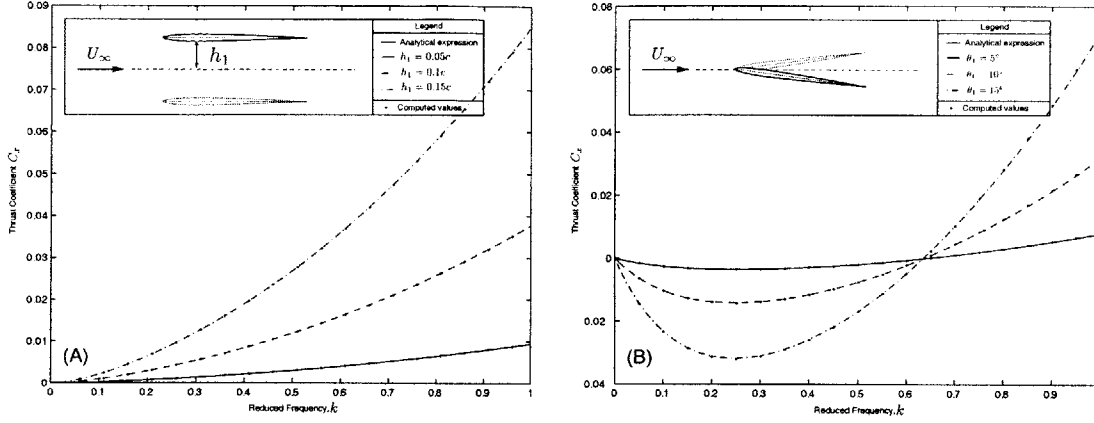
Figure 4-3: Comparison of computed and analytical results for the thrust coefficient in the case of: (A) a pure heaving motion (B) a pure pitching motion around the foil's leading edge. ($N = 50, M = 200$ panels, $n_T = 30$).

Where:

- $C_{t\alpha}$ is the pitch contribution to the total thrust

- C_{th} is the plunge contribution to the total thrust

- C_{tc} is the cross-contribution to the total thrust

These coefficients are respectively defined by Garrick as:

$$
\begin{aligned}
C_{t\alpha} &= \alpha^2 \left\{ (F^2 + G^2)\left[\frac{1}{k^2} + (\frac{1}{2} - a)^2\right] + (\frac{1}{2} - F)(\frac{1}{2} - a) - \frac{F}{k^2} - (\frac{1}{2} + a)\frac{G}{k} \right\} \\
C_{th} &= 4h^2(F^2 + G^2) \\
C_{tc} &= 4\alpha h \left\{ (\frac{F}{2k} + \frac{G}{2} - \frac{F^2 + G^2}{k}) \sin\phi + \left[(F^2 + G^2)(\frac{1}{2} - a) + \frac{1}{4} + \frac{G}{2k} - \frac{F}{2} \right] \cos\phi \right\} \quad (4.6)
\end{aligned}
$$

Note that Garrick uses a foil of chord $2b$ with b being the reference unit length. The leading edge coordinate is $x = -1$ and the trailing edge coordinate is $x = 1$. The coordinate $x = a$ corresponds to the location of the pivot point. With the nomenclature used in this work, $a = 2x_{rot}/c - 1$, $\alpha = \theta_1$, $h = h_1$ and $\phi = \phi_1$. Figure 4-3 shows that the computed results agree very well with the analytical theory of Garrick.

60
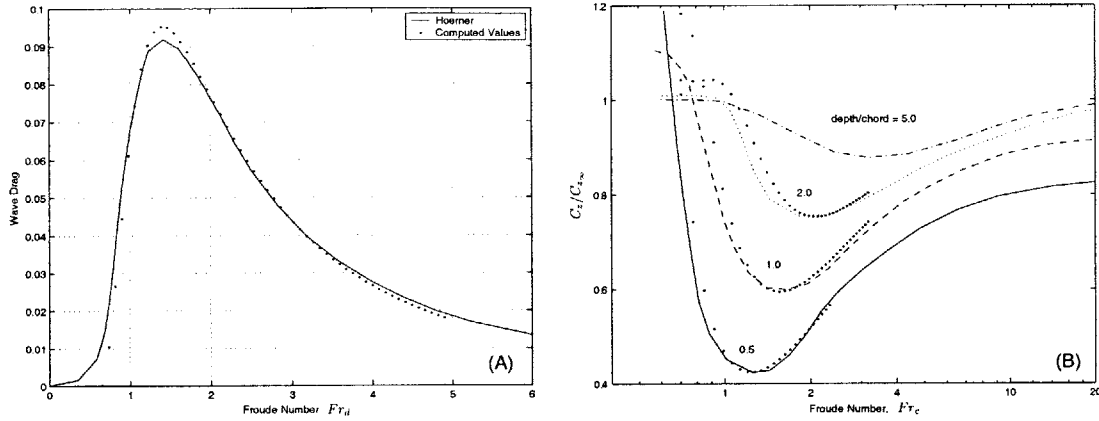
Figure 4-4: (A) Comparison of computed and theoretical results for the wave drag. (B) Comparison of computed and analytical results for the normalized lift with free surface effect as a function of the Froude number Fr_c and various airfoil depths. ($N = 40, M = 40, L = 300$ panels).

4.2 Flows with Free Surface Effects

4.2.1 Steady Flow Validation

Wave Drag

For a foil moving below the surface of the water, a wave train originates from the pressure field around it. The motion associated with this wave train represents a transfer of momentum from the foil to the water and results in a lift-induced drag force known as *wave drag*. Although induced drag usually stems from tip vortices on finite wings, lift-induced drag is present in two-dimensional flow in proximity of the water surface because of this transfer of momentum. Results pertaining to the lift/drag characteristics of a hydrofoil below the surface of the water at a depth d are available in Hoërner [14]. Predictions for the wave drag as a function of the Froude number based on the depth of submergence d are given in Figure 4-4 where the wave drag D_{wave} is defined as the ratio of the foil drag and the square of the lift. Normalized with respect to the depth of submergence and the foil chord,

$$D_{wave} \equiv -\left(\frac{d}{c}\right)\frac{C_x}{C_z^2} \tag{4.7}$$

Note that since C_x corresponds to the thrust, a minus sign is necessary in front of equation (4.7). From Figure 4-4, one sees that the results predicted by the panel method code are in good agreement with the theoretical model given by Hoërner.
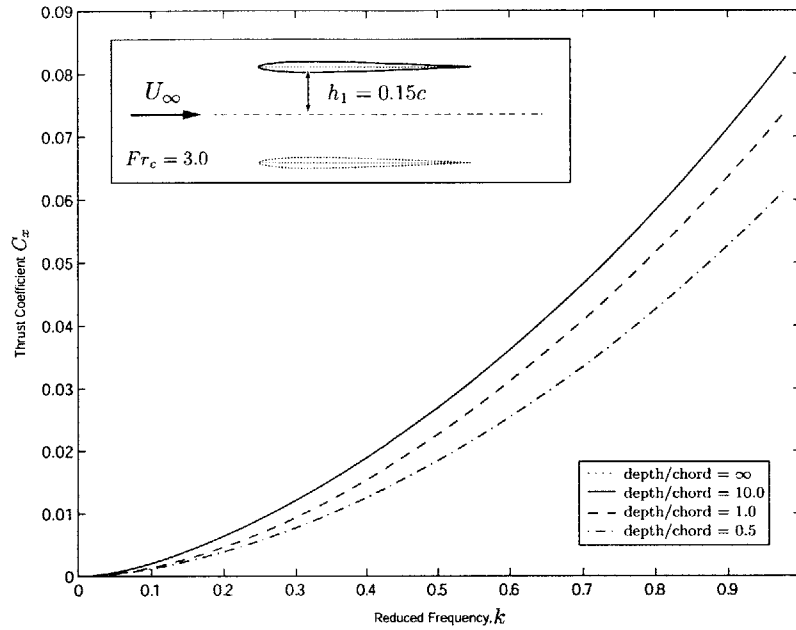
Figure 4-5: Influence of the depth-to-chord ratio on the thrust coefficient. ($h_1 = 0.15c$, $Fr_c = 3.0$, $n_T = 30$, $N = 40$, $M = 200$, $L = 800$ panels).

Lift

When a foil is deeply submerged it produces downwash in the same manner as the wing of an airplane. However, as the foil approaches the free water surface the total circulation decreases resulting in a loss of lift.

Results from Hoërner [15] pertaining to the lift coefficient of a hydrofoil in the proximity of the water surface as a function of Froude number F_{r_c} for various depth of submergence ratios are presented in Figure 4-4-(B). Comparison to computed results is also shown.

4.2.2 Unsteady Flow Validation

Figure 4-5 shows the influence of the depth-to-chord ratio of the foil on the thrust coefficient as a function of the reduced frequency. The results are given for a fixed Froude number based on the chord equal to 3. As expected from looking at Figure 4-4, the thrust coefficient decreases as the free surface induced drag become more significant (for decreasing values of d/c). The unsteady results in the presence of the free surface thus look reasonable.

Chapter 5

Computed Results and Design Implications

Having validated the computational tool, we now turn to the problem of finding the optimal foil motions for efficient propulsion and power extraction. However, before proceeding with the optimization problem per se, we first look at some interesting computed results in an attempt to gain some insight on the behavior of the VSH system. Similarly to the work of Jones and Platzer [19] [18], the influence of the multiple design parameters are reviewed and conclusions pertaining to the efficiency are drawn. Secondly, the optimization problem is described and results for the optimal foil motions are presented and discussed. Finally, design recommendations for a generic VSH system are made based on the optimization results.

5.1   Computed VSH Results

We first take a few 'slices' in the large parameter space to shed some light on how the various design parameters influence the unsteady loads and the efficiency of the VSH system. In this initial trade space exploration, only pure harmonic oscillations are considered for the foil motion. The effects of more complex motions on the performance of the system will be investigated in the optimization problem in section 5.2.

5.1.1   Influence of Design Parameters on Loads and Efficiency

Influence of Reduced Frequency

Figure 5-1-(A) shows that for a heaving foil, C_x increases monotonically with increasing reduced frequency. Also, we remark that the efficiency increases monotonically with decreasing reduced
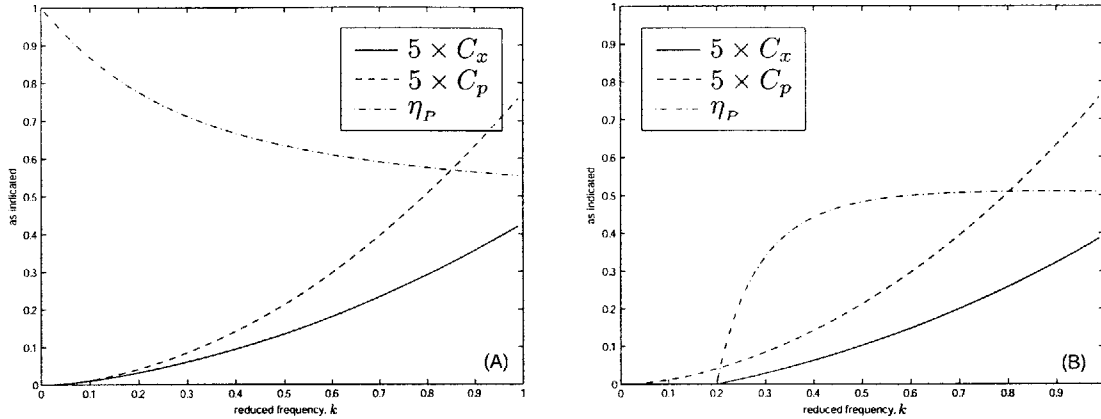
Figure 5-1: Efficiency, thrust and power coefficients as a function of the reduced frequency for a purely heaving foil. (A) Inviscid results, (B) Viscous correction. ($h_1 = 0.15c$)

frequency, suggesting that maximum efficiencies can only be attained for small values of the thrust coefficient. If small thrust coefficients are sufficient for practical applications, the model predicts that very high propulsive efficiencies are possible. In practice, such high efficiencies are unattainable once viscous forces on the foil are taken into account.

Recall that in the VSH model, the flow around the foil is assumed to be inviscid. Although this assumption is valid *around* the foil, in its vicinity, however, there exists a thin boundary layer that imparts viscous shear forces on the foil. Hall&Hall pointed out in [13] that for small reduced frequencies, the effects of this viscous force can be added to the inviscid model by means of a *quasi-steady lift-drag correlation*. For angles-of-attack away from stall and for moderate to large Reynolds numbers, the drag coefficient of a two-dimensional foil is primarily a function of the lift coefficient, and can be approximated by a quadratic function of the lift, such that:

$$C_d \approx C_{d0} + C_{d2}(C_l - C_{l_0})^2 \qquad (5.1)$$

Where the constants C_{d0}, C_{d2} and C_{l_0} are found by interpolation (curve fit) of a foil drag polar.

To account for profile drag in what follows, the author has chosen to use a NACA 0012 foil section. This section was chosen in particular because of its blunt leading edge, which is prone to generating a large suction force and hence a large thrust coefficient. Using the computer code XFOIL [8], a drag polar (see Appendix B) was generated for a Reynolds number of 0.5×10^6, which is in the realm of Reynolds numbers typical of the *Trampofoil®*. For a NACA 0012 the following values where found for the interpolation constants: $C_{d0} = 0.0063$, $C_{d2} = 0.0112$ and $C_{l_0} = 0$.

Figure 5-1-(B) clearly shows that inclusion of the viscous profile drag has a detrimental effect on the propulsive efficiency. In fact, when viscous effects are introduced in the model, the foil must flap at higher frequencies to overcome the added drag to generate thrust, resulting in dramatically
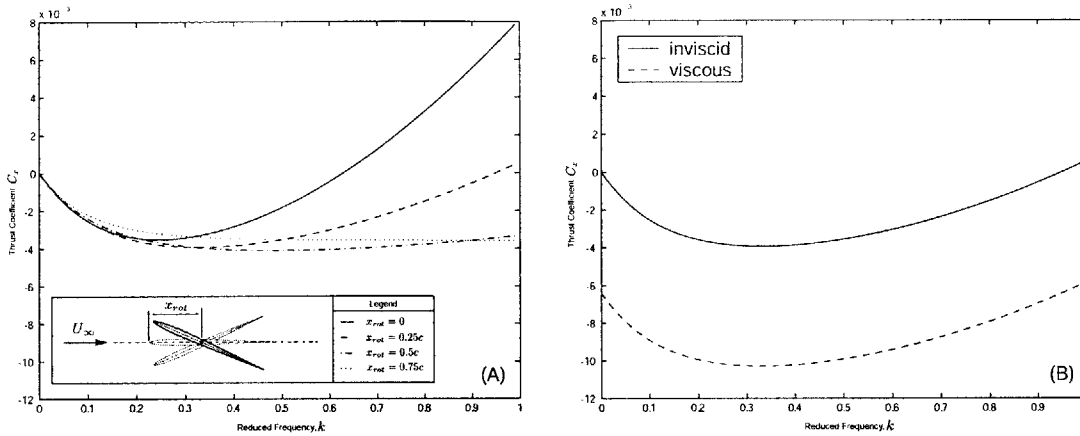
Figure 5-2: (A) Thrust coefficient as a function of the reduced frequency and the pitching axis location for a purely pitching foil ($\theta = 5°$), (B) Comparison between inviscid and viscous results for the thrust coefficient. ($x_{rot} = 0.25c$, $\theta_1 = 5°$)

reduced efficiency.

Influence of Pitching DOF

In the case of a foil pitching about a fixed axis, the model predicts that thrust is produced only at high frequencies ($k > 1$), for both the viscous and the inviscid case (Figure 5-2-(A) and (B)). From these considerations, one may believe that the pitching degree of freedom does not bring any benefit to the thrust producing mechanism at low-to-medium frequencies, and that it should be left out altogether. However, when the pitching degree of freedom is added to the heaving motion, thrust can actually be increased considerably for a given combination of parameters as inviscid losses are alleviated through a better scheduling of the shed vortices. Also, the pitching degree of freedom reduces profile drag stemming from excessive leading edge suction.

Influence of Pitching Axis Location

The pitching axis location of the foil can be set by the designer without impacting the efficiency of the system. Although one may believe otherwise by looking at Figure 5-2(A), similar flowfields can be obtained around the foil with different Fourier coefficients and pitching axis locations resulting in identical efficiencies. For thin uncambered foils, the pitching axis location is chosen to be at the quarter chord point (center of pressure) which is the point on the foil about which the aerodynamic moment is zero.

Influence of Motion Phase

Once a pitching-axis location is set, the phase lead between the heaving and pitching motions plays an important role on the efficiency of the VSH system. In Figure 5-3, C_x, C_p and the propulsive

65
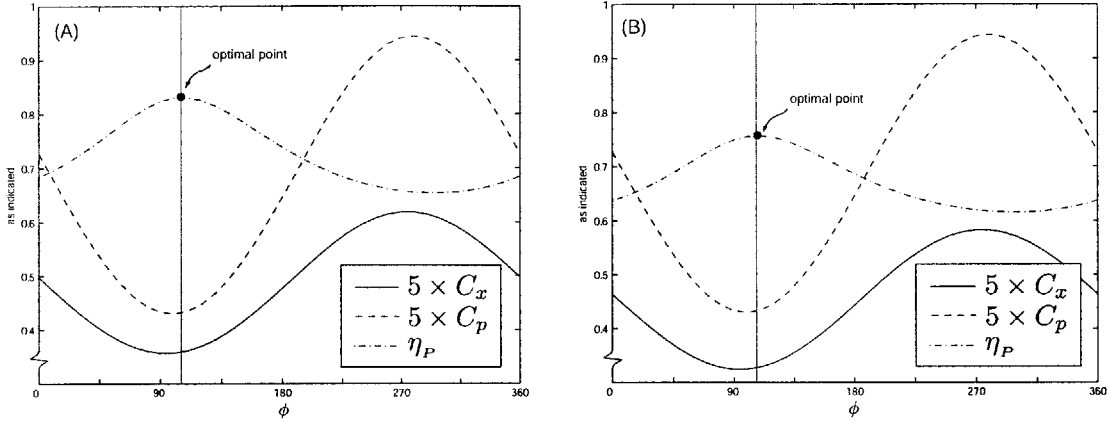
Figure 5-3: Efficiency, thrust and power coefficients as a function of the phase angle ϕ for a propulsive foil. (A) Inviscid results, (B) Viscous results. ($x_{rot} = 0.25c$, $h_1 = 0.5c$, $\theta_1 = 5°$, $k = 0.25$)
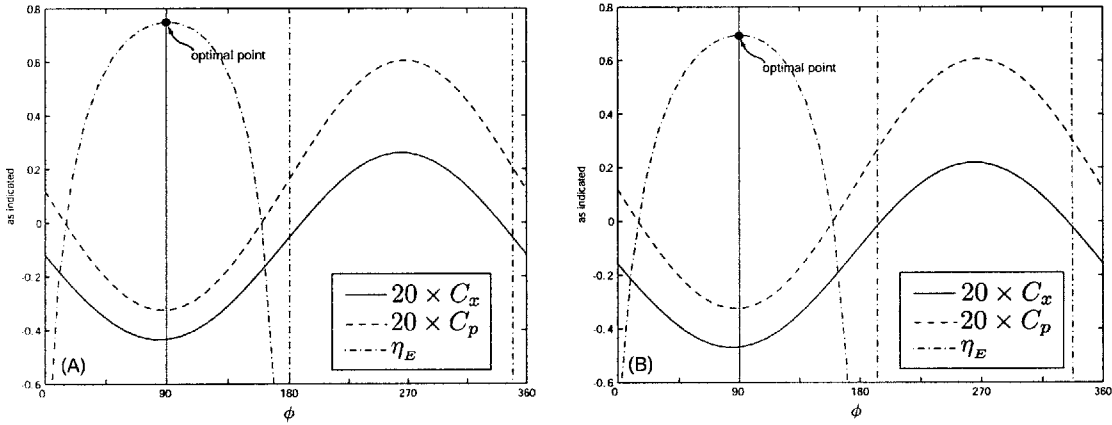
Figure 5-4: Efficiency, C_x and power coefficient as a function of the phase angle ϕ in the case of power extraction. (A) Inviscid results, (B) Viscous results ($x_{rot} = 0.25c$, $h_1 = 0.5c$, $\theta_1 = 20°$, $k = 0.1$)

efficiency η_P are plotted as a function of the heaving phase lead ϕ. The reduced frequency is held constant at $k = 0.25$, with $h_1 = 0.5c$ and $\theta_1 = 5°$. The pitching axis location is placed at the 1/4-chord point.

Figure 5-3 shows that maximum propulsive efficiency is attained for nearly minimum values of C_x and C_p, which means that high efficiencies are only achievable with low thrust coefficients. From a propulsion standpoint this is an unfortunate outcome if practical applications are to be considered. Also, once the effects of viscosity are included (see Figure 5-3-(B)) the values of C_x are reduced even more. It should be noted from Figure 5-3 that maximum propulsive efficiency corresponds to a phase lead of $90 - 130°$.

In Figure 5-4, C_x, C_p and the power-extraction efficiency η_E are plotted as a function of the phase with $k = 0.1$, $h_1 = 0.5c$ and $\theta_1 = 20°$. Once again, the foil is set to pitch around the 1/4-chord axis. The plot of Figure 5-4 suggests that a phase angle in the range of $80° - 120°$ is optimal for

66
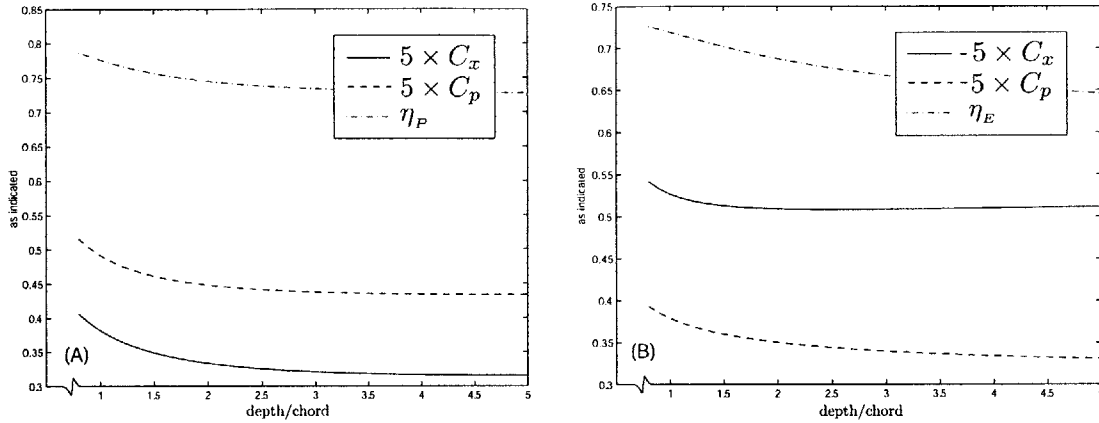
Figure 5-5: (A) Influence of ground effect on propulsion (x_{rot} = 0.25c, h_1 = 0.5c, θ_1 = 5°, ϕ_1 = 110°, k = 0.25) (B) Influence of ground effect on power-extraction (x_{rot} = 0.25c, h_1 = 0.5c, θ_1 = 20°, ϕ_1 = 90°, k = 0.1)

maximum power-extraction efficiency.

Influence of Ground Effect

By setting the Froude parameter to zero, the influence of a ground plane on the loads can be introduced in the model. Since d is defined as the depth of submergence, a positive value of d actually corresponds to an anti-ground effect, and a negative value of d to a ground effect. The efficiency along with the C_x and C_p of the system are plotted in Figure 5-5 as a function of the depth-to-chord ratio for the propulsion (A) and power-extraction (B) configurations. Both η_P and η_E increase with diminishing d/c.

Influence of Free Surface Effect

The depth of submergence of the foil d relative to the water free surface greatly impacts the performance of the VSH system. In Figure 5-6, the efficiency of the system is plotted as a function of the depth of submergence ratio for various Froude numbers Fr_c. Interestingly, for Froude numbers Fr_c between 1 and 2, the efficiencies for both the propulsion (A) and power-extraction (B) cases increase significantly for corresponding depth-to-chord ratios of about 1.5 and 2.5. A closer look at the flowfield for this specific case suggests that a constructive mechanism takes place between the kinetic energy shed in the wake and the momentum transferred to the free surface.

In practice, it is unlikely that the VSH system would work at such low Froude numbers, as it would require the hydrofoil to either advance very slowly[1] or to have a very large chord [2]. In the

---

[1] For Fr_c to be equal to unity in the case of a hydrofoil with a mean chord of 0.15m, the hydrofoil would need to advance at approximately 1.2m/s. Such a low speed would, in turn, limit the lift provided by the wing.

[2] With an advance speed of 4m/s, the chord of the hydrofoil would need to be a staggering $c \approx 1.6$m for the Froude number based on the chord to be equal to one.
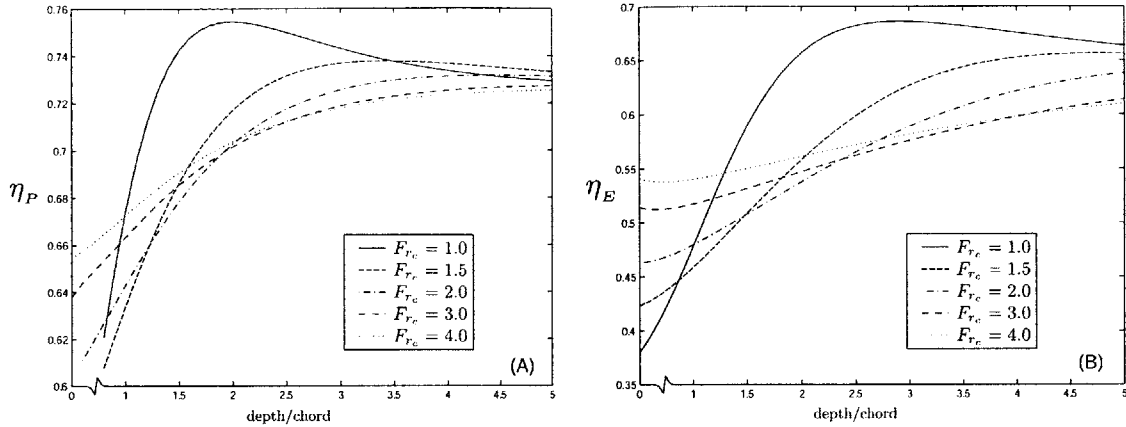
Figure 5-6: (A) Influence of free surface on propulsion efficiency for various Froude numbers ($x_{rot} = 0.25c$, $h_1 = 0.5c$, $\theta_1 = 5°$, $\phi_1 = 110°$, $k = 0.25$) (B) Influence of free surface on power-extraction efficiency for various Froude numbers. ($x_{rot} = 0.25c$, $h_1 = 0.5c$, $\theta_1 = 20°$, $\phi_1 = 90°$, $k = 0.1$)

latter case, the resulting increase in the wetted area of the foil would translate in increased viscous and form drag which in turn would nullify the efficiency gain of working at lower Froude numbers.

5.2 Foil Motion Optimization for Efficiency

The results presented in section 5.1 have helped identify the influence of the design parameters on the unsteady loads generated by the foil. For the computed results to be of practical interest for design, a quasi-steady lift-drag correlation was introduced in the model to account for viscous effects. We now turn to the problem of determining a preferred foil motion in an attempt to achieve optimal efficiency for propulsion and power extraction.

5.2.1 Optimization Problem Description

The optimization problem consists in finding a set of design parameters $\mathcal{X}$ that minimize an *objective function* $\mathcal{F}$ subject to the *constraints* $\mathcal{G}(\mathcal{X})$. For the VSH problem, the parameters correspond to the Fourier coefficients as well as the reduced frequency and phase shift necessary to describe the motion. These design parameters are summarized in Table 5.1.

Objective Function

In the case of the propulsion problem, the power coefficient C_p is chosen as the objective function $\mathcal{F}$ to be minimized. Note that the efficiency is not chosen as the objective function for the simple reason that maximum propulsive efficiency corresponds to a minimum value of the thrust coefficient, which is of little practical value from an engineering standpoint. In selecting a propulsor for a marine vehicle, the engineer generally has an idea of the necessary thrust coefficient and proceeds to achieve

68

Design Parameter, $\mathcal{X}$	LB	UB
Heaving amplitude, h_n	$0c$	$0.5c$
Pitching amplitude, θ_n	$0°$	$20°$
Heaving phase lead, ϕ_n	$0°$	$360°$
Motion reduced frequency, k	0	1

Table 5.1: Summary of the design parameters with upper (UB) and lower bounds (LB) for the foil motion optimization problem.

maximum efficiency subject to the constant thrust constraint. By enforcing an *equality constraint* $\mathcal{G}(\mathcal{X})$ that a prescribed thrust must be provided, the optimization problem translates into maximizing the efficiency for a given thrust.

The power coefficient is also chosen as the objective function to be minimized in the case of the power-extraction problem. This time, a negative thrust coefficient is prescribed as an equality constraint to the optimization problem. Minimizing C_p with a negative prescribed C_x will results in a negative value of C_p, which in turn results in maximizing η_E.

Parameter Bounds

From a design standpoint, the actuators used to drive the foil have limited travel amplitudes, and *bounds* representing the maximum heaving and pitching amplitudes of travel must be set on the design parameters describing the foil motion. Likewise, the frequency of motion might be limited by the actuator dynamics and must thus be bounded. Table 5.1 summarizes the lower (LB) and upper bounds (UB) on the design parameters used in this optimization problem. Note that these values have been chosen arbitrarily and are purely for illustration purposes.

Constraints

As seen previously, an equality constraint specifying the thrust must be set for the results to be of practical use. Since the foil motion is defined as a sum of Fourier coefficients, *inequality constraints* must also be set on the total travel amplitudes $h(t)$ and $\theta(t)$ to ensure that they do not violate the maximum actuator displacement. The following inequality constraints were thus defined and added to the optimization problem:

$$\begin{cases} z(t) \leq h_{max} = 0.5c \\ \theta(t) \leq \theta_{max} = 20° \end{cases} \tag{5.2}$$

Optimization Implementation

A Sequential Quadratic Programming (SQP) method was used to perform the optimizations. Implementation was carried out in MATLAB® using the *Optimization Toolbox* application.
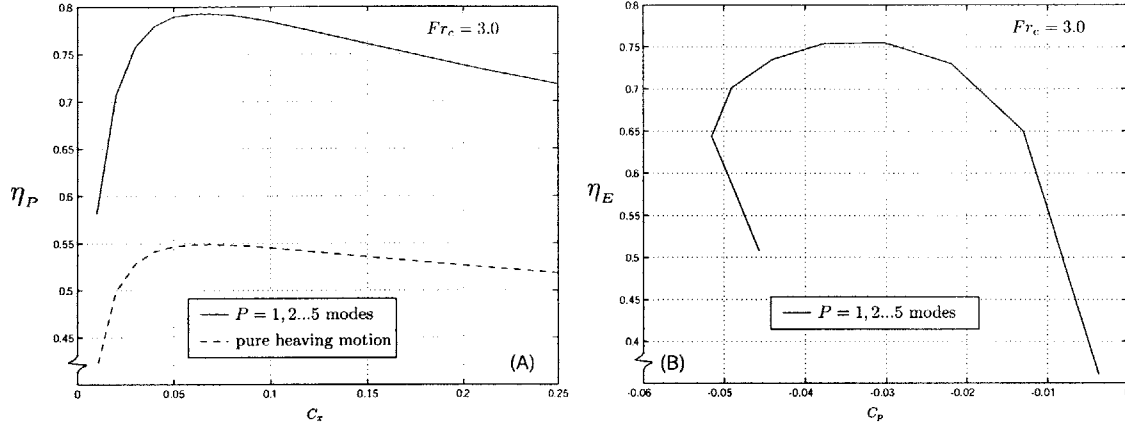
Figure 5-7: (A) Optimal propulsive efficiency found for a foil motion described using $P = 5$ modes. Comparison with the efficiency obtained for a purely heaving foil. (B) Optimal power extraction efficiency found for a foil motion described using $P = 5$ modes. Comparison with the efficiency obtained for a purely pitching foil.

The bounds set on the total amplitudes of travel of the foil, h_{max} and θ_{max}, define a limit in terms of the maximum thrust and power that can be produced by the system. With the bounds specified in this problem, propulsive efficiencies beyond 75% cannot be achieved for thrust coefficients greater than 0.25. Likewise, power coefficients greater than -0.07 are achieveable but with a significant efficiency loss. Throughout the optimization process, the thrust coefficient was thus varied between $0.01 - 0.25$ for the propulsive case, and between $0.01 - 0.09$ for the power-extraction problem. In all cases, the following number of panels were used to discretize the foil, wake and free surface regions: $N = 30$ on the foil, $M = 250$ and $L = 650$.

5.2.2 Optimization Results

Optimal Foil Motion

What motion should the foil be undergoing in order to maximize propulsive and power-extraction efficiency ? To answer this question, an increasing number of Fourier coefficients were progressively introduced in the model to give the optimizer more degrees of freedom to describe the foil motion. The initial optimization was carried out with just *one* Fourier coefficient and a reduced frequency as the design parameters for the propulsive case. Since at least two degrees of freedom are necessary to extract power, initial power-extraction optimizations were done with two Fourier coefficients and a reduced frequency (h_1, θ_1, k). As many as $P = 5$ modes were used in the optimization process, resulting in a design vector of 26 parameters (25 Fourier amplitudes and 1 reduced frequency). Also, to account for the free surface effect, a Froude number of $Fr_c = 3$ and a depth-to-submergence ratio of $0.6c$ were selected.

Figure 5-7 shows the efficiency of the system for the optimal foil motion in the case of propulsion

(A) and power-extraction (B). The plots of Figure 5-7 (A) show that, as expected, the pitching degree of freedom greatly enhances the efficiency of the system for the propulsive case. In fact, people who have ridden the *Trampofoil®* all concur to saying that introduction of a pitching motion noticeably augments its propelling characteristics. Interestingly enough, the results indicate that a *sinusoidal motion* corresponds to the optimal solution for both power extraction (A) and propulsion (B), and this, even though the optimizer could operate on 26 design parameters. In Figure 5-7 the optimal efficiencies found for $P = 1, 2, 3, 4$ and 5 modes all yielded the same sinusoidal motion solution.

As a "reality check", the bounds on the design parameters were lifted. The idea behind performing a set of unbounded optimizations was to give the SQP method more freedom to find solutions that might have been in otherwise unreachable areas of the design space because of the bounds. The unbounded optimization results showed that for a prescribed thrust coefficient, optimal efficiency is achieved through a very slow motion with large heaving amplitudes. The high efficiency resulting from this *quasi-steady motion* can be explained by the fact that little kinetic energy is deposited in the wake with a slowly moving foil. As the frequency of motion increases, so does the kinetic energy lost in the flow, which in turn hinders the efficiency.

Despite the fact that the optimizer could operate on 26 design parameters, the optimal motion was once again found to be sinusoidal. It can be concluded that harmonics of the motion higher than $n = 1$ blow off energy into the flow and are not useful in increasing the propulsive nor the power-extracting efficiency of the VSH system.

Free Surface Interference Effects

Having identified an optimal foil motion, propulsive and power-extraction efficiencies were calculated for various combinations of Froude numbers, Fr_c and depth of submergence ratios d/c to examine the influence of the ocean free surface. To inspect a wide region of the design space, optimizations were carried out with Fr_c ranging from 1 to 6 and depth of submergence ratios of $1c$, $0.8c$ and $0.6c$. Also, since the optimal motion was found to be sinusoidal, all optimizations were conducted with $P = 1$ mode. From the optimization results, a set of efficiency plots were generated that are useful for design. The plots pertaining to the propulsion problem are shown in Figure 5-8. Figure 5-9 shows the results obtained for the power extraction problem. All optimization results are summarized in Tables C.1 to D.18 in Appendices C and D.

For the range of computed Froude numbers, the effect of the free surface is seen to have a notable influence on the propulsive efficiency of the system. For the case considered here, the computations show that as much as 7% efficiency can be lost because of the free surface induced drag, at low depths and Froude numbers.
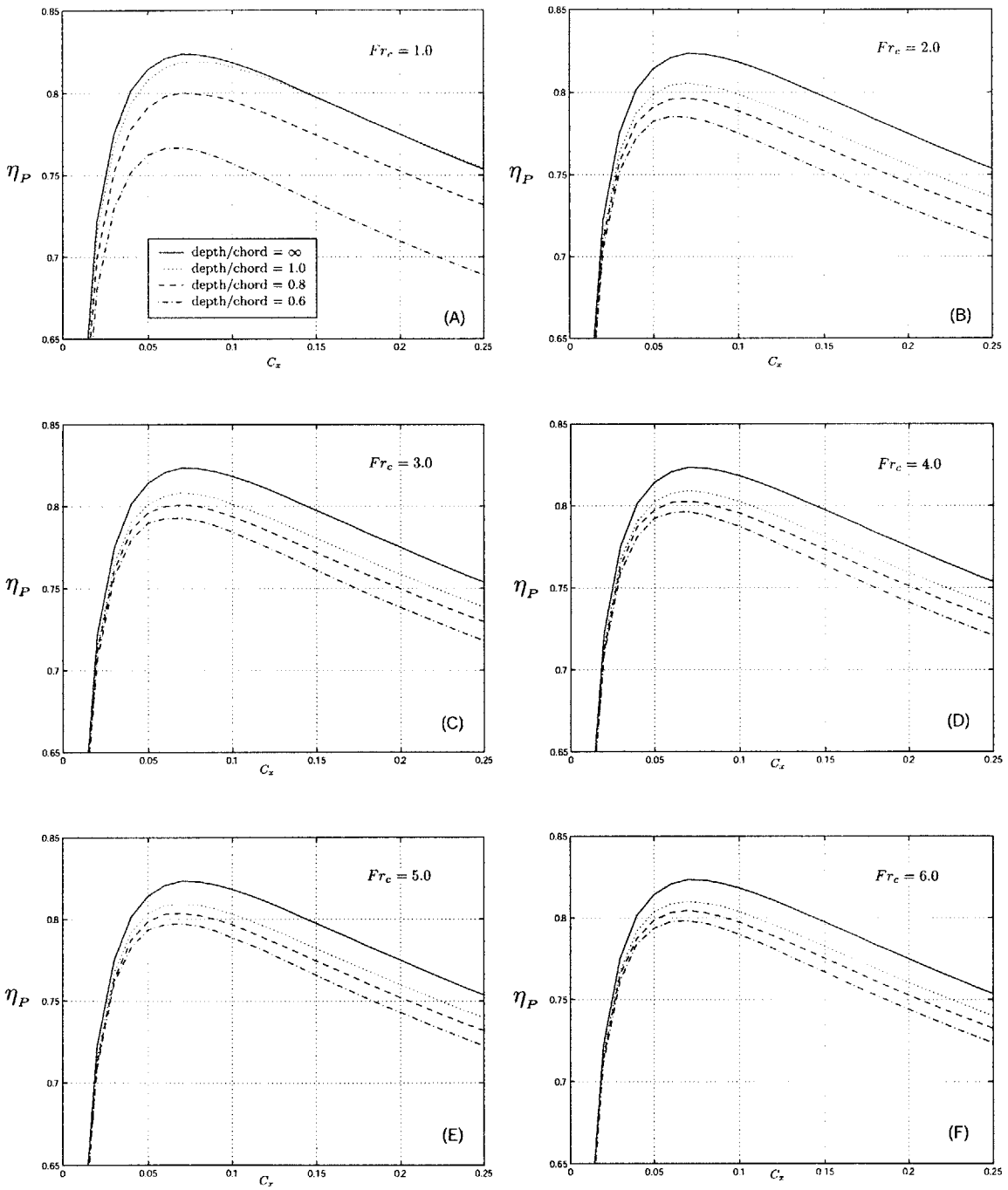
Figure 5-8: VSH design optimization results for the propulsive problem for Froude numbers based on the chord varying between 1 and 6 and various depths of submergence ratios.
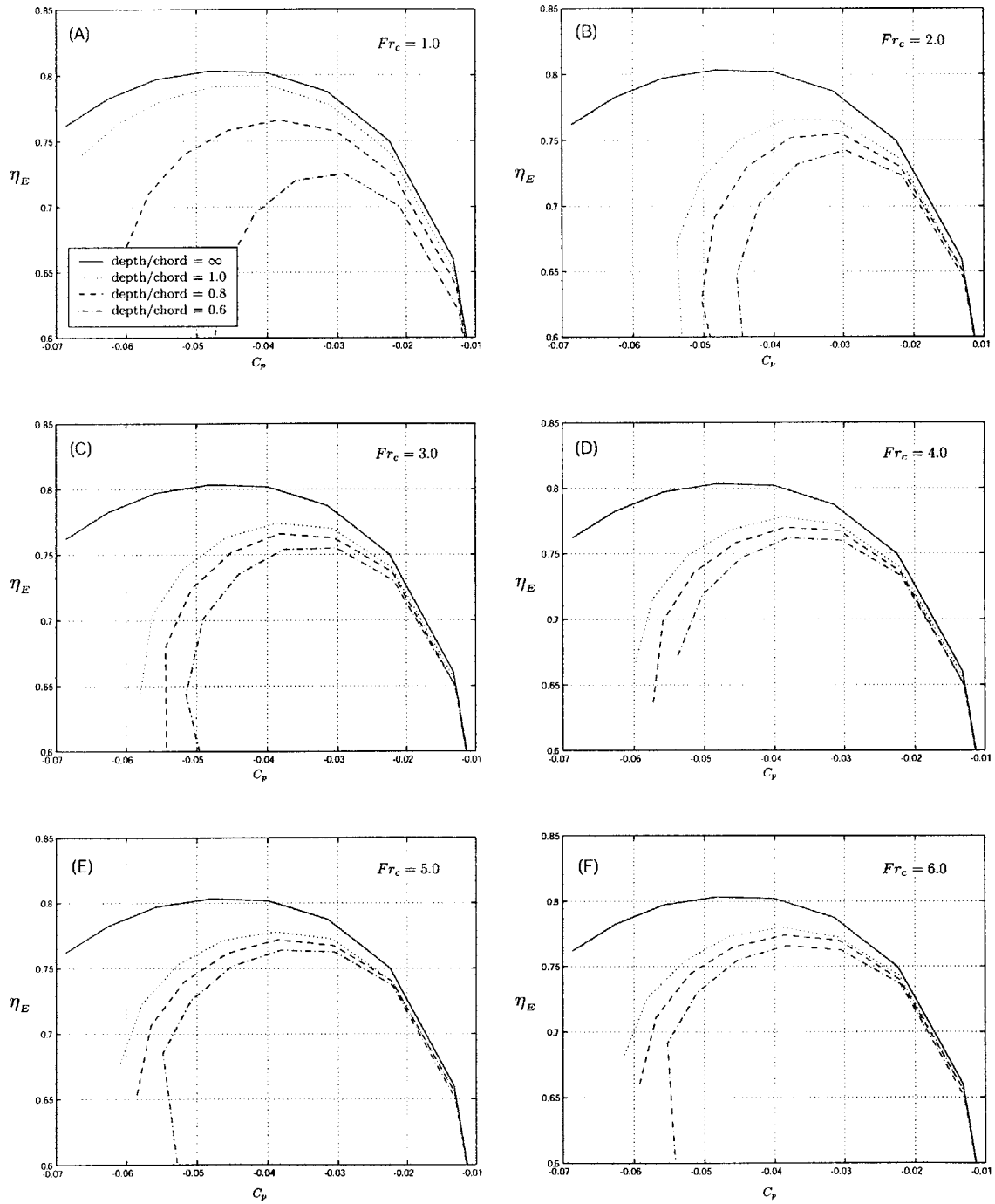
Figure 5-9: VSH design optimization results for the power extraction problem for Froude numbers based on the chord varying between 1 and 6 and various depths of submergence ratios.

Likewise, the optimization results obtained for the case of power-extraction show that the power coefficient is greatly hindered by the free surface. Intriguingly, for certain configurations of Froude numbers and depths of submergence, the VSH system is unable to deliver power extraction performances otherwise achievable at increased depths. Figure 5-9 (B) illustrates the case where a power coefficient of −0.06 is accomplished at an infinite depth, but unrealizable for depths less or equal to one chord length.

Difficulties Encountered

It must be noted that multiple difficulties were encountered while performing these optimizations.

The first difficulty arose from the design space becoming excessively large as more modes were used to describe the foil motion. Finding the globally optimal solution thus became very challenging, especially for the gradient-based optimization method used in this work. To prevent the method from getting trapped into local minimums, the author had to use *many* randomly-chosen initial vectors of design parameters $\mathcal{X}$. Yet, even with this time-consuming approach, global optimality of the solution is not guaranteed. One way to ensure that the solution is globally optimal might be to use heuristic-based optimization techniques such as Simulated Annealing or Genetic Algorithms. Implementation of the equality and inequality constraints with such techniques; however, is usually difficult.

Also, the number of optimizations that could be carried out was contingent on the available time and computing power. Although the panel method code only requires a couple of seconds[3] at most to evaluate the unsteady loads on the foil, the optimization algorithm makes multiple calls to the panel method code and computational times can rapidly become very large.

5.3 VSH Design Implications

The optimization results provide useful indications for the design of a VSH system. Let us review the influence of the elements influencing the performance of the VSH system and look at ways of improving its efficiency.

5.3.1 Interference Effects

Free Surface Effect

The free surface is seen to influence the efficiency of the system for depths less than or equal to approximately $5c$ for the propulsive case (cf Figure 5-6). In the energy-extracting case, the foil

---

[3]Calculations were performed on a Pentium III-750MHz workstation.

needs to operate at a depth greater than $5c$ not to be affected by the free surface induced drag. This suggests that the loss of efficiency (η_P or η_E) due to the free surface effect can be regained or improved in two ways:

- By increasing the depth of the foil so as to limit the influence of the free surface induced drag.

- By increasing the Froude number based on the chord.

Increasing the depth of submergence of the foil is easily done, but care must be taken not to introduce too much friction drag with excessively long struts connecting the body of the vehicle to the foil. Even if the struts are well designed so as to minimize drag, their lengths will also be limited by weight and structural issues.

Increasing the Froude number based on the chord is done by either advancing at higher velocity U_∞, or by reducing the foil's chord length. In the latter case, design considerations, such as the minimum lift that must be provided to support the vehicle weight, or the minimum power that must be extracted from the flow, will affect the size of the foil's chord and a trade off must be sought.

Ground Effect/Multiple Foil Configurations

The investigations of section 5.1.1 clearly indicate that substantial increases in efficiency can be attained by operating in ground effect. In fact, birds are known to take advantage of ground plane effect by flying low over water. For the VSH system, ground effect can be reproduced by introducing a second foil to create an mirror image of the first foil. A configuration similar to the one investigated by Jones and Platzer [19] where two wings work in an opposed-plunge configuration (biplane arrangement) might be a solution to regaining the lost efficiency of working in the free surface effect. It remains to be seen if the addition of a second hydrofoil introduces too much viscous drag.

5.3.2 Dynamic Foil Stall

All results given thus far make no mention of foil stalling. In a real flow, the *effective angle-of-attack* of the foil will likely reach values where stalling occurs, thus placing a threshold on the maximum achievable thrust and extracted power. The effective angle-of-attack is calculated at the 3/4-chord point of the foil and is given by the following expression:

$$\alpha_e = \theta + \frac{\dot{h}}{U_\infty} + \frac{(\frac{3c}{4} - x_{rot})\dot{\theta}}{U_\infty} \tag{5.3}$$

Figures 5-10 and 5-11 give the *maximum* effective angle-of-attack seen by the foil for the optimal motions of Figures 5-8 and 5-9. From the NACA 0012 drag polar (Appendix B), the static stall

75
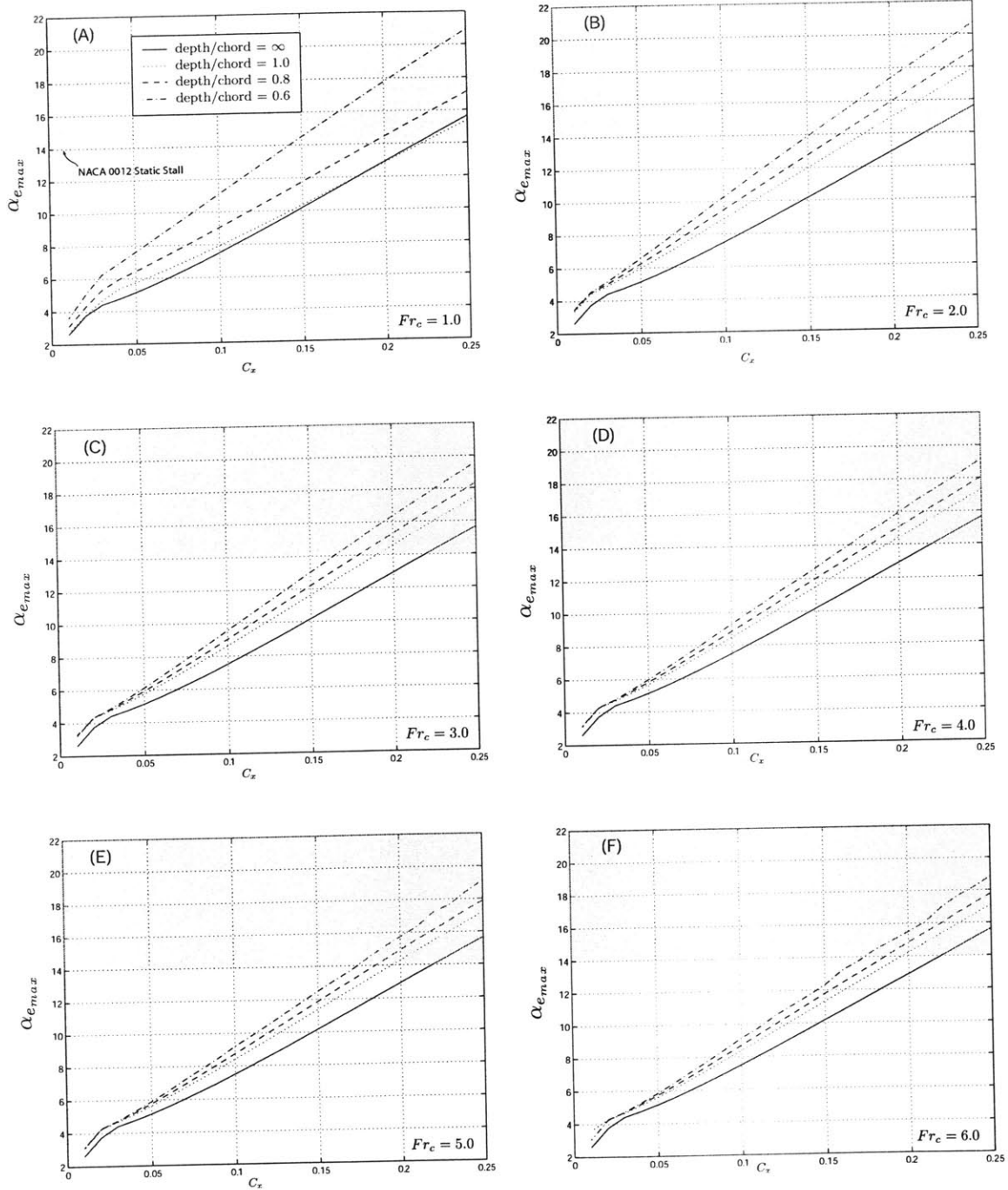
Figure 5-10: Maximum effective angle-of-attack see by the foil for the optimal propulsive motion.
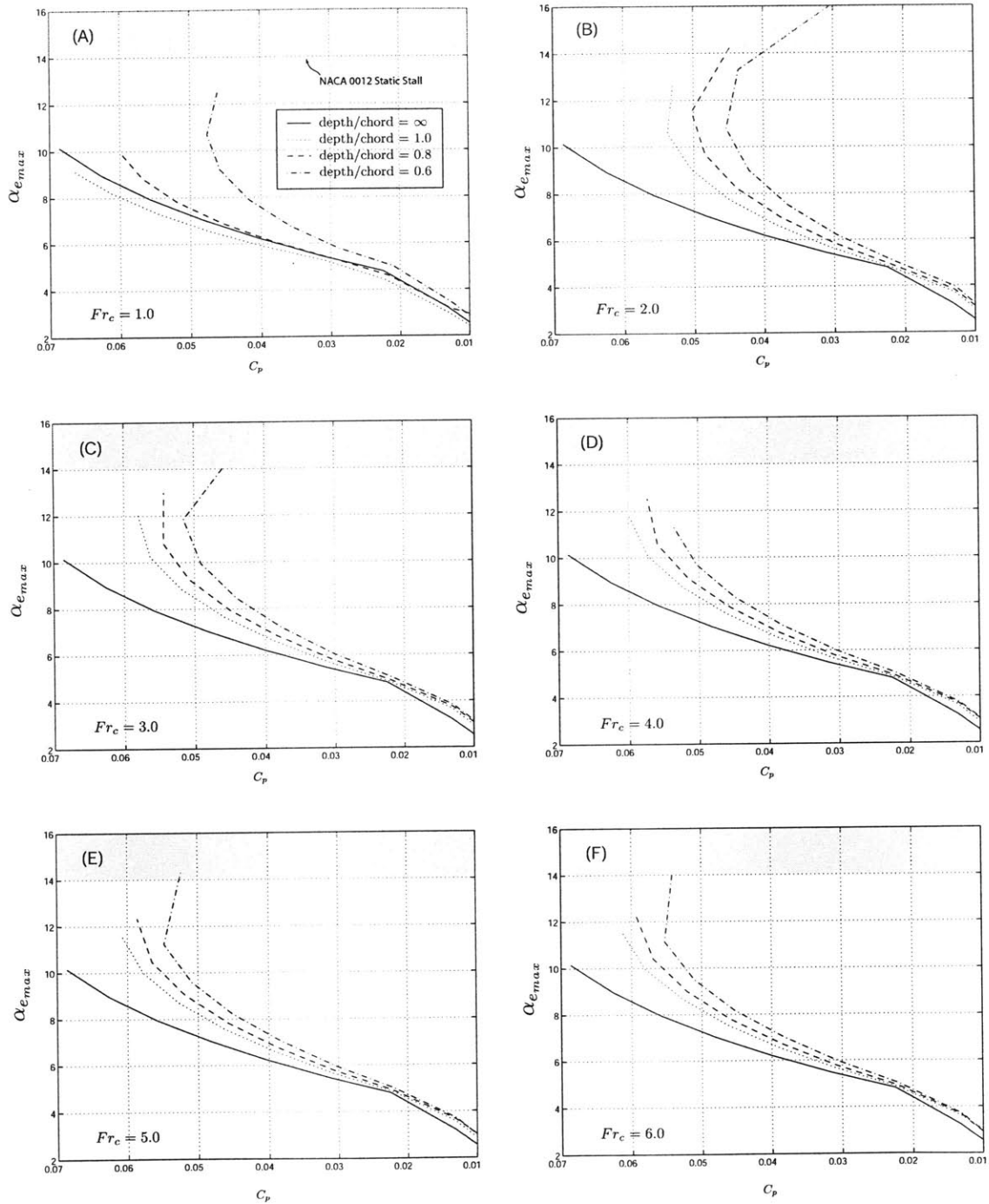
Figure 5-11: Maximum effective angle-of-attack see by the foil for the optimal power-extraction motion.

angle-of-attack is seen to correspond to approximately $14°$ for the Reynolds number considered in this study.

In selecting an operating point, the designer will want to make sure the maximum effective angle-of-attack $\alpha_{e_{max}}$ does not exceed the static stall angle-of-attack by too much. Luckily, dynamic stalls are usually more tolerant than static stalls, so even if the effective angle-of-attack of the foil is close to its static stall value, it is unlikely that the foil will stall for that value.

Predicting dynamic stall is one of the key elements that will allow to push the performance envelope of flapping-wing systems. Unfortunately precise analysis of dynamic stall is extremely difficult. There exist semi-empirical methods of determining the dynamic stall characteristics of a particular foil section based on static data. The method of Erickson and Reding [10],[9] is an example of such a method to determine dynamic stall characteristics for foils oscillating in pitch at low reduced frequencies.

5.3.3 Other Considerations

All mechanical losses as well as the mass and inertia of the wing have been ignored and inclusion of these terms in the model will further diminish the overall efficiency of the system. However, nature shows that it may be possible to overcome most of the inertial energy requirements needed to accelerate the mass of the wing by adding springs to the flapping mechanism to create a tuned harmonic oscillator. In fact, it is believed that insects employ such techniques to generate highly efficient flapping flight [2].

Chapter 6

Summary, Conclusions and Recommendations for Future Work

6.1 Summary

To provide an Autonomous Marine Vehicle with improved endurance, a simple mechanical system based on a Vertically Sculling Hydrofoil was studied. A computer-based tool allowing for the computation of the unsteady loads exerted on a two-dimensional heaving and pitching foil in the presence of free surface effects was devised. With the use of this tool, a series of investigations were carried out to understand how the various VSH design parameters influence the loads and the efficiency of the system. A set of optimizations were conducted to find the ideal foil motion in order to maximize the VSH system's efficiency. From the investigations and the optimization results, it was found that a sinusoidal foil motion is optimal for both propulsion and power extraction in the case of a symmetrical foil. Finally, the influence of the free surface effect on the efficiency of the system was studied. The results show that the free surface greatly impacts the efficiency of the system for foil depths of approximately 5 chord lengths for the case of propulsion and for depths greater than 5 chord lengths for power extraction. Design recommendations to limit the effect of free surface induced drag were provided.

6.2 Future Work

Various recommendations can be made for future work on this project. First of all, the capabilities of the computer tool can be enhanced in the following ways to help in the design of efficient VSH systems:

- Nature suggests that interference effects between multiple wings may be a highly efficient approach to flapping flight (e.g. dragonflies). Among others, experiments by Jones [19], and Schmidt[29] also suggest that this is the case. It would therefore be valuable to enhance the computational tool so as to allow the modeling of multiple foil configurations and assess the resulting interference effects.

- As stated previously, use of spring mechanisms may be another approach to increase the propulsive and power extraction efficiencies of the VSH system. The addition of a dynamics module to the current computational tool could be made to quantify the benefits of using such spring mechanisms.

- Since the wing is assumed to be of high aspect ratio, so as to limit the finite-span induced drag, a two-dimensional computational tool was developed. If the wing's aspect ratio is to be constrained, the high aspect ratio assumption might fail and means of computing the three dimensional flow around the hydrofoil may prove necessary. A vortex lattice tool similar to the one developed by Hall & Hall [13] may be a way of achieving this. In fact, the Fourier solution technique presented in this work could be implemented on such a tool. Finally, with a three dimensional tool, the influence of all types of wing planforms on the unsteady loads could be investigated.

Secondly, further optimizations and VSH experiments may be achieved. These include:

- Looking at heuristic-based methods for the optimization of the foil motion to ensure global optimality of the solution. Because of the large design space, finding the optimal solution was rendered difficult as the SQP algorithm got trapped in multiple local minima. Also, optimizations were only carried out for a symmetrical foil section and it would be interesting to see if the optimal foil motion changes with cambered foil sections.

- Designing a VSH system to conduct a series of experiments to acquire data and correlate this experimental data with results given by the computational tool. Ways of acquiring data may be done with tow tank tests or with a remote control vehicle testbed with adequate on board instrumentation for performance assessment.

Appendix A

Analytic Panel Integrals

In this section, we lay the foundations for the numerical method described in Chapter 3. As seen in Chapter 2, unsteady loads imparted on the foil can be determined by finding the variation of vorticity γ along a foil and its wake by satisfying a set of boundary conditions. In order to find the γ-distribution, one must be able to describe the velocity induced by a singularity distribution. For numerical considerations, a discrete analog to the velocity induced by a continuous distribution is sought.

The continuous vorticity or source distributions are approximated by a set of discrete singularity panels of linearly varying strength. Integrals relating the induced velocities to the singularity strengths are evaluated for a panel and an influence coefficient matrix is build.

A.1 Panel Influence Formulation

The two dimensional inviscid flow around the foil can be represented as an analytical function of the complex argument $\chi = x + iz = re^{i\theta}$:

$$F(\chi) = F(x + iz) = \varphi(x, z) + i\psi(x, z) \tag{A.1}$$

Where $F(\chi)$ is the *complex stream* function and φ and ψ, the perturbation potential and stream functions are real functions of x and z. From elementary potential flows the complex stream function for a point source of strength q is given by,

$$\varphi + i\psi = \frac{q}{2\pi} \ln r + i \frac{q}{2\pi} \theta \tag{A.2}$$

81

And for a point vortex of strength γ, the complex stream function is,

$$\varphi + i\psi = -\frac{\gamma}{2\pi}\theta + i\frac{\gamma}{2\pi}\ln r \tag{A.3}$$

Combining the two singularities allows one to write the complex stream function for a *complex source* of strength $\sigma = q + i\gamma$

$$\varphi + i\psi = \frac{\sigma}{2\pi}\ln\chi = \frac{q + i\gamma}{2\pi}\ln(x + iz) \tag{A.4}$$

Instead of using discrete source or vortices to approximate a continuous singularity distribution, one may consider using a two-dimensional panel of length $\Delta s = |\Delta\chi| = |\chi_2 - \chi_1|$. The complex stream function for such a panel, evaluated at a *control point* χ_0, is obtained by integrating the point source complex stream function over the length of the panel.

$$F(\chi_0) = \varphi + i\psi = \frac{1}{2\pi}\frac{\Delta s}{\Delta\chi}\int_{\chi_1}^{\chi_2}\sigma(\chi)\ln(\chi - \chi_0)d\chi \tag{A.5}$$

Assuming a linearly varying complex source distribution $\sigma(\chi)$ on the panel, as depicted per Figure A-1 yields,

$$\sigma(\chi) = \sigma_1\left(\frac{\chi_2 - \chi}{\Delta\chi}\right) + \sigma_2\left(\frac{\chi - \chi_1}{\Delta\chi}\right) \tag{A.6}$$

Substitution of (A.6) into (A.5) gives for the complex stream function,

$$\varphi + i\psi = \frac{1}{2\pi}\frac{\Delta s}{\Delta\chi^2}\int_{\chi_1}^{\chi_2}\left\{(\sigma_1\chi_2 - \sigma_2\chi_1)\ln(\chi - \chi_0) + (\sigma_2 - \sigma_1)\chi\ln(\chi - \chi_0)\right\}d\chi \tag{A.7}$$

$$\begin{aligned}
\varphi + i\psi = \frac{1}{8\pi}\frac{\Delta s}{\Delta\chi^2}\Big[&\ (\chi_2 - \chi_1)\Big(\sigma_1(2\chi_0 + \chi_1 - 3\chi_2) - \sigma_2(2\chi_0 - 3\chi_1 + \chi_2)\Big)\\
-&\ 2(\chi_0 - \chi_1)\Big(\sigma_2(\chi_1 - \chi_0) + \sigma_1(\chi_0 + \chi_1 - 2\chi_2)\Big)\ln(\chi_1 - \chi_0)\\
+&\ 2(\chi_2 - \chi_0)\Big(\sigma_1(\chi_2 - \chi_0) + \sigma_2(\chi_0 - 2\chi_1 + \chi_2)\Big)\ln(\chi_2 - \chi_0)\Big]
\end{aligned} \tag{A.8}$$

The velocity field in the complex plane is obtained by differentiating the complex stream function with respect to χ_0,

$$u - iw = \frac{d}{d\chi_0}(\varphi + i\psi) \tag{A.9}$$
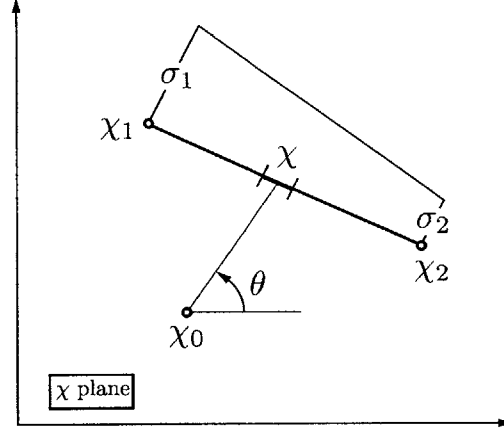
Figure A-1: Panel of linearly varying complex source distribution.

After differentiating and regrouping the σ_1 and σ_2 terms, one obtains,

$$u - iw = \frac{1}{2\pi}\frac{\Delta s}{\Delta \chi^2} \left[\quad \sigma_1\left\{(\chi_2 - \chi_1) + (\chi_2 - \chi_0)\Big(\ln(\chi_1 - \chi_0) - \ln(\chi_2 - \chi_0)\Big)\right\} \right.$$

$$\left. + \quad \sigma_2\left\{(\chi_1 - \chi_2) + (\chi_0 - \chi_1)\Big(\ln(\chi_1 - \chi_0) - \ln(\chi_2 - \chi_0)\Big)\right\} \quad \right] \quad \text{(A.10)}$$

As seen in Chapter 1, the second derivative of the complex stream function with respect to x is necessary in order to introduce the fluid free surface effects in our model. Deriving the velocity field in the complex plane with respect to the complex variable χ_0 yields,

$$\frac{d^2}{d^2\chi_0}(\varphi + i\psi) = \frac{\partial u}{\partial x_0} - i\frac{\partial w}{\partial x_0} - i\frac{\partial u}{\partial z_0} - \frac{\partial w}{\partial z_0} \tag{A.11}$$

From the two-dimensional expression of the continuity equation in cartesian space,

$$\rho\left(\frac{\partial u}{\partial x_0} + \frac{\partial w}{\partial z_0}\right) = 0 \;\; \rightarrow \;\; \frac{\partial u}{\partial x_0} = -\frac{\partial w}{\partial z_0} \tag{A.12}$$

Also, for an irrotational fluid the vorticity ζ is equal to zero yielding,

$$\zeta = \left(\frac{\partial w}{\partial x_0} - \frac{\partial u}{\partial z_0}\right) = 0 \;\; \rightarrow \;\; \frac{\partial w}{\partial x_0} = \frac{\partial u}{\partial z_0} \tag{A.13}$$

Using equations (A.12) and (A.13), the acceleration field in the complex plane finally becomes,

$$\frac{d^2}{d^2\chi_0}(\varphi + i\psi) = 2\frac{\partial u}{\partial x_0} - 2i\frac{\partial w}{\partial x_0} \tag{A.14}$$

83

$$\frac{d^2}{d^2\chi_0}(\varphi + i\psi) = \frac{1}{2\pi}\frac{\Delta s}{\Delta\chi^2}\left[\sigma_1\left\{\frac{(\chi_2 - \chi_1) - (\chi_0 - \chi_1)\Big(\ln(\chi_1 - \chi_0) - \ln(\chi_2 - \chi_0)\Big)}{\chi_0 - \chi_1}\right\}\right.$$
$$\left. + \ \sigma_2\left\{\frac{(\chi_1 - \chi_2) + (\chi_0 - \chi_2)\Big(\ln(\chi_1 - \chi_0) - \ln(\chi_2 - \chi_0)\Big)}{\chi_0 - \chi_2}\right\}\right] \qquad \text{(A.15)}$$

The induced velocities and their derivatives can be rewritten in a more compact form for computer implementation as,

$$\frac{d}{d\chi_0}(\varphi + i\psi) = \sigma_1 C_1(\chi_0) + \sigma_2 C_2(\chi_0)$$
$$= (q_1 + i\gamma_1)(A_1 + iB_1) + (q_2 + i\gamma_2)(A_2 + iB_2) \qquad \text{(A.16)}$$

$$\frac{d^2}{d^2\chi_0}(\varphi + i\psi) = \sigma_1 C_1'(\chi_0) + \sigma_2 C_2'(\chi_0)$$
$$= (q_1 + i\gamma_1)(A_1' + iB_1') + (q_2 + i\gamma_2)(A_2' + iB_2') \qquad \text{(A.17)}$$

Where the *complex influence coefficients* C_1, C_1', C_2 and C_2' are given by:

$$C_1(\chi_0) = A_1 + iB_1$$
$$= \frac{\Delta s}{2\pi\Delta\chi^2}\left\{(\chi_2 - \chi_1) + (\chi_2 - \chi_0)\Big(\ln(\chi_1 - \chi_0) - \ln(\chi_2 - \chi_0)\Big)\right\} \qquad \text{(A.18)}$$

$$C_2(\chi_0) = A_2 + iB_2$$
$$= \frac{\Delta s}{2\pi\Delta\chi^2}\left\{(\chi_1 - \chi_2) + (\chi_0 - \chi_1)\Big(\ln(\chi_1 - \chi_0) - \ln(\chi_2 - \chi_0)\Big)\right\} \qquad \text{(A.19)}$$

$$C_1'(\chi_0) = A_1' + iB_1'$$
$$= \frac{\Delta s}{2\pi\Delta\chi^2}\left\{\frac{(\chi_2 - \chi_1) - (\chi_0 - \chi_1)\Big(\ln(\chi_1 - \chi_0) - \ln(\chi_2 - \chi_0)\Big)}{\chi_0 - \chi_1}\right\} \qquad \text{(A.20)}$$

$$C_2'(\chi_0) = A_1' + iB_1'$$
$$= \frac{\Delta s}{2\pi\Delta\chi^2}\left\{\frac{(\chi_1 - \chi_2) + (\chi_0 - \chi_2)\Big(\ln(\chi_1 - \chi_0) - \ln(\chi_2 - \chi_0)\Big)}{\chi_0 - \chi_2}\right\} \qquad \text{(A.21)}$$

Finally, the x and z-components of the panel-induced velocities are obtained by respectively taking the real part and imaginary part of (A.9). The induced velocities can further be decomposed into

velocities due to the source singularity q and the vortex singularity γ.

$$
\begin{aligned}
u(x_0, z_0) &= \operatorname{Re}(\sigma_1 C_1 + \sigma_2 C_2) = \operatorname{Re}\left((q_1 + i\gamma_1)(A_1 + iB_1) + (q_2 + i\gamma_2)(A_2 + iB_2)\right) \\
&= \left(q_1 \operatorname{Re}(C_1) + q_2 \operatorname{Re}(C_2)\right) + \left(-\gamma_1 \operatorname{Im}(C_1) - \gamma_2 \operatorname{Im}(C_2)\right) \\
&= u^q + u^\gamma
\end{aligned}
\tag{A.22}
$$

$$
\begin{aligned}
w(x_0, z_0) &= -\operatorname{Im}(\sigma_1 C_1 + \sigma_2 C_2) \\
&= \left(-q_1 \operatorname{Im}(C_1) - q_2 \operatorname{Im}(C_2)\right) + \left(-\gamma_1 \operatorname{Re}(C_1) - \gamma_2 \operatorname{Re}(C_2)\right) \\
&= w^q + w^\gamma
\end{aligned}
\tag{A.23}
$$

Likewise, separating real and imaginary parts of (A.14) and regrouping terms induced by the source and vortex singularity yields for the acceleration field,

$$
\begin{aligned}
\frac{\partial u}{\partial x_0}(x_0, z_0) &= \frac{1}{2}\operatorname{Re}(\sigma_1 C_1' + \sigma_2 C_2') \\
&= \frac{1}{2}\left(q_1 \operatorname{Re}(C_1') + q_2 \operatorname{Re}(C_2')\right) + \frac{1}{2}\left(-\gamma_1 \operatorname{Im}(C_1') - \gamma_2 \operatorname{Im}(C_2')\right) \\
&= \frac{\partial u^q}{\partial x_0} + \frac{\partial u^\gamma}{\partial x_0}
\end{aligned}
\tag{A.24}
$$

$$
\begin{aligned}
\frac{\partial w}{\partial x_0}(x_0, z_0) &= -\frac{1}{2}\operatorname{Im}(\sigma_1 C_1' + \sigma_2 C_2') \\
&= -\frac{1}{2}\left(q_1 \operatorname{Im}(C_1') + q_2 \operatorname{Im}(C_2')\right) - \frac{1}{2}\left(\gamma_1 \operatorname{Re}(C_1') + \gamma_2 \operatorname{Re}(C_2')\right) \\
&= \frac{\partial w^q}{\partial x_0} + \frac{\partial w^\gamma}{\partial x_0}
\end{aligned}
\tag{A.25}
$$

The above formulae have been derived for the case of a single panel, where the velocity induced by this panel is calculated at a control point χ_0. If two or more panels are to be considered, the velocity induced by these panels at point χ_0 is now the sum of the influences of the various panels. Generalizing to a panel j of node coordinates χ_j and χ_{j+1} yields for the functions C_1, C_1', C_2 and

C_2' evaluated at a control point χ_{0_i}:

$$C_{1ij} = \frac{\Delta s}{2\pi \Delta \chi^2}\left\{(\chi_{j+1} - \chi_j) + (\chi_{j+1} - \chi_{0_i})\Big(\ln(\chi_j - \chi_{0_i}) - \ln(\chi_{j+1} - \chi_{0i})\Big)\right\} \quad \text{(A.26)}$$

$$C_{2ij} = \frac{\Delta s}{2\pi \Delta \chi^2}\left\{(\chi_j - \chi_{j+1}) + (\chi_{0_i} - \chi_j)\Big(\ln(\chi_j - \chi_{0_i}) - \ln(\chi_{j+1} - \chi_{0_i})\Big)\right\} \quad \text{(A.27)}$$

$$C_{1ij}' = \frac{\Delta s}{2\pi \Delta \chi^2}\left\{\frac{(\chi_{j+1} - \chi_j) - (\chi_{0_i} - \chi_j)\Big(\ln(\chi_j - \chi_{0_i}) - \ln(\chi_{j+1} - \chi_{0_i})\Big)}{\chi_{0_i} - \chi_j}\right)\right\} \quad \text{(A.28)}$$

$$C_{2ij}' = \frac{\Delta s}{2\pi \Delta \chi^2}\left\{\frac{(\chi_j - \chi_{j+1}) + (\chi_{0_i} - \chi_{j+1})\Big(\ln(\chi_j - \chi_{0_i}) - \ln(\chi_{j+1} - \chi_{0_i})\Big)}{\chi_{0_i} - \chi_{j+1}}\right)\right\} \quad \text{(A.29)}$$

Finally, calling a^x and a^z the influence coefficients in the x and z directions respectively for the vortex distribution γ, and b^x, b^z the influence coefficients in the x and z directions respectively for the source distribution q, one may construct the *influence coefficient matrix* for a given geometry by scanning each panel and accumulating the influences.

The pseudo-code below shows the accumulation process for N panels:

```
DO i = 1,N  \\For every control point
  DO j = 1,N  \\Scan each panel

    ax(i,j) = ax(i,j) - Im(C1(i,j))
    ax(i,j+1) = ax(i,j+1) - Im(C2(i,j))


    ax_x(i,j) = ax_x(i,j) + 0.5*Im(C1'(i,j))
    ax_x(i,j+1) = ax_x(i,j+1) + 0.5*Im(C2'(i,j))


    az(i,j) = az(i,j) - Re(C1(i,j))
    az(i,j+1) = az(i,j+1) - Re(C2(i,j))


    az_x(i,j) = az_z(i,j) - 0.5*Re(C1'(i,j))
    az_x(i,j+1) = az_z(i,j+1) - 0.5*Re(C2'(i,j))


    bx(i,j) = bx(i,j) + Re(C1(i,j))
    bx(i,j+1) = bx(i,j+1) + Re(C2(i,j))


    bx_x(i,j) = bx_x(i,j) - 0.5*Re(C1'(i,j))
    bx_x(i,j+1) = bx_x(i,j+1) - 0.5*Re(C2'(i,j))


    bz(i,j) = bz(i,j) - Im(C1(i,j))
    bz(i,j+1) = bz(i,j+1) - Im (C2(i,j))
```

```
bz_x(i,j) = bz_x(i,j) - 0.5*Im(C1'(i,j))

bz_x(i,j+1) = bz_x(i,j+1) - 0.5*Im (C2'(i,j))
```

END

END

The x and z-velocities induced at a control point i by N panels of linearly varying vortex-distribution are given by,

$$u^\gamma = \sum_{j=1}^{N+1} a_{ij}^x \gamma_j \ , \ v^\gamma = \sum_{j=1}^{N+1} a_{ij}^z \gamma_j \qquad (A.30)$$

The x and z-velocities induced at a control point i by N panels of linearly varying source-distribution are given by,

$$u^q = \sum_{j=1}^{N+1} b_{ij}^x q_j \ , \ v^q = \sum_{j=1}^{N+1} b_{ij}^z q_j \qquad (A.31)$$

The first derivatives of the velocities induced at a control point i by N panels of linearly varying source-distribution are given by,

$$\frac{\partial u^q}{\partial x} = \sum_{j=1}^{N+1} b_{x_{ij}}^x q_j \ , \ \frac{\partial v^q}{\partial x} = \sum_{j=1}^{N+1} b_{x_{ij}}^z q_j \qquad (A.32)$$

The first derivatives of the velocities induced at a control point i by N panels of linearly varying vortex-distribution are given by,

$$\frac{\partial u^\gamma}{\partial x} = \sum_{j=1}^{N+1} a_{x_{ij}}^x \gamma_j \ , \ \frac{\partial v^\gamma}{\partial x} = \sum_{j=1}^{N+1} a_{x_{ij}}^z \gamma_j \qquad (A.33)$$

87

Appendix B

NACA 0012 Drag Polar

NACA 0012   Re = 500000   Ma = 0.000   Ncrit = 9.000

XFOIL V 6.94
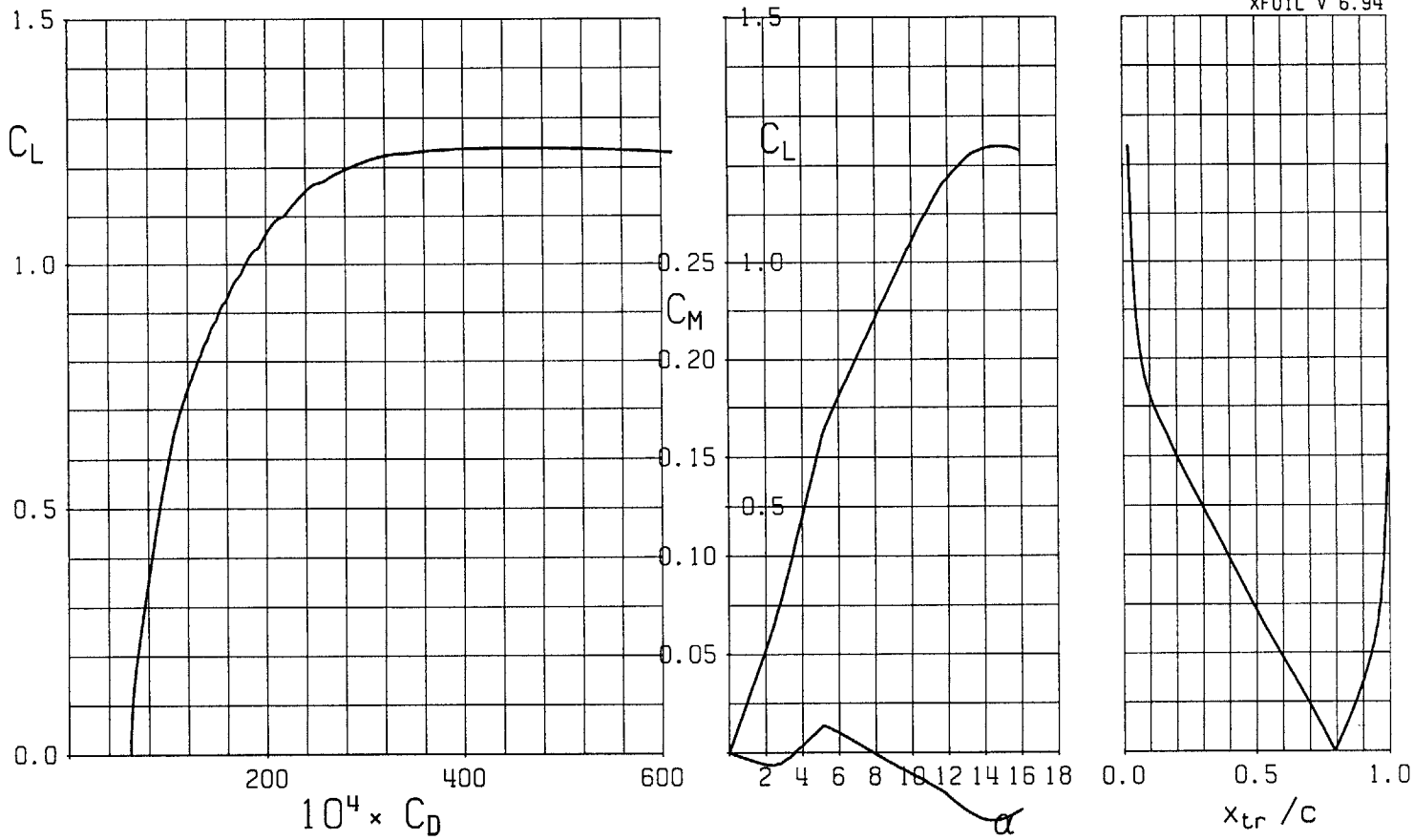
Figure B-1: Polar generated with XFOIL for the NACA 0012 foil section.

89
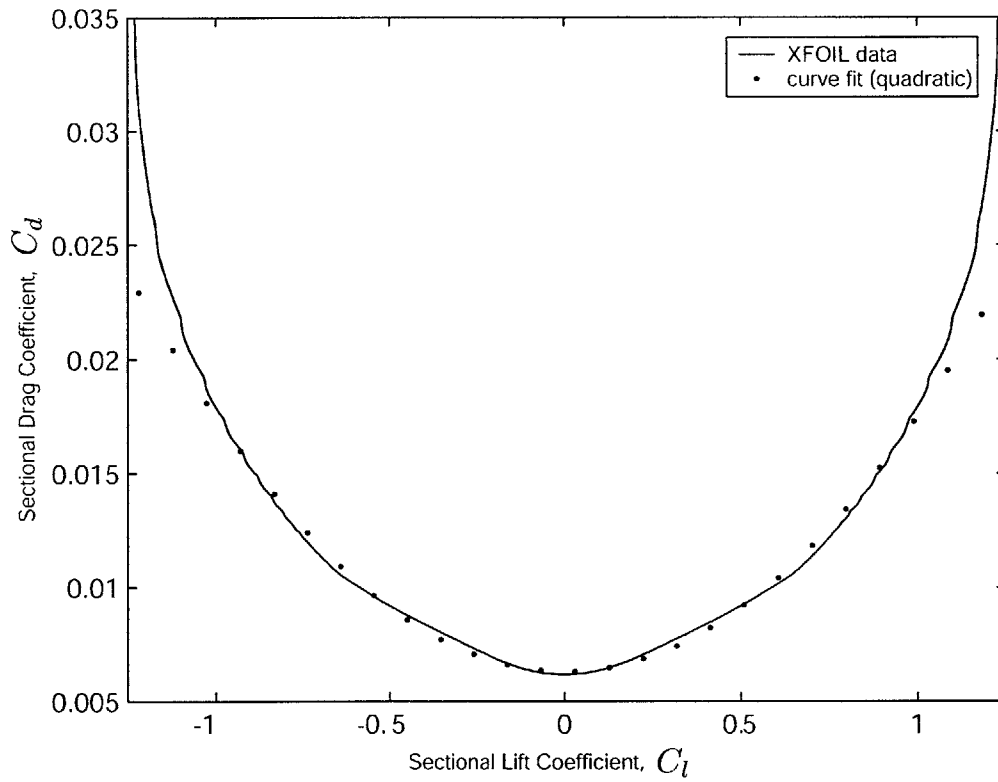
Figure B-2: Curve fit of the NACA 0012 foil section drag bucket by means of a quadratic function.

Appendix C

Optimization Results - Propulsion

This section summarizes the optimization results for the **propulsive case** . In the tables presented below, certain parameters are given to help in the design process and for comparison purposes with other theories and flapping-foil results :

$C_{z_{max}}$ corresponds to the maximum lift coefficient experienced by the foil over a cycle of the optimal motion. From the static stall characteristics of a given foil, the designer can gage whether the foil is close to stalling or not.

$C_{x_{LES}}$ is the part of the thrust coefficient due to leading edge suction. This value is provided here to help in the design process. To achieve large thrust coefficients, the designer will want to select an airfoil that can reach high values of $C_{x_{LES}}$ without flow separation.

$\alpha_{e_{max}}$ is the maximum effective angle-of-attack seen by the foil at the 3/4-chord point. It is given by $\dot{h}/U_\infty + (3/4c - x_{rot})\,\dot{\theta}/U_\infty + \theta$

St_a is the Strouhal number. It is defined as $St_a = fA/U_\infty$, where f is the frequency in Hertz of the motion, A is the maximum excursion of the foil's trailing edge, and U_∞ is the average forward velocity. The Strouhal number is provided in this work for comparative purposes with other results, such as the ones obtained by Triantafyllou [32],[33],[3]

Θ is the *proportional feathering parameter* introduced by Lighthill [24]. It is defined as $\alpha_{e_{max}}\,U_\infty/\dot{h}$.

d/c	C_x	C_p	$C_{z_{max}}$	$C_{x_{LES}}$	$\alpha_{e_{max}}$	h_1	θ_1	ϕ_1	k	St_a	Θ
∞	0.250	0.332	0.953	0.139	15.647	0.500	20.000	115.435	0.713	0.206	0.383
∞	0.240	0.317	0.918	0.133	15.108	0.500	20.000	115.486	0.702	0.203	0.376
∞	0.230	0.302	0.883	0.127	14.567	0.500	20.000	115.531	0.691	0.200	0.368
∞	0.220	0.287	0.847	0.120	14.023	0.500	20.000	115.565	0.680	0.196	0.360
∞	0.210	0.273	0.812	0.114	13.476	0.500	20.000	115.589	0.669	0.193	0.352
∞	0.200	0.258	0.776	0.108	12.927	0.500	20.000	115.600	0.657	0.190	0.343
∞	0.190	0.244	0.740	0.102	12.381	0.500	20.000	115.600	0.646	0.186	0.335
∞	0.180	0.230	0.704	0.096	11.833	0.500	20.000	115.585	0.634	0.183	0.326
∞	0.170	0.216	0.668	0.090	11.282	0.500	20.000	115.556	0.622	0.180	0.317
∞	0.160	0.202	0.632	0.084	10.734	0.500	20.000	115.507	0.610	0.176	0.307
∞	0.150	0.188	0.595	0.078	10.188	0.500	20.000	115.443	0.598	0.173	0.298
∞	0.140	0.175	0.558	0.072	9.640	0.500	20.000	115.359	0.585	0.169	0.288
∞	0.130	0.161	0.521	0.067	9.100	0.500	20.000	115.253	0.572	0.166	0.278
∞	0.120	0.148	0.483	0.061	8.560	0.500	20.000	115.124	0.559	0.162	0.267
∞	0.110	0.135	0.445	0.056	8.031	0.500	20.000	114.968	0.546	0.159	0.257
∞	0.100	0.122	0.407	0.051	7.507	0.500	20.000	114.787	0.532	0.155	0.246
∞	0.090	0.110	0.367	0.046	6.994	0.500	20.000	114.571	0.519	0.151	0.235
∞	0.080	0.097	0.327	0.041	6.498	0.500	20.000	114.321	0.505	0.148	0.225
∞	0.070	0.085	0.287	0.037	6.020	0.500	20.000	114.032	0.491	0.144	0.214
∞	0.060	0.073	0.245	0.032	5.563	0.500	20.000	113.701	0.476	0.140	0.204
∞	0.050	0.061	0.203	0.028	5.140	0.500	20.000	113.322	0.461	0.136	0.195
∞	0.040	0.050	0.159	0.025	4.751	0.500	20.000	112.892	0.446	0.132	0.186
∞	0.030	0.039	0.114	0.021	4.411	0.500	20.000	112.404	0.431	0.128	0.179
∞	0.020	0.028	0.084	0.015	3.739	0.500	18.934	110.906	0.394	0.118	0.166
∞	0.010	0.017	0.068	0.008	2.613	0.500	16.200	107.782	0.324	0.099	0.141

Table C.1: Optimization results for $d/c = \infty$

d/c	C_x	C_p	$C_{z_{max}}$	$C_{x_{LES}}$	$\alpha_{e_{max}}$	h_1	θ_1	ϕ_1	k	St_a	Θ
1.000	0.250	0.331	0.982	0.119	15.377	0.500	20.000	112.307	0.675	0.201	0.398
1.000	0.240	0.317	0.947	0.113	14.873	0.500	20.000	112.346	0.665	0.198	0.390
1.000	0.230	0.302	0.911	0.107	14.365	0.500	20.000	112.383	0.655	0.195	0.383
1.000	0.220	0.287	0.876	0.102	13.868	0.500	20.000	112.389	0.645	0.192	0.375
1.000	0.210	0.272	0.840	0.096	13.368	0.500	20.000	112.396	0.634	0.189	0.368
1.000	0.200	0.258	0.804	0.091	12.860	0.500	20.000	112.410	0.624	0.186	0.360
1.000	0.190	0.244	0.768	0.085	12.354	0.500	20.000	112.408	0.613	0.183	0.352
1.000	0.180	0.230	0.732	0.080	11.852	0.500	20.000	112.386	0.603	0.180	0.343
1.000	0.170	0.216	0.695	0.075	11.353	0.500	20.000	112.354	0.592	0.176	0.335
1.000	0.160	0.202	0.658	0.070	10.850	0.500	20.000	112.319	0.581	0.173	0.326
1.000	0.150	0.188	0.620	0.065	10.354	0.500	20.000	112.256	0.570	0.170	0.317
1.000	0.140	0.175	0.582	0.060	9.864	0.500	20.000	112.178	0.558	0.167	0.308
1.000	0.130	0.161	0.544	0.055	9.368	0.500	20.000	112.101	0.547	0.163	0.299
1.000	0.120	0.148	0.505	0.051	8.886	0.500	20.000	111.998	0.535	0.160	0.290
1.000	0.110	0.135	0.465	0.046	8.403	0.500	20.000	111.880	0.523	0.157	0.280
1.000	0.100	0.123	0.425	0.042	7.932	0.500	20.000	111.745	0.511	0.153	0.271
1.000	0.090	0.110	0.384	0.038	7.470	0.500	20.000	111.588	0.499	0.150	0.261
1.000	0.080	0.098	0.343	0.034	7.016	0.500	20.000	111.412	0.487	0.146	0.252
1.000	0.070	0.086	0.300	0.030	6.575	0.500	20.000	111.216	0.474	0.143	0.242
1.000	0.060	0.074	0.257	0.027	6.151	0.500	20.000	110.997	0.462	0.139	0.233
1.000	0.050	0.062	0.213	0.023	5.749	0.500	20.000	110.754	0.449	0.136	0.224
1.000	0.040	0.050	0.167	0.020	5.372	0.500	20.000	110.486	0.435	0.132	0.215
1.000	0.030	0.039	0.137	0.015	4.681	0.500	19.086	109.390	0.404	0.123	0.202
1.000	0.020	0.028	0.113	0.010	3.769	0.500	17.422	107.580	0.358	0.110	0.184
1.000	0.010	0.017	0.086	0.005	2.740	0.500	15.127	105.110	0.301	0.093	0.159

Table C.2: Optimization results for $Fr_c = 1.0$, $d/c = 1.0$

93

d/c	C_x	C_p	$C_{z_{max}}$	$C_{x_{LES}}$	$\alpha_{e_{max}}$	h_1	θ_1	ϕ_1	k	St_a	Θ
0.800	0.250	0.342	1.011	0.112	17.123	0.500	20.000	109.704	0.684	0.209	0.437
0.800	0.240	0.326	0.975	0.107	16.594	0.500	20.000	109.767	0.674	0.206	0.430
0.800	0.230	0.311	0.938	0.101	16.062	0.500	20.000	109.830	0.664	0.203	0.422
0.800	0.220	0.296	0.902	0.096	15.532	0.500	20.000	109.886	0.653	0.199	0.415
0.800	0.210	0.281	0.865	0.091	14.998	0.500	20.000	109.936	0.643	0.196	0.407
0.800	0.200	0.266	0.827	0.085	14.462	0.500	20.000	109.980	0.633	0.193	0.399
0.800	0.190	0.251	0.790	0.080	13.922	0.500	20.000	110.018	0.622	0.190	0.391
0.800	0.180	0.237	0.752	0.075	13.380	0.500	20.000	110.048	0.611	0.186	0.382
0.800	0.170	0.222	0.714	0.070	12.842	0.500	20.000	110.071	0.600	0.183	0.373
0.800	0.160	0.208	0.675	0.066	12.299	0.500	20.000	110.086	0.589	0.179	0.364
0.800	0.150	0.194	0.637	0.061	11.752	0.500	20.000	110.094	0.578	0.176	0.355
0.800	0.140	0.180	0.598	0.056	11.211	0.500	20.000	110.090	0.566	0.172	0.346
0.800	0.130	0.166	0.558	0.052	10.668	0.500	20.000	110.078	0.555	0.169	0.336
0.800	0.120	0.152	0.518	0.048	10.122	0.500	20.000	110.059	0.543	0.165	0.325
0.800	0.110	0.139	0.477	0.043	9.582	0.500	20.000	110.026	0.531	0.162	0.315
0.800	0.100	0.126	0.436	0.039	9.041	0.500	20.000	109.984	0.519	0.158	0.304
0.800	0.090	0.113	0.394	0.035	8.505	0.500	20.000	109.929	0.506	0.154	0.293
0.800	0.080	0.100	0.351	0.032	7.975	0.500	20.000	109.863	0.493	0.151	0.282
0.800	0.070	0.088	0.308	0.028	7.450	0.500	20.000	109.783	0.480	0.147	0.271
0.800	0.060	0.075	0.264	0.025	6.935	0.500	20.000	109.689	0.467	0.143	0.259
0.800	0.050	0.063	0.218	0.022	6.436	0.500	20.000	109.581	0.453	0.139	0.248
0.800	0.040	0.051	0.172	0.019	5.956	0.500	20.000	109.456	0.439	0.135	0.237
0.800	0.030	0.040	0.133	0.015	5.322	0.500	19.526	108.893	0.416	0.128	0.223
0.800	0.020	0.029	0.110	0.010	4.277	0.500	17.816	107.183	0.369	0.114	0.202
0.800	0.010	0.018	0.084	0.005	3.100	0.500	15.464	104.827	0.310	0.097	0.175

Table C.3: Optimization results for $Fr_c = 1.0$, $d/c = 0.8$

94

d/c	C_x	C_p	$C_{z_{max}}$	$C_{x_{LES}}$	$\alpha_{e_{max}}$	h_1	θ_1	ϕ_1	k	St_a	Θ
0.600	0.250	0.363	1.052	0.107	20.907	0.500	20.000	106.219	0.722	0.228	0.505
0.600	0.240	0.346	1.013	0.102	20.288	0.500	20.000	106.353	0.712	0.224	0.498
0.600	0.230	0.330	0.974	0.097	19.667	0.500	20.000	106.472	0.701	0.221	0.490
0.600	0.220	0.314	0.935	0.092	19.038	0.500	20.000	106.599	0.690	0.217	0.482
0.600	0.210	0.298	0.896	0.087	18.408	0.500	20.000	106.724	0.679	0.213	0.473
0.600	0.200	0.282	0.857	0.082	17.771	0.500	20.000	106.850	0.668	0.209	0.465
0.600	0.190	0.266	0.817	0.077	17.130	0.500	20.000	106.965	0.656	0.206	0.456
0.600	0.180	0.250	0.777	0.072	16.483	0.500	20.000	107.075	0.644	0.202	0.447
0.600	0.170	0.235	0.737	0.068	15.826	0.500	20.000	107.191	0.632	0.198	0.437
0.600	0.160	0.220	0.697	0.063	15.164	0.500	20.000	107.301	0.620	0.194	0.427
0.600	0.150	0.205	0.657	0.058	14.502	0.500	20.000	107.407	0.608	0.190	0.416
0.600	0.140	0.190	0.616	0.054	13.830	0.500	20.000	107.518	0.595	0.186	0.405
0.600	0.130	0.175	0.574	0.050	13.152	0.500	20.000	107.612	0.583	0.181	0.394
0.600	0.120	0.161	0.533	0.046	12.469	0.500	20.000	107.714	0.569	0.177	0.382
0.600	0.110	0.146	0.491	0.042	11.781	0.500	20.000	107.814	0.556	0.173	0.370
0.600	0.100	0.132	0.448	0.038	11.087	0.500	20.000	107.896	0.542	0.168	0.357
0.600	0.090	0.118	0.405	0.034	10.393	0.500	20.000	107.988	0.528	0.164	0.343
0.600	0.080	0.105	0.361	0.030	9.692	0.500	20.000	108.069	0.514	0.159	0.329
0.600	0.070	0.091	0.317	0.027	8.992	0.500	20.000	108.148	0.499	0.155	0.315
0.600	0.060	0.078	0.272	0.024	8.294	0.500	20.000	108.222	0.484	0.150	0.299
0.600	0.050	0.066	0.226	0.021	7.601	0.500	20.000	108.290	0.468	0.145	0.283
0.600	0.040	0.053	0.179	0.018	6.918	0.500	20.000	108.354	0.452	0.140	0.267
0.600	0.030	0.041	0.130	0.015	6.252	0.500	20.000	108.411	0.436	0.135	0.251
0.600	0.020	0.029	0.107	0.010	5.019	0.500	18.310	106.905	0.387	0.120	0.226
0.600	0.010	0.018	0.081	0.006	3.611	0.500	15.897	104.708	0.325	0.101	0.194

Table C.4: Optimization results for $Fr_c = 1.0$, $d/c = 0.6$

d/c	C_x	C_p	$C_{z_{max}}$	$C_{x_{LES}}$	$\alpha_{e_{max}}$	h_1	θ_1	ϕ_1	k	St_a	Θ
1.000	0.250	0.340	0.970	0.139	17.907	0.500	20.000	113.042	0.734	0.217	0.426
1.000	0.240	0.324	0.934	0.132	17.335	0.500	20.000	113.106	0.723	0.214	0.418
1.000	0.230	0.309	0.898	0.126	16.745	0.500	20.000	113.211	0.712	0.210	0.410
1.000	0.220	0.294	0.862	0.120	16.167	0.500	20.000	113.254	0.701	0.207	0.403
1.000	0.210	0.279	0.826	0.114	15.581	0.500	20.000	113.305	0.689	0.203	0.395
1.000	0.200	0.265	0.789	0.108	14.987	0.500	20.000	113.358	0.678	0.200	0.386
1.000	0.190	0.250	0.753	0.101	14.396	0.500	20.000	113.396	0.666	0.196	0.377
1.000	0.180	0.235	0.716	0.095	13.801	0.500	20.000	113.425	0.654	0.193	0.369
1.000	0.170	0.221	0.679	0.090	13.201	0.500	20.000	113.442	0.641	0.189	0.359
1.000	0.160	0.207	0.641	0.084	12.596	0.500	20.000	113.449	0.629	0.185	0.350
1.000	0.150	0.193	0.604	0.078	11.992	0.500	20.000	113.443	0.616	0.182	0.340
1.000	0.140	0.179	0.566	0.072	11.385	0.500	20.000	113.425	0.603	0.178	0.330
1.000	0.130	0.165	0.528	0.067	10.772	0.500	20.000	113.392	0.590	0.174	0.319
1.000	0.120	0.152	0.489	0.061	10.164	0.500	20.000	113.345	0.576	0.170	0.308
1.000	0.110	0.138	0.450	0.056	9.550	0.500	20.000	113.281	0.563	0.166	0.296
1.000	0.100	0.125	0.411	0.051	8.941	0.500	20.000	113.199	0.548	0.162	0.285
1.000	0.090	0.112	0.371	0.046	8.330	0.500	20.000	113.095	0.534	0.158	0.272
1.000	0.080	0.100	0.330	0.041	7.727	0.500	20.000	112.974	0.519	0.154	0.260
1.000	0.070	0.087	0.289	0.037	7.130	0.500	20.000	112.827	0.504	0.150	0.247
1.000	0.060	0.075	0.247	0.033	6.543	0.500	20.000	112.654	0.489	0.145	0.234
1.000	0.050	0.063	0.204	0.028	5.970	0.500	20.000	112.452	0.473	0.141	0.221
1.000	0.040	0.051	0.160	0.025	5.421	0.500	20.000	112.214	0.456	0.136	0.207
1.000	0.030	0.039	0.115	0.021	4.902	0.500	20.000	111.955	0.440	0.131	0.195
1.000	0.020	0.028	0.070	0.018	4.438	0.500	20.000	111.632	0.422	0.127	0.184
1.000	0.010	0.017	0.047	0.011	3.355	0.500	17.973	109.270	0.364	0.111	0.161

Table C.5: Optimization results for $Fr_c = 2.0$, $d/c = 1.0$

96

d/c	C_x	C_p	$C_{z_{max}}$	$C_{x_{LES}}$	$\alpha_{e_{max}}$	h_1	θ_1	ϕ_1	k	St_a	Θ
0.800	0.250	0.345	0.980	0.141	19.006	0.500	20.000	112.554	0.751	0.223	0.442
0.800	0.240	0.329	0.944	0.134	18.403	0.500	20.000	112.652	0.740	0.220	0.434
0.800	0.230	0.314	0.907	0.128	17.796	0.500	20.000	112.743	0.729	0.216	0.426
0.800	0.220	0.299	0.870	0.122	17.181	0.500	20.000	112.836	0.717	0.213	0.418
0.800	0.210	0.284	0.832	0.115	16.572	0.500	20.000	112.883	0.705	0.209	0.410
0.800	0.200	0.269	0.795	0.109	15.945	0.500	20.000	112.965	0.693	0.205	0.401
0.800	0.190	0.254	0.758	0.103	15.318	0.500	20.000	113.038	0.681	0.202	0.393
0.800	0.180	0.239	0.721	0.097	14.699	0.500	20.000	113.064	0.669	0.198	0.384
0.800	0.170	0.224	0.683	0.091	14.060	0.500	20.000	113.120	0.656	0.194	0.374
0.800	0.160	0.210	0.645	0.085	13.420	0.500	20.000	113.153	0.643	0.190	0.364
0.800	0.150	0.196	0.607	0.079	12.773	0.500	20.000	113.176	0.630	0.186	0.354
0.800	0.140	0.182	0.569	0.074	12.128	0.500	20.000	113.187	0.616	0.182	0.343
0.800	0.130	0.168	0.530	0.068	11.475	0.500	20.000	113.185	0.603	0.178	0.332
0.800	0.120	0.154	0.491	0.063	10.816	0.500	20.000	113.170	0.589	0.174	0.321
0.800	0.110	0.140	0.452	0.057	10.159	0.500	20.000	113.140	0.574	0.170	0.309
0.800	0.100	0.127	0.412	0.052	9.495	0.500	20.000	113.093	0.560	0.166	0.296
0.800	0.090	0.114	0.372	0.047	8.836	0.500	20.000	113.028	0.544	0.161	0.283
0.800	0.080	0.101	0.331	0.042	8.175	0.500	20.000	112.942	0.529	0.157	0.270
0.800	0.070	0.088	0.290	0.038	7.517	0.500	20.000	112.833	0.513	0.152	0.256
0.800	0.060	0.075	0.247	0.033	6.868	0.500	20.000	112.697	0.497	0.148	0.241
0.800	0.050	0.063	0.204	0.029	6.233	0.500	20.000	112.530	0.480	0.143	0.227
0.800	0.040	0.051	0.161	0.025	5.617	0.500	20.000	112.335	0.463	0.138	0.212
0.800	0.030	0.040	0.116	0.022	5.027	0.500	20.000	112.108	0.445	0.133	0.197
0.800	0.020	0.028	0.071	0.018	4.495	0.500	20.000	111.815	0.426	0.128	0.184
0.800	0.010	0.017	0.045	0.011	3.446	0.500	18.224	109.713	0.372	0.113	0.162

Table C.6: Optimization results for $Fr_c = 2.0$, $d/c = 0.8$

97

d/c	C_x	C_p	$C_{z_{max}}$	$C_{x_{LES}}$	$\alpha_{e_{max}}$	h_1	θ_1	ϕ_1	k	St_a	Θ
0.600	0.250	0.352	0.993	0.145	20.696	0.500	20.000	112.160	0.781	0.233	0.463
0.600	0.240	0.336	0.956	0.139	20.043	0.500	20.000	112.297	0.769	0.229	0.455
0.600	0.230	0.321	0.918	0.132	19.387	0.500	20.000	112.421	0.758	0.226	0.447
0.600	0.220	0.305	0.880	0.126	18.727	0.500	20.000	112.530	0.745	0.222	0.439
0.600	0.210	0.289	0.842	0.119	18.057	0.500	20.000	112.647	0.733	0.218	0.430
0.600	0.200	0.274	0.804	0.113	17.382	0.500	20.000	112.753	0.720	0.214	0.421
0.600	0.190	0.259	0.765	0.107	16.697	0.500	20.000	112.860	0.708	0.210	0.412
0.600	0.180	0.244	0.727	0.101	16.007	0.500	20.000	112.950	0.694	0.206	0.402
0.600	0.170	0.229	0.689	0.095	15.316	0.500	20.000	113.028	0.681	0.202	0.393
0.600	0.160	0.214	0.650	0.089	14.616	0.500	20.000	113.103	0.667	0.197	0.382
0.600	0.150	0.199	0.611	0.083	13.908	0.500	20.000	113.167	0.653	0.193	0.372
0.600	0.140	0.185	0.572	0.077	13.194	0.500	20.000	113.212	0.639	0.189	0.360
0.600	0.130	0.171	0.533	0.071	12.473	0.500	20.000	113.248	0.624	0.184	0.349
0.600	0.120	0.157	0.493	0.065	11.749	0.500	20.000	113.269	0.609	0.180	0.337
0.600	0.110	0.143	0.454	0.060	11.010	0.500	20.000	113.288	0.594	0.175	0.324
0.600	0.100	0.129	0.414	0.055	10.268	0.500	20.000	113.298	0.578	0.171	0.310
0.600	0.090	0.116	0.373	0.049	9.531	0.500	20.000	113.245	0.562	0.166	0.296
0.600	0.080	0.102	0.332	0.044	8.787	0.500	20.000	113.204	0.545	0.161	0.281
0.600	0.070	0.089	0.290	0.039	8.042	0.500	20.000	113.132	0.528	0.156	0.266
0.600	0.060	0.076	0.248	0.035	7.301	0.500	20.000	113.033	0.510	0.151	0.250
0.600	0.050	0.064	0.205	0.030	6.570	0.500	20.000	112.902	0.492	0.146	0.233
0.600	0.040	0.052	0.162	0.026	5.857	0.500	20.000	112.733	0.473	0.140	0.216
0.600	0.030	0.040	0.117	0.022	5.170	0.500	20.000	112.529	0.453	0.135	0.199
0.600	0.020	0.028	0.073	0.019	4.543	0.500	20.000	112.247	0.433	0.129	0.183
0.600	0.010	0.017	0.044	0.012	3.504	0.500	18.446	110.345	0.380	0.115	0.161

Table C.7: Optimization results for $Fr_c = 2.0$, $d/c = 0.6$

d/c	C_x	C_p	$C_{z_{max}}$	$C_{x_{LES}}$	$\alpha_{e_{max}}$	h_1	θ_1	ϕ_1	k	St_a	Θ
1.000	0.250	0.339	0.967	0.140	17.460	0.500	20.000	113.752	0.733	0.215	0.416
1.000	0.240	0.323	0.931	0.134	16.892	0.500	20.000	113.826	0.722	0.212	0.409
1.000	0.230	0.308	0.895	0.127	16.321	0.500	20.000	113.892	0.711	0.209	0.401
1.000	0.220	0.293	0.859	0.121	15.745	0.500	20.000	113.953	0.699	0.205	0.393
1.000	0.210	0.278	0.823	0.115	15.167	0.500	20.000	113.999	0.688	0.202	0.385
1.000	0.200	0.264	0.786	0.109	14.584	0.500	20.000	114.040	0.676	0.198	0.377
1.000	0.190	0.249	0.750	0.102	13.997	0.500	20.000	114.071	0.664	0.195	0.368
1.000	0.180	0.235	0.713	0.096	13.406	0.500	20.000	114.092	0.652	0.191	0.359
1.000	0.170	0.220	0.676	0.090	12.816	0.500	20.000	114.103	0.640	0.187	0.350
1.000	0.160	0.206	0.639	0.085	12.222	0.500	20.000	114.101	0.628	0.184	0.340
1.000	0.150	0.192	0.602	0.079	11.622	0.500	20.000	114.088	0.615	0.180	0.330
1.000	0.140	0.178	0.564	0.073	11.025	0.500	20.000	114.057	0.602	0.176	0.320
1.000	0.130	0.165	0.526	0.068	10.426	0.500	20.000	114.011	0.589	0.173	0.309
1.000	0.120	0.151	0.488	0.062	9.823	0.500	20.000	113.949	0.575	0.169	0.298
1.000	0.110	0.138	0.449	0.057	9.226	0.500	20.000	113.867	0.561	0.165	0.287
1.000	0.100	0.125	0.409	0.052	8.627	0.500	20.000	113.763	0.547	0.161	0.275
1.000	0.090	0.112	0.370	0.047	8.033	0.500	20.000	113.637	0.533	0.157	0.263
1.000	0.080	0.099	0.329	0.042	7.447	0.500	20.000	113.485	0.518	0.153	0.251
1.000	0.070	0.087	0.288	0.037	6.868	0.500	20.000	113.305	0.503	0.148	0.238
1.000	0.060	0.074	0.246	0.033	6.303	0.500	20.000	113.094	0.488	0.144	0.226
1.000	0.050	0.062	0.203	0.029	5.758	0.500	20.000	112.843	0.472	0.140	0.213
1.000	0.040	0.051	0.160	0.025	5.236	0.500	20.000	112.557	0.455	0.135	0.201
1.000	0.030	0.039	0.115	0.021	4.751	0.500	20.000	112.239	0.439	0.131	0.189
1.000	0.020	0.028	0.070	0.018	4.328	0.500	20.000	111.841	0.421	0.126	0.179
1.000	0.010	0.017	0.049	0.010	3.212	0.500	17.764	109.232	0.359	0.109	0.156

Table C.8: Optimization results for $Fr_c = 3.0$, $d/c = 1.0$

d/c	C_x	C_p	$C_{z_{max}}$	$C_{x_{LES}}$	$\alpha_{e_{max}}$	h_1	θ_1	ϕ_1	k	St_a	Θ
0.800	0.250	0.343	0.974	0.142	18.290	0.500	20.000	113.436	0.746	0.220	0.428
0.800	0.240	0.327	0.938	0.135	17.700	0.500	20.000	113.530	0.735	0.217	0.420
0.800	0.230	0.312	0.901	0.129	17.108	0.500	20.000	113.611	0.724	0.213	0.413
0.800	0.220	0.297	0.865	0.123	16.507	0.500	20.000	113.696	0.712	0.209	0.405
0.800	0.210	0.282	0.828	0.116	15.906	0.500	20.000	113.761	0.701	0.206	0.396
0.800	0.200	0.267	0.791	0.110	15.298	0.500	20.000	113.821	0.689	0.202	0.388
0.800	0.190	0.252	0.754	0.104	14.685	0.500	20.000	113.872	0.677	0.199	0.379
0.800	0.180	0.237	0.717	0.098	14.067	0.500	20.000	113.913	0.664	0.195	0.370
0.800	0.170	0.223	0.679	0.092	13.450	0.500	20.000	113.940	0.652	0.191	0.360
0.800	0.160	0.209	0.642	0.086	12.826	0.500	20.000	113.965	0.639	0.187	0.351
0.800	0.150	0.194	0.604	0.080	12.199	0.500	20.000	113.969	0.626	0.183	0.340
0.800	0.140	0.180	0.566	0.074	11.564	0.500	20.000	113.965	0.612	0.180	0.330
0.800	0.130	0.167	0.527	0.069	10.933	0.500	20.000	113.945	0.599	0.176	0.319
0.800	0.120	0.153	0.489	0.063	10.298	0.500	20.000	113.903	0.585	0.172	0.308
0.800	0.110	0.139	0.450	0.058	9.660	0.500	20.000	113.849	0.571	0.168	0.296
0.800	0.100	0.126	0.410	0.053	9.022	0.500	20.000	113.773	0.556	0.163	0.283
0.800	0.090	0.113	0.370	0.047	8.388	0.500	20.000	113.675	0.541	0.159	0.271
0.800	0.080	0.100	0.330	0.043	7.755	0.500	20.000	113.550	0.526	0.155	0.258
0.800	0.070	0.087	0.288	0.038	7.130	0.500	20.000	113.396	0.510	0.150	0.244
0.800	0.060	0.075	0.246	0.033	6.518	0.500	20.000	113.210	0.494	0.146	0.230
0.800	0.050	0.063	0.204	0.029	5.925	0.500	20.000	112.986	0.477	0.141	0.217
0.800	0.040	0.051	0.160	0.025	5.358	0.500	20.000	112.718	0.460	0.137	0.203
0.800	0.030	0.039	0.116	0.022	4.819	0.500	20.000	112.422	0.443	0.132	0.190
0.800	0.020	0.028	0.070	0.019	4.352	0.500	20.000	112.029	0.425	0.127	0.179
0.800	0.010	0.017	0.049	0.011	3.228	0.500	17.840	109.509	0.363	0.110	0.155

Table C.9: Optimization results for $Fr_c = 3.0$, $d/c = 0.8$

d/c	C_x	$\bar{C}_p$	$C_{z_{max}}$	$C_{x_{LES}}$	$\alpha_{e_{max}}$	h_1	θ_1	ϕ_1	k	St_a	Θ
0.600	0.250	0.348	0.984	0.146	19.544	0.500	20.000	113.240	0.770	0.227	0.443
0.600	0.240	0.333	0.947	0.139	18.907	0.500	20.000	113.383	0.758	0.224	0.435
0.600	0.230	0.317	0.909	0.133	18.283	0.500	20.000	113.457	0.746	0.220	0.428
0.600	0.220	0.301	0.872	0.126	17.637	0.500	20.000	113.587	0.734	0.216	0.419
0.600	0.210	0.286	0.834	0.120	16.989	0.500	20.000	113.701	0.722	0.212	0.411
0.600	0.200	0.271	0.796	0.114	16.360	0.500	20.000	113.732	0.710	0.209	0.402
0.600	0.190	0.256	0.758	0.107	15.706	0.500	20.000	113.810	0.697	0.205	0.393
0.600	0.180	0.241	0.721	0.101	15.040	0.500	20.000	113.898	0.684	0.201	0.384
0.600	0.170	0.226	0.683	0.095	14.361	0.500	20.000	113.994	0.671	0.197	0.374
0.600	0.160	0.212	0.645	0.089	13.691	0.500	20.000	114.030	0.658	0.193	0.364
0.600	0.150	0.197	0.606	0.083	13.009	0.500	20.000	114.091	0.644	0.189	0.353
0.600	0.140	0.183	0.568	0.077	12.325	0.500	20.000	114.125	0.630	0.184	0.342
0.600	0.130	0.169	0.529	0.071	11.636	0.500	20.000	114.134	0.616	0.180	0.330
0.600	0.120	0.155	0.490	0.066	10.945	0.500	20.000	114.125	0.601	0.176	0.318
0.600	0.110	0.141	0.451	0.060	10.254	0.500	20.000	114.090	0.586	0.172	0.306
0.600	0.100	0.128	0.411	0.055	9.557	0.500	20.000	114.041	0.570	0.167	0.293
0.600	0.090	0.114	0.371	0.049	8.857	0.500	20.000	113.977	0.554	0.163	0.279
0.600	0.080	0.101	0.330	0.044	8.161	0.500	20.000	113.884	0.538	0.158	0.265
0.600	0.070	0.088	0.289	0.039	7.471	0.500	20.000	113.752	0.521	0.153	0.250
0.600	0.060	0.076	0.247	0.035	6.790	0.500	20.000	113.589	0.504	0.148	0.235
0.600	0.050	0.063	0.205	0.030	6.125	0.500	20.000	113.384	0.486	0.143	0.220
0.600	0.040	0.051	0.161	0.026	5.487	0.500	20.000	113.124	0.468	0.138	0.205
0.600	0.030	0.040	0.117	0.022	4.879	0.500	20.000	112.837	0.449	0.133	0.190
0.600	0.020	0.028	0.073	0.019	4.350	0.500	20.000	112.429	0.429	0.128	0.177
0.600	0.010	0.017	0.047	0.011	3.294	0.500	18.147	110.155	0.372	0.112	0.155

Table C.10: Optimization results for $Fr_c = 3.0$, $d/c = 0.6$

101

d/c	C_x	C_p	$C_{z_{max}}$	$C_{x_{LES}}$	$\alpha_{e_{max}}$	h_1	θ_1	ϕ_1	k	St_a	Θ
1.000	0.250	0.338	0.966	0.141	17.293	0.500	20.000	114.033	0.732	0.215	0.412
1.000	0.240	0.323	0.930	0.134	16.725	0.500	20.000	114.103	0.721	0.211	0.405
1.000	0.230	0.308	0.894	0.128	16.157	0.500	20.000	114.159	0.710	0.208	0.397
1.000	0.220	0.293	0.858	0.121	15.583	0.500	20.000	114.221	0.699	0.204	0.389
1.000	0.210	0.278	0.822	0.115	15.008	0.500	20.000	114.268	0.687	0.201	0.381
1.000	0.200	0.264	0.786	0.109	14.428	0.500	20.000	114.304	0.676	0.197	0.373
1.000	0.190	0.249	0.749	0.103	13.845	0.500	20.000	114.329	0.664	0.194	0.364
1.000	0.180	0.234	0.713	0.097	13.255	0.500	20.000	114.350	0.652	0.190	0.355
1.000	0.170	0.220	0.676	0.091	12.667	0.500	20.000	114.354	0.639	0.187	0.346
1.000	0.160	0.206	0.638	0.085	12.077	0.500	20.000	114.349	0.627	0.183	0.336
1.000	0.150	0.192	0.601	0.079	11.483	0.500	20.000	114.325	0.614	0.179	0.326
1.000	0.140	0.178	0.563	0.073	10.885	0.500	20.000	114.290	0.601	0.176	0.316
1.000	0.130	0.165	0.525	0.068	10.292	0.500	20.000	114.236	0.588	0.172	0.306
1.000	0.120	0.151	0.487	0.062	9.691	0.500	20.000	114.167	0.574	0.168	0.295
1.000	0.110	0.138	0.448	0.057	9.099	0.500	20.000	114.077	0.561	0.164	0.283
1.000	0.100	0.125	0.409	0.052	8.504	0.500	20.000	113.964	0.546	0.160	0.272
1.000	0.090	0.112	0.369	0.047	7.916	0.500	20.000	113.829	0.532	0.156	0.260
1.000	0.080	0.099	0.329	0.042	7.336	0.500	20.000	113.666	0.517	0.152	0.248
1.000	0.070	0.087	0.288	0.037	6.764	0.500	20.000	113.473	0.502	0.148	0.235
1.000	0.060	0.074	0.246	0.033	6.208	0.500	20.000	113.245	0.487	0.144	0.223
1.000	0.050	0.062	0.203	0.029	5.674	0.500	20.000	112.978	0.471	0.140	0.210
1.000	0.040	0.051	0.160	0.025	5.163	0.500	20.000	112.674	0.455	0.135	0.198
1.000	0.030	0.039	0.115	0.022	4.698	0.500	20.000	112.319	0.438	0.131	0.187
1.000	0.020	0.028	0.070	0.018	4.291	0.500	20.000	111.895	0.421	0.126	0.178
1.000	0.010	0.017	0.050	0.010	3.163	0.500	17.695	109.213	0.357	0.109	0.155

Table C.11: Optimization results for $Fr_c = 4.0$, $d/c = 1.0$

102

d/c	C_x	C_p	$C_{z_{max}}$	$C_{x_{LES}}$	$\alpha_{e_{max}}$	h_1	θ_1	ϕ_1	k	St_a	Θ
0.800	0.250	0.342	0.973	0.142	18.042	0.500	20.000	113.763	0.745	0.219	0.423
0.800	0.240	0.327	0.936	0.136	17.456	0.500	20.000	113.846	0.733	0.215	0.416
0.800	0.230	0.311	0.900	0.129	16.860	0.500	20.000	113.940	0.722	0.212	0.408
0.800	0.220	0.296	0.863	0.123	16.270	0.500	20.000	114.004	0.711	0.208	0.400
0.800	0.210	0.281	0.827	0.117	15.667	0.500	20.000	114.086	0.699	0.205	0.391
0.800	0.200	0.266	0.790	0.111	15.066	0.500	20.000	114.139	0.687	0.201	0.383
0.800	0.190	0.252	0.753	0.104	14.455	0.500	20.000	114.195	0.675	0.198	0.374
0.800	0.180	0.237	0.716	0.098	13.845	0.500	20.000	114.224	0.663	0.194	0.365
0.800	0.170	0.223	0.678	0.092	13.235	0.500	20.000	114.228	0.650	0.190	0.355
0.800	0.160	0.208	0.641	0.086	12.617	0.500	20.000	114.246	0.637	0.186	0.346
0.800	0.150	0.194	0.603	0.080	11.997	0.500	20.000	114.244	0.624	0.183	0.336
0.800	0.140	0.180	0.565	0.075	11.368	0.500	20.000	114.233	0.611	0.179	0.325
0.800	0.130	0.166	0.527	0.069	10.744	0.500	20.000	114.197	0.597	0.175	0.314
0.800	0.120	0.153	0.488	0.063	10.111	0.500	20.000	114.160	0.583	0.171	0.303
0.800	0.110	0.139	0.449	0.058	9.481	0.500	20.000	114.093	0.569	0.167	0.291
0.800	0.100	0.126	0.410	0.053	8.855	0.500	20.000	113.996	0.554	0.163	0.279
0.800	0.090	0.113	0.370	0.048	8.227	0.500	20.000	113.891	0.540	0.158	0.266
0.800	0.080	0.100	0.329	0.043	7.605	0.500	20.000	113.749	0.524	0.154	0.253
0.800	0.070	0.087	0.288	0.038	6.991	0.500	20.000	113.581	0.509	0.150	0.240
0.800	0.060	0.075	0.246	0.033	6.392	0.500	20.000	113.374	0.493	0.145	0.227
0.800	0.050	0.063	0.204	0.029	5.815	0.500	20.000	113.130	0.476	0.141	0.213
0.800	0.040	0.051	0.160	0.025	5.266	0.500	20.000	112.834	0.459	0.136	0.200
0.800	0.030	0.039	0.115	0.022	4.752	0.500	20.000	112.499	0.442	0.131	0.188
0.800	0.020	0.028	0.070	0.019	4.306	0.500	20.000	112.079	0.424	0.127	0.177
0.800	0.010	0.017	0.049	0.011	3.177	0.500	17.821	109.563	0.362	0.110	0.153

Table C.12: Optimization results for $Fr_c = 4.0$, $d/c = 0.8$

103

d/c	C_x	C_p	$C_{z_{max}}$	$C_{x_{LES}}$	$\alpha_{e_{max}}$	h_1	θ_1	ϕ_1	k	St_a	Θ
0.600	0.250	0.347	0.981	0.146	19.131	0.500	20.000	113.671	0.766	0.225	0.436
0.600	0.240	0.331	0.945	0.140	18.494	0.500	20.000	113.833	0.755	0.222	0.428
0.600	0.230	0.316	0.907	0.133	17.871	0.500	20.000	113.930	0.743	0.218	0.420
0.600	0.220	0.300	0.870	0.127	17.248	0.500	20.000	114.002	0.731	0.214	0.412
0.600	0.210	0.285	0.831	0.120	16.648	0.500	20.000	113.976	0.718	0.211	0.405
0.600	0.200	0.270	0.795	0.115	15.942	0.500	20.000	114.261	0.707	0.207	0.394
0.600	0.190	0.255	0.758	0.109	15.277	0.500	20.000	114.400	0.694	0.203	0.384
0.600	0.180	0.240	0.719	0.101	14.704	0.500	20.000	114.227	0.681	0.199	0.377
0.600	0.170	0.225	0.682	0.096	14.001	0.500	20.000	114.419	0.668	0.195	0.366
0.600	0.160	0.211	0.644	0.089	13.348	0.500	20.000	114.429	0.654	0.191	0.356
0.600	0.150	0.196	0.606	0.084	12.632	0.500	20.000	114.600	0.641	0.187	0.344
0.600	0.140	0.182	0.568	0.078	11.971	0.500	20.000	114.589	0.627	0.183	0.333
0.600	0.130	0.168	0.528	0.071	11.356	0.500	20.000	114.403	0.612	0.179	0.324
0.600	0.120	0.154	0.490	0.066	10.642	0.500	20.000	114.482	0.598	0.174	0.311
0.600	0.110	0.141	0.450	0.060	9.981	0.500	20.000	114.387	0.583	0.170	0.299
0.600	0.100	0.127	0.410	0.055	9.309	0.500	20.000	114.285	0.567	0.166	0.287
0.600	0.090	0.114	0.370	0.049	8.622	0.500	20.000	114.215	0.552	0.161	0.273
0.600	0.080	0.101	0.330	0.044	7.936	0.500	20.000	114.121	0.535	0.157	0.259
0.600	0.070	0.088	0.289	0.039	7.267	0.500	20.000	113.959	0.519	0.152	0.245
0.600	0.060	0.075	0.247	0.035	6.613	0.500	20.000	113.756	0.502	0.147	0.230
0.600	0.050	0.063	0.205	0.030	5.968	0.500	20.000	113.537	0.484	0.143	0.215
0.600	0.040	0.051	0.161	0.026	5.358	0.500	20.000	113.241	0.466	0.138	0.201
0.600	0.030	0.040	0.117	0.022	4.786	0.500	20.000	112.905	0.447	0.133	0.187
0.600	0.020	0.028	0.073	0.019	4.282	0.500	20.000	112.481	0.428	0.127	0.175
0.600	0.010	0.017	0.051	0.011	3.137	0.500	17.763	109.823	0.363	0.110	0.151

Table C.13: Optimization results for $Fr_c = 4.0$, $d/c = 0.6$

d/c	C_x	C_p	$C_{z_{max}}$	$C_{x_{LES}}$	$\alpha_{e_{max}}$	h_1	θ_1	ϕ_1	k	St_a	Θ
1.000	0.250	0.338	0.966	0.141	17.171	0.500	20.000	114.162	0.731	0.214	0.410
1.000	0.240	0.323	0.930	0.134	16.605	0.500	20.000	114.230	0.720	0.211	0.403
1.000	0.230	0.308	0.894	0.128	16.034	0.500	20.000	114.294	0.709	0.207	0.395
1.000	0.220	0.293	0.858	0.121	15.465	0.500	20.000	114.348	0.698	0.204	0.387
1.000	0.210	0.278	0.822	0.115	14.891	0.500	20.000	114.395	0.686	0.200	0.379
1.000	0.200	0.263	0.785	0.109	14.312	0.500	20.000	114.437	0.675	0.197	0.370
1.000	0.190	0.249	0.749	0.103	13.732	0.500	20.000	114.459	0.663	0.193	0.362
1.000	0.180	0.234	0.712	0.097	13.148	0.500	20.000	114.470	0.651	0.190	0.353
1.000	0.170	0.220	0.675	0.091	12.557	0.500	20.000	114.484	0.638	0.186	0.343
1.000	0.160	0.206	0.638	0.085	11.972	0.500	20.000	114.472	0.626	0.183	0.334
1.000	0.150	0.192	0.601	0.079	11.382	0.500	20.000	114.445	0.613	0.179	0.324
1.000	0.140	0.178	0.563	0.073	10.786	0.500	20.000	114.410	0.600	0.175	0.314
1.000	0.130	0.164	0.525	0.068	10.196	0.500	20.000	114.354	0.587	0.171	0.303
1.000	0.120	0.151	0.487	0.062	9.602	0.500	20.000	114.277	0.574	0.168	0.292
1.000	0.110	0.138	0.448	0.057	9.013	0.500	20.000	114.184	0.560	0.164	0.281
1.000	0.100	0.125	0.409	0.052	8.422	0.500	20.000	114.068	0.546	0.160	0.269
1.000	0.090	0.112	0.369	0.047	7.841	0.500	20.000	113.926	0.531	0.156	0.258
1.000	0.080	0.099	0.329	0.042	7.266	0.500	20.000	113.757	0.517	0.152	0.246
1.000	0.070	0.087	0.288	0.037	6.701	0.500	20.000	113.556	0.502	0.148	0.233
1.000	0.060	0.074	0.246	0.033	6.152	0.500	20.000	113.320	0.486	0.144	0.221
1.000	0.050	0.062	0.203	0.029	5.625	0.500	20.000	113.043	0.471	0.139	0.209
1.000	0.040	0.051	0.160	0.025	5.127	0.500	20.000	112.719	0.454	0.135	0.197
1.000	0.030	0.039	0.115	0.022	4.669	0.500	20.000	112.355	0.438	0.130	0.186
1.000	0.020	0.028	0.070	0.018	4.271	0.500	20.000	111.919	0.421	0.126	0.177
1.000	0.010	0.017	0.054	0.010	3.057	0.500	17.374	108.916	0.351	0.107	0.152

Table C.14: Optimization results for $Fr_c = 5.0$, $d/c = 1.0$

d/c	C_x	C_p	$C_{z_{max}}$	$C_{x_{LES}}$	$\alpha_{e_{max}}$	h_1	θ_1	ϕ_1	k	St_a	Θ
0.800	0.250	0.342	0.972	0.142	17.867	0.500	20.000	113.968	0.743	0.218	0.420
0.800	0.240	0.326	0.935	0.135	17.324	0.500	20.000	113.922	0.732	0.215	0.413
0.800	0.230	0.311	0.899	0.129	16.696	0.500	20.000	114.120	0.721	0.211	0.404
0.800	0.220	0.296	0.862	0.123	16.117	0.500	20.000	114.153	0.709	0.208	0.397
0.800	0.210	0.281	0.826	0.116	15.533	0.500	20.000	114.187	0.697	0.204	0.389
0.800	0.200	0.266	0.789	0.110	14.933	0.500	20.000	114.244	0.686	0.200	0.380
0.800	0.190	0.251	0.752	0.104	14.321	0.500	20.000	114.313	0.674	0.197	0.371
0.800	0.180	0.237	0.715	0.098	13.718	0.500	20.000	114.331	0.661	0.193	0.362
0.800	0.170	0.222	0.678	0.092	13.096	0.500	20.000	114.376	0.649	0.189	0.352
0.800	0.160	0.208	0.640	0.086	12.492	0.500	20.000	114.362	0.636	0.186	0.343
0.800	0.150	0.194	0.603	0.080	11.867	0.500	20.000	114.382	0.623	0.182	0.333
0.800	0.140	0.180	0.565	0.074	11.244	0.500	20.000	114.367	0.610	0.178	0.322
0.800	0.130	0.166	0.526	0.069	10.620	0.500	20.000	114.339	0.596	0.174	0.311
0.800	0.120	0.152	0.488	0.063	10.006	0.500	20.000	114.258	0.582	0.170	0.300
0.800	0.110	0.139	0.449	0.058	9.378	0.500	20.000	114.197	0.568	0.166	0.288
0.800	0.100	0.126	0.409	0.053	8.749	0.500	20.000	114.121	0.553	0.162	0.276
0.800	0.090	0.113	0.370	0.048	8.132	0.500	20.000	113.996	0.539	0.158	0.264
0.800	0.080	0.100	0.329	0.043	7.516	0.500	20.000	113.853	0.523	0.154	0.251
0.800	0.070	0.087	0.288	0.038	6.913	0.500	20.000	113.669	0.508	0.149	0.238
0.800	0.060	0.075	0.246	0.033	6.323	0.500	20.000	113.455	0.492	0.145	0.224
0.800	0.050	0.063	0.203	0.029	5.756	0.500	20.000	113.196	0.475	0.141	0.211
0.800	0.040	0.051	0.160	0.025	5.217	0.500	20.000	112.890	0.459	0.136	0.199
0.800	0.030	0.039	0.115	0.022	4.718	0.500	20.000	112.535	0.441	0.131	0.187
0.800	0.020	0.028	0.070	0.019	4.284	0.500	20.000	112.099	0.423	0.126	0.177
0.800	0.010	0.017	0.051	0.010	3.125	0.500	17.630	109.338	0.358	0.108	0.153

Table C.15: Optimization results for $Fr_c = 5.0$, $d/c = 0.8$

d/c	C_x	C_p	$C_{z_{max}}$	$C_{x_{LES}}$	$\alpha_{e_{max}}$	h_1	θ_1	ϕ_1	k	St_a	Θ
0.600	0.250	0.346	0.976	0.143	19.098	0.500	20.000	113.241	0.761	0.225	0.438
0.600	0.240	0.330	0.940	0.137	18.435	0.500	20.000	113.496	0.750	0.221	0.429
0.600	0.230	0.315	0.906	0.133	17.659	0.500	20.000	114.093	0.740	0.217	0.417
0.600	0.220	0.300	0.866	0.125	17.183	0.500	20.000	113.719	0.727	0.214	0.413
0.600	0.210	0.284	0.833	0.122	16.318	0.500	20.000	114.526	0.717	0.209	0.397
0.600	0.200	0.269	0.794	0.114	15.735	0.500	20.000	114.432	0.704	0.206	0.390
0.600	0.190	0.254	0.756	0.108	15.120	0.500	20.000	114.432	0.691	0.202	0.382
0.600	0.180	0.240	0.719	0.102	14.442	0.500	20.000	114.596	0.679	0.198	0.371
0.600	0.170	0.225	0.683	0.097	13.726	0.500	20.000	114.842	0.666	0.194	0.360
0.600	0.160	0.210	0.644	0.090	13.113	0.500	20.000	114.743	0.653	0.190	0.351
0.600	0.150	0.196	0.605	0.083	12.492	0.500	20.000	114.635	0.639	0.186	0.342
0.600	0.140	0.182	0.567	0.077	11.829	0.500	20.000	114.646	0.625	0.182	0.331
0.600	0.130	0.168	0.528	0.071	11.180	0.500	20.000	114.582	0.610	0.178	0.320
0.600	0.120	0.154	0.489	0.066	10.479	0.500	20.000	114.634	0.596	0.174	0.307
0.600	0.110	0.140	0.450	0.060	9.840	0.500	20.000	114.493	0.581	0.169	0.296
0.600	0.100	0.127	0.410	0.054	9.199	0.500	20.000	114.326	0.565	0.165	0.284
0.600	0.090	0.114	0.370	0.049	8.493	0.500	20.000	114.329	0.550	0.161	0.270
0.600	0.080	0.101	0.330	0.044	7.834	0.500	20.000	114.177	0.534	0.156	0.256
0.600	0.070	0.088	0.288	0.039	7.187	0.500	20.000	113.981	0.517	0.152	0.243
0.600	0.060	0.075	0.247	0.035	6.510	0.500	20.000	113.862	0.500	0.147	0.227
0.600	0.050	0.063	0.205	0.030	5.891	0.500	20.000	113.596	0.483	0.142	0.213
0.600	0.040	0.051	0.161	0.026	5.293	0.500	20.000	113.293	0.465	0.137	0.199
0.600	0.030	0.039	0.117	0.022	4.741	0.500	20.000	112.932	0.446	0.132	0.185
0.600	0.020	0.028	0.073	0.019	4.257	0.500	20.000	112.479	0.427	0.127	0.174
0.600	0.010	0.017	0.052	0.011	3.103	0.500	17.709	109.774	0.362	0.109	0.150

Table C.16: Optimization results for $Fr_c = 5.0$, $d/c = 0.6$

d/c	C_x	C_p	$C_{z_{max}}$	$C_{x_{LES}}$	$\alpha_{e_{max}}$	h_1	θ_1	ϕ_1	k	St_a	Θ
1.000	0.250	0.338	0.965	0.140	17.080	0.500	20.000	114.252	0.730	0.213	0.409
1.000	0.240	0.323	0.929	0.134	16.522	0.500	20.000	114.301	0.719	0.210	0.401
1.000	0.230	0.308	0.893	0.128	15.950	0.500	20.000	114.376	0.708	0.207	0.393
1.000	0.220	0.293	0.857	0.121	15.383	0.500	20.000	114.426	0.697	0.203	0.385
1.000	0.210	0.278	0.821	0.115	14.811	0.500	20.000	114.474	0.685	0.200	0.377
1.000	0.200	0.263	0.785	0.109	14.236	0.500	20.000	114.510	0.674	0.197	0.369
1.000	0.190	0.249	0.748	0.103	13.659	0.500	20.000	114.532	0.662	0.193	0.360
1.000	0.180	0.234	0.712	0.097	13.076	0.500	20.000	114.547	0.650	0.190	0.351
1.000	0.170	0.220	0.675	0.091	12.489	0.500	20.000	114.554	0.638	0.186	0.342
1.000	0.160	0.206	0.638	0.085	11.906	0.500	20.000	114.542	0.625	0.182	0.332
1.000	0.150	0.192	0.600	0.079	11.318	0.500	20.000	114.515	0.613	0.179	0.323
1.000	0.140	0.178	0.563	0.073	10.725	0.500	20.000	114.479	0.600	0.175	0.312
1.000	0.130	0.164	0.525	0.068	10.139	0.500	20.000	114.419	0.586	0.171	0.302
1.000	0.120	0.151	0.487	0.062	9.548	0.500	20.000	114.340	0.573	0.167	0.291
1.000	0.110	0.138	0.448	0.057	8.963	0.500	20.000	114.240	0.559	0.164	0.280
1.000	0.100	0.124	0.409	0.052	8.374	0.500	20.000	114.125	0.545	0.160	0.268
1.000	0.090	0.112	0.369	0.047	7.797	0.500	20.000	113.979	0.531	0.156	0.256
1.000	0.080	0.099	0.329	0.042	7.226	0.500	20.000	113.806	0.516	0.152	0.244
1.000	0.070	0.086	0.288	0.037	6.665	0.500	20.000	113.600	0.501	0.148	0.232
1.000	0.060	0.074	0.246	0.033	6.121	0.500	20.000	113.359	0.486	0.143	0.220
1.000	0.050	0.062	0.203	0.029	5.598	0.500	20.000	113.077	0.470	0.139	0.208
1.000	0.040	0.051	0.160	0.025	5.105	0.500	20.000	112.746	0.454	0.135	0.196
1.000	0.030	0.039	0.115	0.021	4.653	0.500	20.000	112.373	0.438	0.130	0.186
1.000	0.020	0.028	0.070	0.018	4.261	0.500	20.000	111.931	0.421	0.126	0.177
1.000	0.010	0.017	0.040	0.015	3.613	0.500	19.579	111.485	0.395	0.118	0.160

Table C.17: Optimization results for $Fr_c = 6.0$, $d/c = 1.0$

d/c	C_x	C_p	$C_{z_{max}}$	$C_{x_{LES}}$	$\alpha_{e_{max}}$	h_1	θ_1	ϕ_1	k	St_a	Θ
0.800	0.250	0.341	0.971	0.142	17.769	0.500	20.000	114.030	0.742	0.217	0.418
0.800	0.240	0.326	0.935	0.136	17.193	0.500	20.000	114.096	0.731	0.214	0.411
0.800	0.230	0.311	0.898	0.129	16.633	0.500	20.000	114.089	0.719	0.211	0.404
0.800	0.220	0.296	0.862	0.123	15.999	0.500	20.000	114.295	0.708	0.207	0.394
0.800	0.210	0.281	0.825	0.117	15.427	0.500	20.000	114.300	0.696	0.204	0.387
0.800	0.200	0.266	0.788	0.110	14.850	0.500	20.000	114.296	0.684	0.200	0.379
0.800	0.190	0.251	0.751	0.104	14.244	0.500	20.000	114.356	0.672	0.196	0.370
0.800	0.180	0.236	0.715	0.098	13.614	0.500	20.000	114.464	0.660	0.193	0.360
0.800	0.170	0.222	0.677	0.092	13.011	0.500	20.000	114.460	0.648	0.189	0.351
0.800	0.160	0.208	0.640	0.086	12.407	0.500	20.000	114.451	0.635	0.185	0.341
0.800	0.150	0.194	0.602	0.080	11.792	0.500	20.000	114.450	0.622	0.182	0.331
0.800	0.140	0.180	0.564	0.074	11.168	0.500	20.000	114.448	0.609	0.178	0.320
0.800	0.130	0.166	0.526	0.069	10.542	0.500	20.000	114.431	0.595	0.174	0.309
0.800	0.120	0.152	0.487	0.063	9.938	0.500	20.000	114.332	0.581	0.170	0.299
0.800	0.110	0.139	0.449	0.058	9.312	0.500	20.000	114.270	0.567	0.166	0.287
0.800	0.100	0.125	0.409	0.053	8.689	0.500	20.000	114.189	0.553	0.162	0.274
0.800	0.090	0.112	0.370	0.048	8.077	0.500	20.000	114.058	0.538	0.158	0.262
0.800	0.080	0.100	0.329	0.043	7.467	0.500	20.000	113.905	0.523	0.153	0.249
0.800	0.070	0.087	0.288	0.038	6.868	0.500	20.000	113.718	0.507	0.149	0.236
0.800	0.060	0.075	0.246	0.033	6.285	0.500	20.000	113.494	0.491	0.145	0.223
0.800	0.050	0.063	0.203	0.029	5.724	0.500	20.000	113.229	0.475	0.140	0.210
0.800	0.040	0.051	0.160	0.025	5.191	0.500	20.000	112.917	0.458	0.136	0.198
0.800	0.030	0.039	0.115	0.022	4.699	0.500	20.000	112.551	0.441	0.131	0.186
0.800	0.020	0.028	0.070	0.019	4.271	0.500	20.000	112.109	0.423	0.126	0.176

Table C.18: Optimization results for $Fr_c = 6.0$, $d/c = 0.8$

Appendix D

Optimization Results - Power Extraction

d/c	C_x	C_p	$C_{z_{max}}$	$C_{x_{LES}}$	$\alpha_{e_{max}}$	h_1	θ_1	ϕ_1	k	St_a	Θ
∞	-0.010	-0.004	0.051	0.001	1.192	0.500	10.210	99.147	0.172	0.054	0.121
∞	-0.020	-0.013	0.135	0.005	3.220	0.500	16.681	104.988	0.279	0.087	0.202
∞	-0.030	-0.023	0.205	0.011	4.798	0.500	20.000	107.849	0.331	0.103	0.253
∞	-0.040	-0.032	0.270	0.012	5.469	0.500	20.000	106.706	0.313	0.098	0.305
∞	-0.050	-0.040	0.339	0.014	6.215	0.500	20.000	105.409	0.294	0.093	0.369
∞	-0.060	-0.048	0.416	0.018	7.036	0.500	20.000	103.907	0.274	0.088	0.448
∞	-0.070	-0.056	0.503	0.023	7.939	0.500	20.000	102.151	0.253	0.083	0.548
∞	-0.080	-0.063	0.605	0.032	8.954	0.500	20.000	100.027	0.230	0.077	0.680
∞	-0.090	-0.069	0.730	0.045	10.149	0.500	20.000	97.275	0.204	0.069	0.870

Table D.1: Optimization results for $Fr_c = 1.0$, $d/c = \infty$

d/c	C_x	C_p	$C_{z_{max}}$	$C_{x_{LES}}$	$\alpha_{e_{max}}$	h_1	θ_1	ϕ_1	k	St_a	Θ
1.000	-0.010	-0.004	0.050	0.001	1.224	0.500	10.323	99.220	0.174	0.055	0.123
1.000	-0.020	-0.013	0.132	0.004	2.971	0.500	15.752	103.920	0.260	0.082	0.199
1.000	-0.030	-0.022	0.200	0.008	4.417	0.500	18.968	106.644	0.311	0.097	0.248
1.000	-0.040	-0.031	0.263	0.011	5.274	0.500	20.000	107.181	0.318	0.099	0.290
1.000	-0.050	-0.040	0.329	0.012	5.880	0.500	20.000	106.585	0.301	0.095	0.341
1.000	-0.060	-0.048	0.401	0.015	6.561	0.500	20.000	105.934	0.283	0.089	0.405
1.000	-0.070	-0.055	0.478	0.019	7.327	0.500	20.000	105.190	0.264	0.084	0.485
1.000	-0.080	-0.061	0.563	0.024	8.180	0.500	20.000	104.333	0.244	0.078	0.586
1.000	-0.090	-0.067	0.659	0.031	9.144	0.500	20.000	103.415	0.221	0.072	0.721

Table D.2: Optimization results for $Fr_c = 1.0$, $d/c = 1.0$

d/c	C_x	C_p	$C_{z_{max}}$	$C_{x_{LES}}$	$\alpha_{e_{max}}$	h_1	θ_1	ϕ_1	k	St_a	Θ
0.800	-0.010	-0.003	0.055	0.003	2.360	0.465	14.452	104.282	0.272	0.079	0.163
0.800	-0.020	-0.013	0.130	0.004	3.167	0.500	16.332	104.735	0.269	0.084	0.205
0.800	-0.030	-0.022	0.197	0.009	4.599	0.500	19.359	107.409	0.316	0.098	0.254
0.800	-0.040	-0.030	0.260	0.010	5.388	0.500	20.000	107.743	0.312	0.097	0.302
0.800	-0.050	-0.038	0.326	0.012	6.086	0.500	20.000	107.418	0.293	0.091	0.363
0.800	-0.060	-0.046	0.397	0.014	6.888	0.500	20.000	107.042	0.273	0.085	0.441
0.800	-0.070	-0.052	0.474	0.018	7.794	0.500	20.000	106.624	0.251	0.079	0.542
0.800	-0.080	-0.057	0.559	0.024	8.820	0.500	20.000	106.149	0.227	0.072	0.677
0.800	-0.090	-0.060	0.654	0.031	9.999	0.500	20.000	105.617	0.201	0.064	0.867

Table D.3: Optimization results for $Fr_c = 1.0$, $d/c = 0.8$

d/c	C_x	C_p	$C_{z_{max}}$	$C_{x_{LES}}$	$\alpha_{e_{max}}$	h_1	θ_1	ϕ_1	k	St_a	Θ
0.600	-0.010	-0.004	0.049	0.001	1.313	0.500	10.504	99.949	0.173	0.055	0.133
0.600	-0.020	-0.012	0.127	0.004	3.385	0.500	16.647	105.449	0.269	0.084	0.219
0.600	-0.030	-0.021	0.193	0.009	4.996	0.500	20.000	108.608	0.321	0.099	0.272
0.600	-0.040	-0.029	0.256	0.010	5.799	0.500	20.000	108.623	0.298	0.092	0.339
0.600	-0.050	-0.036	0.323	0.012	6.766	0.500	20.000	108.635	0.274	0.085	0.431
0.600	-0.060	-0.042	0.395	0.015	7.890	0.500	20.000	108.638	0.248	0.077	0.555
0.600	-0.070	-0.046	0.475	0.019	9.182	0.500	20.000	108.629	0.219	0.068	0.731
0.600	-0.080	-0.048	0.564	0.025	10.692	0.500	20.000	108.476	0.187	0.058	0.997
0.600	-0.090	-0.046	0.669	0.035	12.488	0.500	20.000	108.387	0.150	0.046	1.455

Table D.4: Optimization results for $Fr_c = 1.0$, $d/c = 0.6$

d/c	C_x	C_p	$C_{z_{max}}$	$C_{x_{LES}}$	$\alpha_{e_{max}}$	h_1	θ_1	ϕ_1	k	St_a	Θ
1.000	-0.010	-0.004	0.050	0.001	1.441	0.500	11.994	101.784	0.204	0.064	0.124
1.000	-0.020	-0.013	0.139	0.008	3.712	0.500	18.728	108.396	0.318	0.098	0.204
1.000	-0.030	-0.022	0.205	0.011	4.812	0.500	20.000	109.198	0.325	0.100	0.259
1.000	-0.040	-0.031	0.269	0.012	5.667	0.500	20.000	108.450	0.302	0.093	0.327
1.000	-0.050	-0.038	0.340	0.014	6.643	0.500	20.000	107.609	0.278	0.087	0.417
1.000	-0.060	-0.045	0.419	0.018	7.758	0.500	20.000	106.494	0.252	0.079	0.538
1.000	-0.070	-0.050	0.511	0.025	9.047	0.500	20.000	105.060	0.223	0.071	0.709
1.000	-0.080	-0.054	0.623	0.035	10.592	0.500	20.000	103.225	0.189	0.061	0.980
1.000	-0.090	-0.053	0.779	0.054	12.685	0.500	20.000	100.313	0.144	0.048	1.537

Table D.5: Optimization results for $Fr_c = 2.0$, $d/c = 1.0$

d/c	C_x	C_p	$C_{z_{max}}$	$C_{x_{LES}}$	$\alpha_{e_{max}}$	h_1	θ_1	ϕ_1	k	St_a	Θ
0.800	-0.010	-0.004	0.051	0.002	1.603	0.500	12.945	102.967	0.222	0.069	0.126
0.800	-0.020	-0.013	0.140	0.009	3.813	0.500	19.024	108.959	0.323	0.099	0.206
0.800	-0.030	-0.022	0.205	0.011	4.908	0.500	20.000	109.401	0.321	0.098	0.267
0.800	-0.040	-0.030	0.270	0.012	5.867	0.500	20.000	108.592	0.297	0.092	0.345
0.800	-0.050	-0.038	0.342	0.014	6.964	0.500	20.000	107.614	0.270	0.084	0.450
0.800	-0.060	-0.044	0.423	0.019	8.218	0.500	20.000	106.341	0.241	0.076	0.595
0.800	-0.070	-0.048	0.519	0.026	9.682	0.500	20.000	104.661	0.208	0.067	0.811
0.800	-0.080	-0.050	0.643	0.039	11.507	0.500	20.000	102.265	0.169	0.055	1.189
0.800	-0.090	-0.044	0.848	0.067	14.384	0.500	20.000	97.624	0.109	0.037	2.302

Table D.6: Optimization results for $Fr_c = 2.0$, $d/c = 0.8$

d/c	C_x	C_p	$C_{z_{max}}$	$C_{x_{LES}}$	$\alpha_{e_{max}}$	h_1	θ_1	ϕ_1	k	St_a	Θ
0.600	-0.010	-0.004	0.050	0.002	1.562	0.500	12.725	102.912	0.216	0.068	0.126
0.600	-0.020	-0.013	0.140	0.009	3.947	0.500	19.335	109.595	0.327	0.100	0.211
0.600	-0.030	-0.022	0.204	0.011	5.084	0.500	20.000	109.618	0.316	0.097	0.281
0.600	-0.040	-0.030	0.270	0.012	6.210	0.500	20.000	108.610	0.288	0.089	0.377
0.600	-0.050	-0.037	0.345	0.015	7.496	0.500	20.000	107.365	0.258	0.080	0.508
0.600	-0.060	-0.042	0.432	0.021	8.986	0.500	20.000	105.676	0.224	0.071	0.701
0.600	-0.070	-0.045	0.540	0.030	10.785	0.500	20.000	103.300	0.184	0.060	1.021
0.600	-0.080	-0.044	0.700	0.050	13.298	0.500	20.000	99.321	0.131	0.044	1.767
0.600	-0.090	-0.030	0.856	0.075	16.028	0.285	19.976	90.187	0.137	0.030	3.429

Table D.7: Optimization results for $Fr_c = 2.0$, $d/c = 0.6$

d/c	C_x	C_p	$C_{z_{max}}$	$C_{x_{LES}}$	$\alpha_{e_{max}}$	h_1	θ_1	ϕ_1	k	St_a	Θ
1.000	-0.010	-0.004	0.050	0.001	1.429	0.500	11.826	101.400	0.201	0.063	0.124
1.000	-0.020	-0.013	0.138	0.008	3.663	0.500	18.446	107.770	0.312	0.096	0.205
1.000	-0.030	-0.022	0.205	0.011	4.831	0.500	20.000	108.751	0.326	0.100	0.259
1.000	-0.040	-0.031	0.270	0.012	5.658	0.500	20.000	107.769	0.304	0.095	0.325
1.000	-0.050	-0.039	0.341	0.014	6.595	0.500	20.000	106.591	0.281	0.088	0.410
1.000	-0.060	-0.046	0.420	0.018	7.642	0.500	20.000	105.162	0.256	0.082	0.521
1.000	-0.070	-0.052	0.512	0.025	8.833	0.500	20.000	103.318	0.229	0.074	0.674
1.000	-0.080	-0.056	0.623	0.035	10.232	0.500	20.000	100.860	0.198	0.065	0.903
1.000	-0.090	-0.058	0.776	0.053	12.040	0.500	20.000	97.077	0.159	0.054	1.322

Table D.8: Optimization results for $Fr_c = 3.0$, $d/c = 1.0$

d/c	C_x	C_p	$C_{z_{max}}$	$C_{x_{LES}}$	$\alpha_{e_{max}}$	h_1	θ_1	ϕ_1	k	St_a	Θ
0.800	-0.010	-0.004	0.051	0.002	1.628	0.500	13.019	102.893	0.224	0.070	0.127
0.800	-0.020	-0.013	0.138	0.008	3.739	0.500	18.642	108.094	0.315	0.097	0.207
0.800	-0.030	-0.022	0.205	0.011	4.903	0.500	20.000	108.819	0.323	0.100	0.265
0.800	-0.040	-0.031	0.270	0.012	5.802	0.500	20.000	107.745	0.300	0.093	0.338
0.800	-0.050	-0.038	0.342	0.014	6.815	0.500	20.000	106.423	0.275	0.087	0.432
0.800	-0.060	-0.045	0.423	0.019	7.953	0.500	20.000	104.805	0.249	0.079	0.558
0.800	-0.070	-0.051	0.518	0.026	9.252	0.500	20.000	102.646	0.219	0.071	0.736
0.800	-0.080	-0.054	0.638	0.038	10.804	0.500	20.000	99.670	0.185	0.062	1.017
0.800	-0.090	-0.054	0.820	0.062	12.975	0.500	20.000	94.477	0.140	0.049	1.622

Table D.9: Optimization results for $Fr_c = 3.0$, $d/c = 0.8$

d/c	C_x	C_p	$C_{z_{max}}$	$C_{x_{LES}}$	$\alpha_{e_{max}}$	h_1	θ_1	ϕ_1	k	St_a	Θ
0.600	-0.010	-0.004	0.051	0.002	1.672	0.500	13.101	102.894	0.225	0.070	0.130
0.600	-0.020	-0.013	0.139	0.009	3.824	0.500	18.845	108.530	0.318	0.098	0.210
0.600	-0.030	-0.022	0.205	0.011	5.027	0.500	20.000	108.858	0.319	0.098	0.275
0.600	-0.040	-0.030	0.271	0.012	6.037	0.500	20.000	107.596	0.294	0.092	0.359
0.600	-0.050	-0.038	0.345	0.015	7.173	0.500	20.000	106.024	0.267	0.084	0.470
0.600	-0.060	-0.044	0.430	0.020	8.456	0.500	20.000	103.973	0.237	0.076	0.622
0.600	-0.070	-0.049	0.534	0.029	9.946	0.500	20.000	101.249	0.204	0.067	0.851
0.600	-0.080	-0.052	0.676	0.045	11.841	0.500	20.000	97.077	0.164	0.056	1.264
0.600	-0.090	-0.046	0.812	0.063	14.115	0.370	19.835	99.611	0.171	0.050	1.962

Table D.10: Optimization results for $Fr_c = 3.0$, $d/c = 0.6$

113

d/c	C_x	C_p	$C_{z_{max}}$	$C_{x_{LES}}$	$\alpha_{e_{max}}$	h_1	θ_1	ϕ_1	k	St_a	Θ
1.000	-0.010	-0.004	0.050	0.001	1.385	0.500	11.491	100.903	0.195	0.061	0.124
1.000	-0.020	-0.013	0.137	0.008	3.615	0.500	18.205	107.331	0.307	0.095	0.205
1.000	-0.030	-0.022	0.205	0.011	4.845	0.500	20.000	108.534	0.326	0.101	0.259
1.000	-0.040	-0.031	0.270	0.012	5.658	0.500	20.000	107.468	0.305	0.095	0.324
1.000	-0.050	-0.039	0.341	0.014	6.572	0.500	20.000	106.191	0.282	0.089	0.407
1.000	-0.060	-0.046	0.420	0.018	7.594	0.500	20.000	104.610	0.258	0.083	0.514
1.000	-0.070	-0.052	0.511	0.025	8.742	0.500	20.000	102.635	0.232	0.075	0.659
1.000	-0.080	-0.057	0.622	0.035	10.077	0.500	20.000	99.999	0.202	0.067	0.871
1.000	-0.090	-0.060	0.772	0.053	11.768	0.500	20.000	96.001	0.166	0.057	1.238

Table D.11: Optimization results for $Fr_c = 4.0$, $d/c = 1.0$

d/c	C_x	C_p	$C_{z_{max}}$	$C_{x_{LES}}$	$\alpha_{e_{max}}$	h_1	θ_1	ϕ_1	k	St_a	Θ
0.800	-0.010	-0.004	0.051	0.002	1.653	0.500	13.044	102.780	0.224	0.070	0.129
0.800	-0.020	-0.013	0.138	0.008	3.682	0.500	18.380	107.615	0.310	0.096	0.207
0.800	-0.030	-0.022	0.205	0.011	4.908	0.500	20.000	108.570	0.324	0.100	0.265
0.800	-0.040	-0.031	0.270	0.012	5.781	0.500	20.000	107.412	0.301	0.094	0.335
0.800	-0.050	-0.039	0.342	0.014	6.764	0.500	20.000	105.999	0.277	0.088	0.426
0.800	-0.060	-0.046	0.423	0.019	7.859	0.500	20.000	104.207	0.252	0.081	0.545
0.800	-0.070	-0.052	0.517	0.026	9.097	0.500	20.000	101.938	0.224	0.073	0.710
0.800	-0.080	-0.056	0.635	0.037	10.556	0.500	20.000	98.855	0.192	0.064	0.961
0.800	-0.090	-0.057	0.808	0.060	12.523	0.500	20.000	93.675	0.150	0.053	1.454

Table D.12: Optimization results for $Fr_c = 4.0$, $d/c = 0.8$

d/c	C_x	C_p	$C_{z_{max}}$	$C_{x_{LES}}$	$\alpha_{e_{max}}$	h_1	θ_1	ϕ_1	k	St_a	Θ
0.600	-0.010	-0.004	0.051	0.002	1.652	0.500	13.092	102.956	0.225	0.070	0.128
0.600	-0.020	-0.013	0.137	0.008	3.739	0.500	18.439	107.764	0.309	0.095	0.211
0.600	-0.030	-0.022	0.205	0.011	5.017	0.500	20.000	108.580	0.320	0.099	0.273
0.600	-0.040	-0.030	0.271	0.012	5.987	0.500	20.000	107.229	0.296	0.093	0.353
0.600	-0.050	-0.038	0.344	0.015	7.070	0.500	20.000	105.577	0.270	0.086	0.457
0.600	-0.060	-0.045	0.429	0.020	8.288	0.500	20.000	103.448	0.242	0.078	0.598
0.600	-0.070	-0.050	0.531	0.029	9.684	0.500	20.000	100.636	0.211	0.070	0.802
0.600	-0.080	-0.054	0.668	0.044	11.410	0.500	20.000	96.518	0.174	0.060	1.146

Table D.13: Optimization results for $Fr_c = 4.0$, $d/c = 0.6$

d/c	C_x	C_p	$C_{z_{max}}$	$C_{x_{LES}}$	$\alpha_{e_{max}}$	h_1	θ_1	ϕ_1	k	St_a	Θ
1.000	-0.010	-0.004	0.050	0.001	1.376	0.500	11.385	100.708	0.193	0.061	0.125
1.000	-0.020	-0.013	0.137	0.007	3.570	0.500	17.999	106.997	0.303	0.094	0.206
1.000	-0.030	-0.022	0.205	0.011	4.850	0.500	20.000	108.427	0.326	0.101	0.259
1.000	-0.040	-0.031	0.270	0.012	5.655	0.500	20.000	107.321	0.305	0.095	0.324
1.000	-0.050	-0.039	0.341	0.014	6.558	0.500	20.000	105.998	0.283	0.089	0.405
1.000	-0.060	-0.046	0.420	0.018	7.568	0.500	20.000	104.345	0.259	0.083	0.510
1.000	-0.070	-0.053	0.511	0.025	8.696	0.500	20.000	102.320	0.233	0.076	0.651
1.000	-0.080	-0.058	0.621	0.035	10.005	0.500	20.000	99.600	0.204	0.068	0.855
1.000	-0.090	-0.061	0.770	0.052	11.648	0.500	20.000	95.532	0.169	0.058	1.202

Table D.14: Optimization results for $Fr_c = 5.0$, $d/c = 1.0$

d/c	C_x	C_p	$C_{z_{max}}$	$C_{x_{LES}}$	$\alpha_{e_{max}}$	h_1	θ_1	ϕ_1	k	St_a	Θ
0.800	-0.010	-0.004	0.051	0.002	1.654	0.500	13.084	102.848	0.225	0.070	0.128
0.800	-0.020	-0.013	0.137	0.008	3.665	0.500	18.281	107.395	0.308	0.095	0.208
0.800	-0.030	-0.022	0.205	0.011	4.910	0.500	20.000	108.453	0.324	0.100	0.264
0.800	-0.040	-0.031	0.270	0.012	5.772	0.500	20.000	107.252	0.302	0.094	0.334
0.800	-0.050	-0.039	0.342	0.014	6.739	0.500	20.000	105.797	0.278	0.088	0.423
0.800	-0.060	-0.046	0.423	0.019	7.816	0.500	20.000	103.954	0.253	0.081	0.539
0.800	-0.070	-0.052	0.517	0.026	9.028	0.500	20.000	101.637	0.226	0.074	0.698
0.800	-0.080	-0.057	0.634	0.037	10.447	0.500	20.000	98.502	0.195	0.066	0.937
0.800	-0.090	-0.059	0.804	0.059	12.330	0.500	20.000	93.350	0.155	0.054	1.388

Table D.15: Optimization results for $Fr_c = 5.0$, $d/c = 0.8$

d/c	C_x	C_p	$C_{z_{max}}$	$C_{x_{LES}}$	$\alpha_{e_{max}}$	h_1	θ_1	ϕ_1	k	St_a	Θ
0.600	-0.010	-0.004	0.050	0.001	1.448	0.500	11.816	101.338	0.200	0.063	0.126
0.600	-0.020	-0.013	0.137	0.008	3.700	0.500	18.290	107.515	0.306	0.095	0.211
0.600	-0.030	-0.022	0.205	0.011	5.011	0.500	20.000	108.448	0.321	0.099	0.273
0.600	-0.040	-0.031	0.271	0.012	5.964	0.500	20.000	107.062	0.297	0.093	0.351
0.600	-0.050	-0.038	0.344	0.015	7.028	0.500	20.000	105.328	0.272	0.086	0.452
0.600	-0.060	-0.045	0.429	0.020	8.211	0.500	20.000	103.196	0.244	0.079	0.587
0.600	-0.070	-0.051	0.530	0.028	9.567	0.500	20.000	100.381	0.214	0.071	0.781
0.600	-0.080	-0.055	0.664	0.043	11.228	0.500	20.000	96.305	0.178	0.061	1.100
0.600	-0.090	-0.052	0.957	0.088	14.351	0.500	20.000	84.284	0.116	0.043	2.159

Table D.16: Optimization results for $Fr_c = 5.0$, $d/c = 0.6$

d/c	C_x	C_p	$C_{z_{max}}$	$C_{x_{LES}}$	$\alpha_{e_{max}}$	h_1	θ_1	ϕ_1	k	St_a	Θ
1.000	-0.010	-0.004	0.052	0.002	1.803	0.500	13.627	103.242	0.236	0.074	0.133
1.000	-0.020	-0.013	0.137	0.007	3.592	0.500	18.070	107.044	0.305	0.094	0.206
1.000	-0.030	-0.022	0.205	0.011	4.852	0.500	20.000	108.367	0.327	0.101	0.259
1.000	-0.040	-0.031	0.270	0.012	5.653	0.500	20.000	107.244	0.305	0.095	0.323
1.000	-0.050	-0.039	0.341	0.014	6.550	0.500	20.000	105.897	0.283	0.090	0.404
1.000	-0.060	-0.046	0.420	0.018	7.551	0.500	20.000	104.218	0.260	0.083	0.508
1.000	-0.070	-0.053	0.511	0.025	8.670	0.500	20.000	102.145	0.234	0.077	0.647
1.000	-0.080	-0.058	0.621	0.035	9.963	0.500	20.000	99.410	0.205	0.069	0.847
1.000	-0.090	-0.061	0.769	0.052	11.582	0.500	20.000	95.321	0.171	0.059	1.183

Table D.17: Optimization results for $Fr_c = 6.0$, $d/c = 1.0$

d/c	C_x	C_p	$C_{z_{max}}$	$C_{x_{LES}}$	$\alpha_{e_{max}}$	h_1	θ_1	ϕ_1	k	St_a	Θ
0.800	-0.010	-0.004	0.050	0.001	1.386	0.500	11.450	100.833	0.194	0.061	0.125
0.800	-0.020	-0.013	0.137	0.008	3.651	0.500	18.222	107.296	0.307	0.095	0.208
0.800	-0.030	-0.022	0.205	0.011	4.911	0.500	20.000	108.385	0.325	0.100	0.264
0.800	-0.040	-0.031	0.270	0.012	5.767	0.500	20.000	107.164	0.302	0.095	0.333
0.800	-0.050	-0.039	0.342	0.014	6.724	0.500	20.000	105.692	0.279	0.088	0.421
0.800	-0.060	-0.046	0.423	0.019	7.791	0.500	20.000	103.827	0.254	0.082	0.535
0.800	-0.070	-0.052	0.517	0.026	8.988	0.500	20.000	101.487	0.227	0.075	0.691
0.800	-0.080	-0.057	0.633	0.037	10.389	0.500	20.000	98.335	0.196	0.066	0.924
0.800	-0.090	-0.059	0.801	0.058	12.234	0.500	20.000	93.214	0.157	0.055	1.356

Table D.18: Optimization results for $Fr_c = 6.0$, $d/c = 0.8$

Bibliography

[1] ABBOT, I., AND VON DOENHOFF, A. *Theory of Wing Sections.* Dover Publications, Inc., 1959.

[2] ALEXANDER, R. M. "Springs for Wings". *Science, Vol. 268* (April 1995), pp. 50–51.

[3] ANDERSON, J., STREITLIEN, K., BARRET, D., AND TRIANTAFYLLOU, M. "Oscillating Foils of High Propulsive Efficiency". *Journal of Fluid Mechanics, Vol. 360* (1998), pp. 41–72.

[4] ANDERSON, J. J. *Fundamentals of Aerodynamics, Third Edition.* McGraw-Hill Book Company, 2001.

[5] BETZ, A. "Ein Beitrag zur Erklärung des Segeslfluges". *Zeitschrift für Flugtechnik und Motorluftschiffahrt, Vol. 3* (1912), pp. 269–272.

[6] BISPLINGHOFF, R., ASHLEY, H., AND HALFMAN, R. *Aeroelasticity.* Dover Publications, Inc., 1955.

[7] DELAURIER, J., AND HARRIS, J. "Experimental Study of Oscillating-Wing Propulsion". *Journal of Aircraft, Vol. 19*, No. 5 (May 1982), pp. 368–373.

[8] DRELA, M. "XFOIL: An Analysis and Design System for Low Reynolds Number Airfoils". *Low Reynolds Number Aerodynamics, edited by T.J. Mueller, Vol. 54 of Lecture Notes in Engineering, Springer-Verlag, New-York* (June 1989), pp. 1–12.

[9] ERICSSON, L., AND REDING, J. "Analytic Prediction of Dynamic Stall Characteristics". In *Paper AIAA-72-682.* (June 1972).

[10] ERICSSON, L., AND REDING, J. "Dynamic Stall Analysis in Light of Recent Numerical and Experimental Results". *Journal of Aircraft, Vol. 13*, No. 4 (April 1976).

[11] GARRICK, I. "Propulsion of a Flapping and Oscillating Airfoil". Tech. Rep. No. 567, NACA, 1936.

[12] GARRICK, I. *Nonsteady wing Characteristics*, vol. VII High Speed Aerodynamics and Jet Propulsion: Aerodynamic Components of Aircraft at High Speeds, Eds. Donovan, A.F and Lawrence, H.R. Princeton University Press, 1957.

[13] HALL, K., AND HALL, S. "Minimum Induced Power Requirements for Flapping Flight". *Journal of Fluid Mechanics, Vol. 323* (Sept. 1982), pp. 285–315.

[14] HOERNER, S. *Fluid Dynamic Lift.* Bakersfield, CA : Hoerner Fluid Dynamics, 1985.

[15] HOERNER, S. *Fluid Dynamic Drag: Practical Information on Aerodynamic Drag and Hydrodynamic Resistance.* Bakersfield, CA : Hoerner Fluid Dynamics, 1992.

[16] HORNFELD, W. "Germany Enters the AUV Wars with DeepC". *Underwater Magazine* (January/February 2002).

[17] JONES, K., CASTRO, B., MAHMOUD, O., AND PLATZER, M. "A Numerical and Experimental Investigation of Flapping-Wing Propulsion in Ground Effect". In *40th AIAA Aerospace Sciences Meeting and Exhibit, Reno, NV, Paper AIAA-2002-0866.* (Jan. 2002).

[18] JONES, K., AND PLATZER, M. "Numerical Computation of Flapping-Wing Propulsion and Power Extraction". In *37th AIAA Aerospace Sciences Meeting and Exhibit, Reno, NV, Paper AIAA-99-0826.* (Jan. 1997).

[19] JONES, K., AND PLATZER, M. "An Experimental and Numerical Investigation of Flapping-Wing propulsion". In *37th AIAA Aerospace Sciences Meeting and Exhibit, Reno, NV, Paper AIAA-99-0995.* (Jan. 1999).

[20] JONES, K., PLATZER, M., AND DAVIDS, S. "Oscillating-Wing Power Generation". In *Proceedings of the 3rd ASME/JSME Joint Fluids Engineering Conference, San francisco, California, Paper FEDSM99-7050* (July 1999).

[21] KATZ, J., AND PLOTKIN, A. *Low Speed Aerodynamics, Second Edition.* Cambridge University Press, 2001.

[22] KNOLLER, R. "Die Gesetze des Luftwiderstandes". *Flug- und Motortechnik (Wien), Vol. 3*, No. 21 (1909), pp. 1–7.

[23] KUETHE, A., AND CHOW, C. *Foundations of Aerodynamics, Bases of Aerodynamic Design, Fifth Edition.* John Wiley and Sons, Inc., 1998.

[24] LIGHTHILL, M. J. "Aquatic Animal Propulsion of High Hydromechanical Efficiency". *Journal of Fluid Mechanics, Vol. 44*, No. 2 (January 1970), pp. 265–301.

[25] MACCREADY, P. "Hydrofoil Boats with Flapping-Wing Propulsion". *Human Power, Vol. 8,* No. 1 (1990), pp. 9–16.

[26] MCKINNEY, W., AND DELAURIER, J. "The Wingmill: An Oscillating-Wing Windmill". *Journal of Energy, Vol. 5,* No. 2 (1981), pp. 109–115.

[27] MORAN, J. *An Introduction to Theoretical and Computational Aerodynamics.* John Wiley & Sons, 1984.

[28] NEWMAN, J. *Marine Hydrodynamics.* MIT Press, Inc., 1971.

[29] SCHMIDT, W. "Der Wellpropeller, ein neuer Antrieb fuer Wasser-, Land-, und Luft- fahrzeuge". *Z. Flugwiss, Vol. 13* (1965), pp. 472–479.

[30] SFAKIOTAKIS, M., LANE, D., AND DAVIES, J. "Review of Fish Swimming Modes for Aquatic Locomotion". *IEEE Journal of Oceanic Engineering, Vol. 24* (April 1999), pp. 237–252.

[31] THEODORSEN, T. "General Theory of Aerodynamic Instability and the Mechanism of Flutter". Tech. Rep. No. 496, NACA, 1935.

[32] TRIANTAFYLLOU, G., TRIANTAFYLLOU, M., AND GROSENBAUGH, M. "Optimal Thrust Development in Oscillating Foils with Application to Fish Propulsion". *Journal of Fluid and Structures, Vol. 7* (1993), pp. 205–224.

[33] TRIANTAFYLLOU, M., TRIANTAFYLLOU, G., AND YUE, D. "Hydrodynamics of Fishlike Swimming". *Annual Review of Fluid Mechanics, Vol. 32* (2000), pp. 33–53.

[34] TRIPP, S. "Autonomous Underwater Vehicles (AUV's). A Look at Coast Guard Needs to Close Performance Gaps and Enhance Current Mission Performance.". *U.S.C.G. research and Development Center.*

[35] VON KÁRMÁN, T., AND BURGERS, J. *General Aerodynamic Theory-Perfect Fluids.* Aerodynamic Theory, W.F. Durand, ed. vol. II, Julius Springer (Berlin), 1935.